NOVEL CAPILLARY AND MICROFLUIDIC DEVICES FOR BIOLOGICAL ANALYSES

by

SCOTT A. KLASNER

B.S., Truman State University, 2003

AN ABSTRACT OF A DISSERTATION

submitted in partial fulfillment of the requirements for the degree

DOCTOR OF PHILOSOPHY

Department of Chemistry
College of Arts and Sciences

KANSAS STATE UNIVERSITY
Manhattan, Kansas

2010

Abstract

As the field of separation science evolves so do the techniques, tools and capabilities of the discipline. The introduction of microfluidics stemmed from a desire to perform traditional analyses faster and on a much smaller scale. The small device sizes exploited in microfluidics permits the investigation of very small volumes of very dilute samples yielding information inaccessible by traditional macroscale techniques. All of the chapters presented in this dissertation illustrate attempts to supplement current microscale techniques with new tools, techniques and analysis schemes for looking at biologically relevant analytes.

In chapter two I present the development and characterization of an amphiphilic polymer that has potential as a material for the fabrication of microfluidic devices. This material is composed of a poly(dimethylsiloxane)-poly(ethylene oxide) block copolymer and is dramatically more hydrophilic than the other polymeric materials currently used for the fabrication of microfluidic templates, mainly poly(dimethylsiloxane). Biomolecules such as proteins are notoriously hydrophobic and will tend to adsorb to other hydrophobic surfaces thus the use of a hydrophilic material may serve to reduce or eliminate this problem. The amphiphilic material is of a suitable durability for micromolding and molded channel architectures can be sealed between two layers of the material by simple conformal contact permitting the execution of high speed electrophoretic separations.

Chapter three contains initial results obtained while investigating the fluorescent labeling and electrophoretic separation of ecdysteroids. Ecdysteroids are hormones found in insects that are responsible for controlling the process of molting. Here we attempted to analyze these molecules by employing a reactive fluorescent probe, BODIPY FL® hydrazide, that would target the α,β-unsaturated ketone group on the steroid, permitting its analysis by capillary electrophoresis with laser induced fluorescence detection. While optimistic initial results were obtained with the labeling and analysis of similar functional groups on model compounds such as progesterone, labeling of the ecdysteroid molecules was never achieved to a degree that would permit reliable analysis.

In chapter four I report the development and use of a microimmunoaffinity column for the analysis of insect serine protease inhibitors, or serpins. These proteins play a very important

role in the regulation of insect immune responses and their activity may play an integral role in the effective transmission of the malaria parasite by the mosquito *Anopheles gambiae.* A microimmunoaffinity column was constructed from magnets, poly(dimethylsiloxane), fused silica capillary and Protein A coated magnetic microspheres. In these initial studies, purified antibodies to serpin protein, as well as purified serpin protein, were used to prepare and investigate the ability to isolate, preconcentrate, and elute serpin proteins for subsequent analysis. By implementing this miniaturized system which incorporates very small fluid volumes we hoped to extend this technique to the analysis of very small samples, and eventually to the analysis of individual small insects. Our work indicates that it is possible to isolate, elute, and detect serpin protein on a traditional western blot membrane.

Chapter five presents the development of a novel polymer blend for the fabrication of paper-based microfluidic devices and use of these devices in the performance of diagnostically relevant clinical assays. We took the concept of paper-based microfluidic devices and improved upon the current photoactive polymers used for their fabrication by developing a polymer blend using an acryloxy modified siloxane polymer as well as a commercially available photoactive adhesive, Norland Optical Adhesive 74. This blended polymer resulted in a dramatic reduction in fabrication time as well as improved resolution permitting the reliable patterning of small feature sizes. We also report for the first time a demonstration of these devices performing a two-step spatially separated online chemical derivatization facilitating the analysis of urinary ketones. These devices are predominantly used for the analysis of urine, and their application was extended to the quantitation of nitrite in saliva for the purposes of hemodialysis monitoring.

While varied in application, all of the data presented in this dissertation exploits the power of miniaturization to improve current methods of analysis and to extend macroscale techniques to trace biological analytes.

NOVEL CAPILLARY AND MICROFLUIDIC DEVICES FOR BIOLOGICAL ANALYSES

by

SCOTT A. KLASNER

B.S., Truman State University, 2003

A DISSERTATION

submitted in partial fulfillment of the requirements for the degree

DOCTOR OF PHILOSOPHY

Department of Chemistry
College of Arts and Sciences

KANSAS STATE UNIVERSITY
Manhattan, Kansas

2010

Approved by:

Major Professor
Christopher T. Culbertson

Copyright

Abstract

As the field of separation science evolves so do the techniques, tools and capabilities of the discipline. The introduction of microfluidics stemmed from a desire to perform traditional analyses faster and on a much smaller scale. The small device sizes exploited in microfluidics permits the investigation of very small volumes of very dilute samples yielding information inaccessible by traditional macroscale techniques. All of the chapters presented in this dissertation illustrate attempts to supplement current microscale techniques with new tools, techniques and analysis schemes for looking at biologically relevant analytes.

In chapter two I present the development and characterization of an amphiphilic polymer that has potential as a material for the fabrication of microfluidic devices. This material is composed of a poly(dimethylsiloxane)-poly(ethylene oxide) block copolymer and is dramatically more hydrophilic than the other polymeric materials currently used for the fabrication of microfluidic templates, mainly poly(dimethylsiloxane). Biomolecules such as proteins are notoriously hydrophobic and will tend to absorb to other hydrophobic surfaces thus the use of a hydrophilic material may serve to reduce or eliminate this problem. The amphiphilic material is of a suitable durability for micromolding and molded channel architectures can be sealed between two layers of the material by simple conformal contact permitting the execution of high speed electrophoretic separations.

Chapter three contains initial results obtained while investigating the fluorescent labeling and electrophoretic separation of ecdysteroids. Ecdysteroids are hormones found in insects that are responsible for controlling the process of molting. Here we attempted to analyze these molecules by employing a reactive fluorescent probe, BODIPY FL® hydrazide, that would target the α,β-unsaturated ketone group on the steroid, permitting its analysis by capillary electrophoresis with laser induced fluorescence detection. While optimistic initial results were obtained with the labeling and analysis of similar functional groups on model compounds such as progesterone, labeling of the ecdysteroid molecules was never achieved to a degree that would permit reliable analysis.

In chapter four we report the development and use of a microimmunoaffinity column for the analysis of insect serine protease inhibitors or serpins. These proteins play a very important

role in the regulation of insect immune responses and their activity may play an integral role in the effective transmission of the malaria parasite by the mosquito *Anopheles gambiae.* A microimmunoaffinity column was constructed from magnets, poly(dimethylsiloxane), fused silica capillary and Protein A coated magnetic microspheres. In these initial studies, purified antibodies to serpin protein, as well as purified serpin protein, were used to prepare and investigate the ability to isolate, preconcentrate, and elute serpin proteins for subsequent analysis. By implementing this miniaturized system which incorporates very small fluid volumes we hoped to extend this technique to the analysis of very small samples, and eventually to the analysis of individual small insects. Our work indicates that it is possible to isolate, elute, and detect serpin protein on a traditional western blot membrane.

Chapter five presents the development of a novel polymer blend for the fabrication of paper-based microfluidic devices and use of these devices in the performance of diagnostically relevant clinical assays. We took the concept of paper-based microfluidic devices and improved upon the current photoactive polymers used for their fabrication by developing a polymer blend using an acryloxy modified siloxane polymer as well as a commercially available photoactive adhesive, Norland Optical Adhesive 74. This blended polymer resulted in a dramatic reduction in fabrication time as well as improved resolution permitting the reliable patterning of small feature sizes. We also report for the first time a demonstration of these devices performing a two-step spatially separated online chemical derivatization facilitating the analysis of urinary ketones. These devices are predominantly used for the analysis of urine, and their application was extended to the quantitation of nitrite in saliva for the purposes of hemodialysis monitoring.

While varied in application, all of the data presented in this dissertation exploits the power of miniaturization to improve current methods of analysis and to extend macroscale techniques to trace biological analytes.

Table of Contents

List of Figures

List of Tables

Acknowledgements

I would like to take a moment to extend my thanks to everyone who has helped me along the way. Without any of you I may never have achieved this goal.

To my advisor Dr. Chris Culbertson, thank you for all of your help, expertise, patience and friendship. With some of the horror stories you hear about graduate advisors, I would say I was lucky to work for you. You truly helped make this experience an enjoyable one…most of the time. I have a great deal of respect for you.

To all of my fellow research group members, thank you for putting up with me. We were able to have a good time while also getting some good work accomplished. Thank you for all of your help.

To all of my friends, Kurt, Karcher, Everett, Jeff, Tom, Travis, Nate, Alex and Rodney…I never would have been able to accomplish this without your constant efforts to distract me. I will be keeping in touch with all of you.

To the chemistry department at Kansas State University, thank you for your time and efforts. To the support staff, Jim Hodgson, Tobe Eggers, Ron Jackson, and Richard Bachamp; I appreciate your constantly bailing me out by fixing what I've broken and by helping me to develop and build the tools that made much of my research possible. To the office staff, Donna Wright, Connie Cusimano, and Kim Ross; thank you for all of the behind the scenes work you do to make sure everything in the department is running smoothly. You were all an enormous help.

To Neal, Emily, Chunju, Stewart, and Dr. Michael Kanost of the Biochemistry department of Kansas State University for help with many of the biological experiments.

I would like to thank my committee members, Dr. Daniel Higgins, Dr. Stefan Bossmann, Dr. Yoonsong Park, and Dr. Susan Brown. I appreciate all of your time.

To my girlfriend Sherry for enduring my moaning and groaning when my experiments failed as well as pretending to be interested in all of my work.

Lastly I would like to thank my family. To my Mom and Dad, thank you for your constant love and support. I would have never gotten this far without you believing in me. You helped me become what I am today and I am ever grateful. Also, I'm sorry I spent such a shitload of your money.

Dedication

To my parents Bill and Jean, thank you for everything.

Chapter 1 - Introduction

1.1 Chemical Separations

The field of chemical separations is as broad and elegant as the numerous different techniques and principles that it encompasses. The fundamental challenge associated with a chemical separation is premised in the idea that the separation of components from a complex mixture runs counter to the second law of thermodynamics. The second law of thermodynamics states that the entropy of the universe is ever increasing. Entropy, or more simply disorder, is thus increased by the mixing of a system rather than the isolation of its individual components. To realize a separation therefore, requires the addition of external work.[1]

The field of chemical separations can be divided into two major categories; preparative and analytical. Preparative separations are generally large scale and used in an industrial setting for the production of bulk materials for commercial use. Analytical separations are typically very small scale, and the analytes of interest are traditionally very dilute. For an analytical separation, it is not uncommon for the target analytes to be at concentrations of parts per million or lower. The aim of these types of separations is to identify and quantify the components of complex mixtures.[1] Both types of separations involve selective movement of one component out of a region shared by multiple components into a region where it is the major occupant. As a result, the driving force of all separations is based in transport phenomena. The movement of components in a mixture is achieved by fluid displacement.

Fluid displacement is divided into two categories; bulk flow displacement and relative displacement. Of the two types, only relative displacement is selective and thus useful for achieving a successful separation, however, the two types of fluid displacement will often be used in combination with one another. A simple example of relative displacement can be illustrated by a liquid-liquid extraction. If an organic solvent was added to an aqueous solution containing a mixture of both a polar and a nonpolar compound, the analytes would position themselves such that the nonpolar analyte would be predominantly found in the organic layer, while the polar analyte would primarily occupy the aqueous layer. The concentration profile of the two analytes in their respective phases is dictated by the equilibrium of the system. The molecules, having partitioned into their respective solvents now experience a similar bulk environment, however, on a much smaller scale, each molecule's own microenvironment may be

slightly different and as a result they often display different individual characteristics even though they reside in a similar bulk environment.

The concept of entropy is vividly illustrated by the tendency of molecules to diffuse, occupy different energy states, and to reside in different phases and positions.[1] Due to the heterogeneity of individual molecules within a given population, it is much simpler to observe statistical distributions of molecules rather than individual ones. In terms of separations chemistry, this means that investigators are primarily concerned with concentration profiles of different molecules. Before one can understand the meaning of these parameters however, an understanding of the formation of these different analyte zones must be understood.

A variety of analytical techniques are available for the separation of complex mixtures such as high performance liquid chromatography (HPLC), gas chromatography (GC), capillary electrophoresis (CE), field flow fractionation (FFF), and gel electrophoresis (GE). Each technique exploits the different properties of analyte molecules to achieve useful separations, and thus certain techniques will be better suited for certain molecules based on their physical properties. This work focuses primarily on the use of capillary electrophoresis as a separation technique, thus an explanation of the origin of fluid transport and the mechanism of separation will be presented.

In this dissertation I will discuss the application of capillary electrophoresis to the analysis of biological molecules as well as the development of an amphiphilic block copolymer with the potential for improved performance for the analysis of hydrophobic biomolecules. Also, a simple paper-based microfluidic device fabricated from a novel polymer blend for use as a point-of-care (POC) diagnostic tool for clinically relevant biological assays was developed and these results will be presented as well.

Chapter 2 of this document begins with a discussion of the different types of materials useful for the fabrication of polymeric microfluidic devices for performing CE. A novel block copolymer composed of poly(dimethylsiloxane) and poly(ethylene oxide) was used to fabricate microfluidic systems of an amphiphilic nature, and their material characteristics and performance was evaluated. Chapter 3 will discuss the application of micellar electrokinetic chromatography (MEKC) with laser induced fluorescence detection for the analysis of model steroid compounds as well as some initial results regarding the analysis of insect hormones known as ecdysteroids. In chapter 4, I present preliminary results for the purification of serine protease inhibitors from

insect hemolymph using a micro-immunoaffinity column. Finally, in Chapter 5, the development of a novel polymer blend was used for the fabrication of paper-based microfluidic devices for the execution of clinically relevant biological assays.

1.1.1 Capillary Electrophoresis

1.1.1.1 Electrophoretic Mobility

Capillary electrophoresis is typically performed in an open tube that is filled with a conductive buffer. The open tube, a capillary, has a very small inner diameter on the order of tens to a few hundred microns which results in a high surface area to volume ratio. The capillary can either be a length of fused silica or polymer capillary, or a channel formed in a microfluidic device. These small dimensions result in high resistances when an electric field is applied across them, permitting the use of high electric fields with little heat being generated. The high surface area to volume ratio also results in increased heat dissipation. These two features as well as some others to be discussed later result in the realization of very high efficiency separations.[2]

By applying an electric field across the length of a capillary that has been filled with a conductive buffer solution, an electrical force is exerted on charged particles. This electrical force initiates the motion of ions in solution as they are either attracted to or repelled by the electric field. The equation describing the velocity of an ion under the influence of an electric field is given by equation (1.1) where v_{ep} is the velocity of the charged particle, μ_{ep} is the electrophoretic mobility, and E is the magnitude of the electric field strength.

$$v_{ep} = \mu_{ep} E \tag{1.1}$$

The electrical force, F_E, responsible for the motion of the charged particle in the presence of this electric field is represented by equation (1.2) and is based on the charge of the particle, q, and the applied electrical field strength

$$F_E = qE \tag{1.2}$$

The electrical field strength referenced by equations (1.1) and (1.2) is simply described by equation (1.3) where V is the voltage applied and L is the length of the capillary over which the voltage is applied.

$$E = \frac{V}{L} \tag{1.3}$$

While the electrical force is driving the particle in a certain direction relative to the applied electrical field, there is a second force operating in the opposite direction as a result of viscous forces acting on the particle in motion. The frictional force, F_F, is given by equation (1.4) where r is the hydrodynamic radius and η is the viscosity of the background solution.

$$F_F = -6\pi v_{ep} r\eta \tag{1.4}$$

Upon the application of the electric field, the ion, under the influence of the electrical force begins to accelerate, however the electrical force and the frictional force quickly reach a steady state and the particle will then move at a constant velocity. Under these steady state conditions, the electrical and frictional forces are balanced as shown in (1.5).

$$qE = 6\pi v_{ep} r\eta \tag{1.5}$$

Solving for v_{ep}, by using substitution equation (1.1) into equation (1.5) produces the expression for electrophoretic mobility as represented by equation (1.6).

$$\mu_{ep} = \frac{q}{6\pi\eta r} \tag{1.6}$$

As is indicated by this relationship, the electrophoretic mobility of a particle is maximized by increasing its charge while decreasing its radius. Thus, to effectively separate two different particles, of the same radius they must possess different charges. Likewise, to separate two particles of the same charge requires that they possess differing radii. Simply put, it is the charge to size ratio that effects the separation of particles by capillary electrophoresis.

While the differing electrophoretic mobilities of analytes in solution will result in their having different electrophoretic velocities, the electrophoretic velocity is likely not the actual observed velocity of a particle under the influence of an applied electric field. A phenomena known as electroosmotic flow (EOF) arises as a result of the surface charge on the capillary wall and can have a dramatic impact on a particles observed velocity. EOF defines the movement of the bulk solution in these capillaries and the electroosmotic velocity, v_{eo}, is often much greater in magnitude than the electrophoretic velocity.[1-4]

1.1.1.2 Electroosmotic Mobility

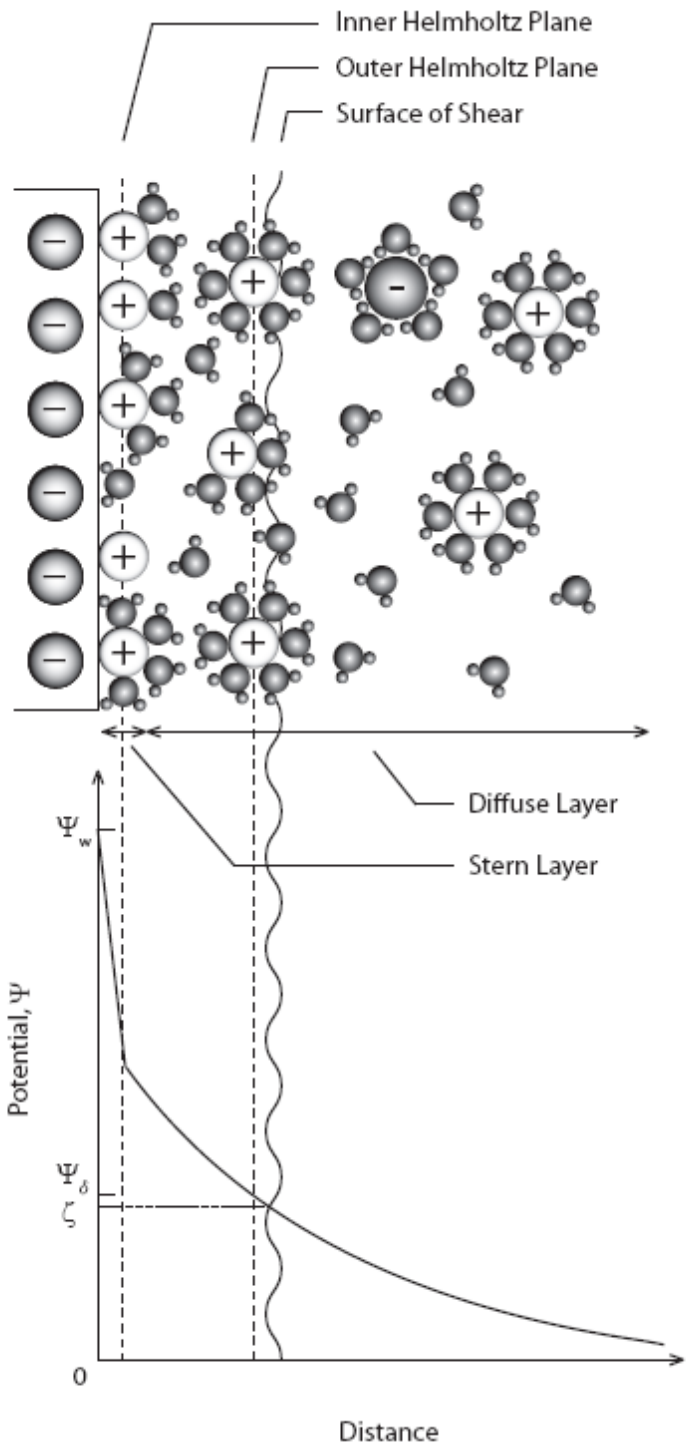

Figure 1.1 – Gouy-Chapman model of the EDL with Ψ_w representing the potential at the surface, Ψ_δ representing the potential at the outer Helmholtz plane, and ζ representing the zeta potential

The formation of an electrical double layer (EDL) at the solid-liquid interface of an insulator, such as the glass of a capillary, in contact with an electrolyte solution facilitates the bulk movement of fluid when an electric field is applied across the length of a capillary (Figure 1.1). This fluid motion is a result of acid base equilibria with respect to glass or fused silica and a result of ion adsorption with regard to many polymers such as Teflon. The surfaces of glass and fused silica are dominated by SiOH groups. Under conditions of pH 2 and higher, these SiOH groups are deprotonated resulting in SiO^- groups. This dissociation results in a surface dominated by negative charge. The background electrolyte supplies cations that arrange themselves near the negatively charged surface in an attempt to maintain charge neutrality. The layer of cations nearest to the surface of the glass is referred to as the compact layer or the Stern layer. These ions are considered adsorbed to the surface and immobile. The plane running parallel to the surface of the glass and bisecting the ions in the compact layer is referred to as the inner Helmholtz plane. Directly adjacent to the ions comprising the compact layer is a layer of solvated ions that serve to neutralize the excess surface charge not compensated for by the ions in the compact layer. These ions are less tightly bound and somewhat mobile. The plane bisecting this layer of solvated ions is the outer Helmholtz plane. Directly adjacent to the outer Helmholtz plane is what is known as the surface of shear, sometimes referred to as the slip plane. The term slip plane can be somewhat confusing, since it is not a true plane. The surface of shear is the boundary where the more mobile ions in solution are able to move along the ions bound to the material surface neutralizing its charge. The potential between the charged glass surface and the surface of shear is known as the zeta potential and is represented by ζ. The surface of shear is normally very close to the outer Helmholtz plane and thus the potential at the outer Helmholtz plane is often a good approximation of the zeta potential.[5] Generally speaking, ζ, is most often between 0 and 100 mV.[6]

Typically the thickness of the EDL, known as the Debye length, λ_D, is small (10 nm - 100 nm) and at 25° C is given by equation (1.7) where z_i is the valency of ion i, c_i is the concentration of ion i, and I_s is the ionic strength defined by equation (1.8).

$$\lambda_D = \frac{3.04 \times 10^{-10}}{z_i\sqrt{c_i}} = \frac{2.15 \times 10^{-10}}{\sqrt{I_s}} \tag{1.7}$$

$$I_s = \frac{1}{2}\sum c_i z_i^2 \tag{1.8}$$

As the distance from the substrate surface increases, the potential in the diffuse layer decreases exponentially until, after a certain distance, the bulk solution is reached and electroneutrality is again observed. It is at this point that the bulk solution "begins" and here ζ equals zero. One can manipulate the Debye length by changing the concentration of the ions in the electrolyte solution. As the ion concentration increases the Debye length decreases as indicated by equation (1.7).[5]

The presence of the EDL is what permits electroosmotic flow (EOF) to occur. When a voltage is applied parallel to the surface of a material in contact with a liquid, the ions that compose the diffuse region of the EDL are attracted towards the electrode of opposite charge. Since these ions are also solvated, the bulk solution gets pulled towards the cathode as well. This creates bulk fluid flow that is dependent on the zeta potential of the surface in question. The bulk fluid flow generated by EOF has a constant velocity denoted v_{eo} and a flow profile that is planar and perpendicular to the surface. The electroosmotic velocity is given by the Smoluchowski equation (1.9) where η is the viscosity, ε_0 is the permittivity in a vacuum, and κ is the dielectric constant.

$$v_{eo} = -(\varepsilon_0 \kappa \zeta / \eta) E \tag{1.9}$$

Since the electroosmotic velocity is dependent on the zeta potential, the pH of the solution filling the capillary plays a key role in determining the magnitude of the EOF. For instance with glass, as the pH increases and more of the SiOH groups become deprotonated forming SiO^- groups, the zeta potential increases resulting in increased EOF. Conversely at low pH where more of the SiOH groups are likely to be protonated, the zeta potential decreases and thus the overall EOF velocity decreases as well.

As recalled from equation (1.1) the electrophoretic velocity is equal to the product of the mobility and the electric field strength, thus the electroosmotic mobility, μ_{eo}, can be calculated using simple substitution as illustrated in equation (1.10).

$$\mu_{eo} = \frac{\varepsilon_0 \kappa \zeta}{\eta} \tag{1.10}$$

Thus, by substitution, the electroosmotic velocity can be simplified by substituting equation (1.10) in to equation (1.9) yielding equation (1.11).

$$v_{eo} = \mu_{eo} E \tag{1.11}$$

The observed velocity of a charged analyte under the influence of an electric field is a combination of the electrophoretic velocity of that analyte and electroosmotic velocity of the system. These two velocities can be in the same or opposite directions. Under traditional CE conditions, a positive potential is applied across a capillary with a negatively charged surface (generally glass or fused silica), and the direction of the resulting EOF will be towards the cathode. Cationic species, repelled by the positive voltage will migrate towards the cathode as well, moving in the same direction as the EOF. Anions, however, will be attracted to this positively charged electrode and possess and electrophoretic velocity counter to the EOF. Neutral species do not posses electrophoretic mobility and are thus simply dragged along with a velocity equal to v_{eo}. So the net velocity, v_{TOT}, of analytes can be described by equation (1.12).

$$v_{TOT} = v_{ep} + v_{eo} \tag{1.12}$$

Electroosmotic velocity is often much greater in magnitude than the electrophoretic velocity and this has many consequences, both positive a negative. One nice feature of having a dominant electroosmotic velocity is the ability to detect all molecules (positive, negative, and neutral) with the same detector, as all molecules regardless of their electrophoretic velocities, will eventually be dragged by the EOF to the point of detection. High EOF also favors very rapid separations as analytes can be separated based on differences in their electrophoretic velocities and then rapidly carried by EOF to the point of detection. High EOF can be undesirable, however when trying to resolve two closely spaced peaks. Resolving closely spaced peaks under conditions of high EOF can lead to longer capillaries requiring the use of higher electrical potentials as well as longer separation times.[6]

At the channel wall where ζ is greatest, v_{eo} is zero, but increases rapidly further away from the surface and remains constant throughout the bulk solution. The constant v_{eo} in the bulk solution is what gives fluid flow in capillary electrophoretic systems a flat profile (Figure 1.2). The flat profile also serves to reduce band broadening when compared to the parabolic flow profiles found in pressure driven systems. In pressure driven systems, the position of the particle in the capillary will dictate its velocity, whereas in electrokinetic systems, the velocity of all particles in the bulk solution is uniform. The flow in pressure driven systems will be described more thoroughly in a later section.

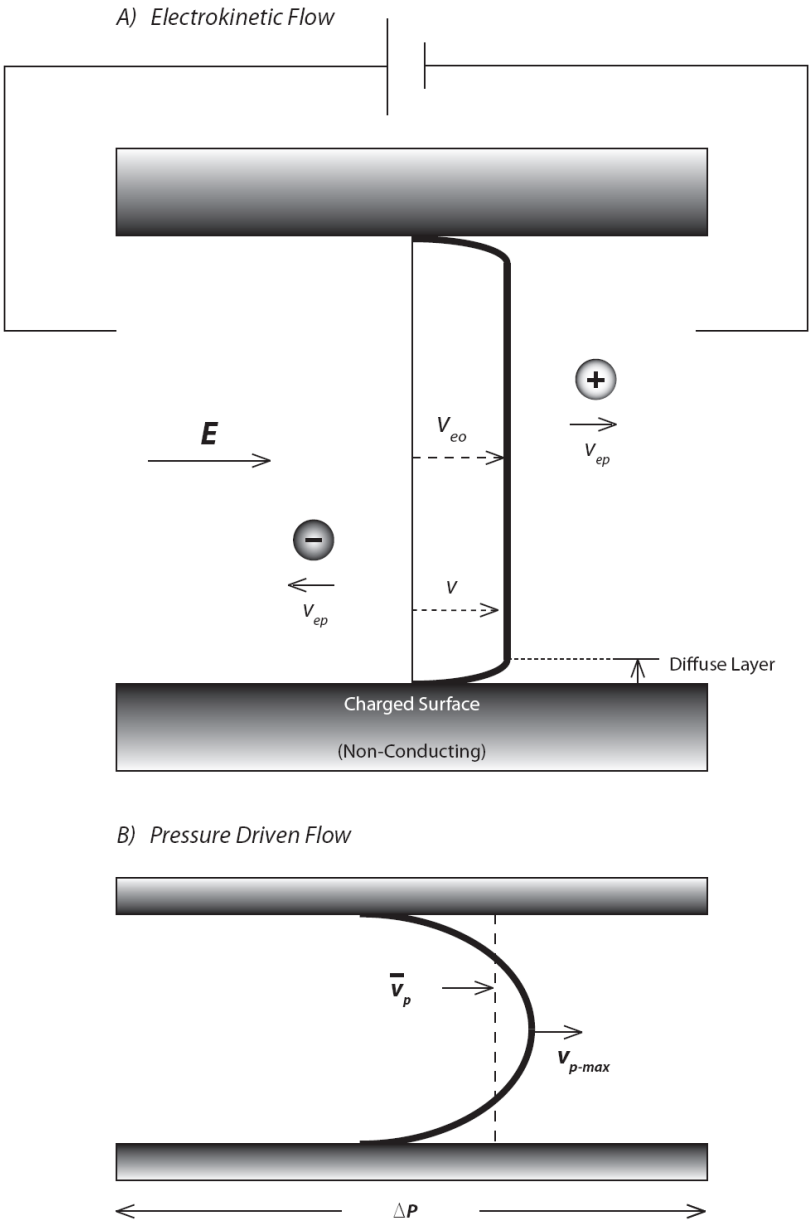

Figure 1.2 – A) Diagram representing the flow profile in an electrokinetically driven environment. The fluid velocity falls off rapidly close to the channel wall and reaches a uniform velocity throughout the bulk solution. Also displayed are the electrophoretic velocities of positively and negatively charged ions relative to the applied electric field. B) Diagram representing flow in a pressure driven system. In the center of the channel, the fluid velocity reaches a maximum and decreases as the channel walls are approached. Commonly, an average velocity will be used to represent flow in these systems and here, its magnitude is denoted by the dashed line.

Since analytes are separated based on their charge to size ratios in CE, peaks corresponding to analytes of similar charge and hydrodynamic radius can be difficult to resolve. For instance two amino acids of similar size and charge may not be completely resolved and two neutral analytes cannot be separated at all based on charge. Thus, it is often necessary to introduce a second orthogonal separation mechanism into the system to separate analytes based on their hydrophobic character. This practice often uses surfactants that, at high enough concentrations will form micelles into which analytes can partition. This technique was developed by Terabe et al.[7] and is known as micellar electrokinetic chromatography (MEKC).

1.1.2 Micellar Electrokinetic Chromatography

1.1.3 Separation Parameters

The evaluation of an analytical separation is based on a set of parameters that can be used to describe the separation as either "high" or "low" quality. It is the difference in the mobilities of the individual analytes that affects the separation in a CE system. As discussed earlier, similar molecules of a population will diffuse, occupy different energy states, and reside within different phases and positions.[1] As a result, analyte zones will typically adopt a Gaussian distribution due to the micro heterogeneities within the population of sample molecules which results in a narrow range of different mobilities. In order to completely separate two analyte zones a variety of dispersive forces must be taken into account as it is these dispersive forces that will dictate the length of each analyte zone and the mobility differences necessary for zone separation.[2] Dispersion can be numerically described by the baseline width (w_b) of a Gaussian peak where σ represents the standard deviation of the peak as in equation (1.13). The standard deviation of the peak can have a variety of units such as time, length or volume. Conceptually, dispersion describes the broadening of solute bands.

$$w_b = 4\sigma \tag{1.13}$$

The variance of a peak is described by equation (1.14) where D is the diffusion coefficient of the corresponding analyte and t is migration time. A representative electropherogram is shown in Figure 1.3, pointing out some of these important parameters.

$$\sigma^2 = 2Dt \tag{1.14}$$

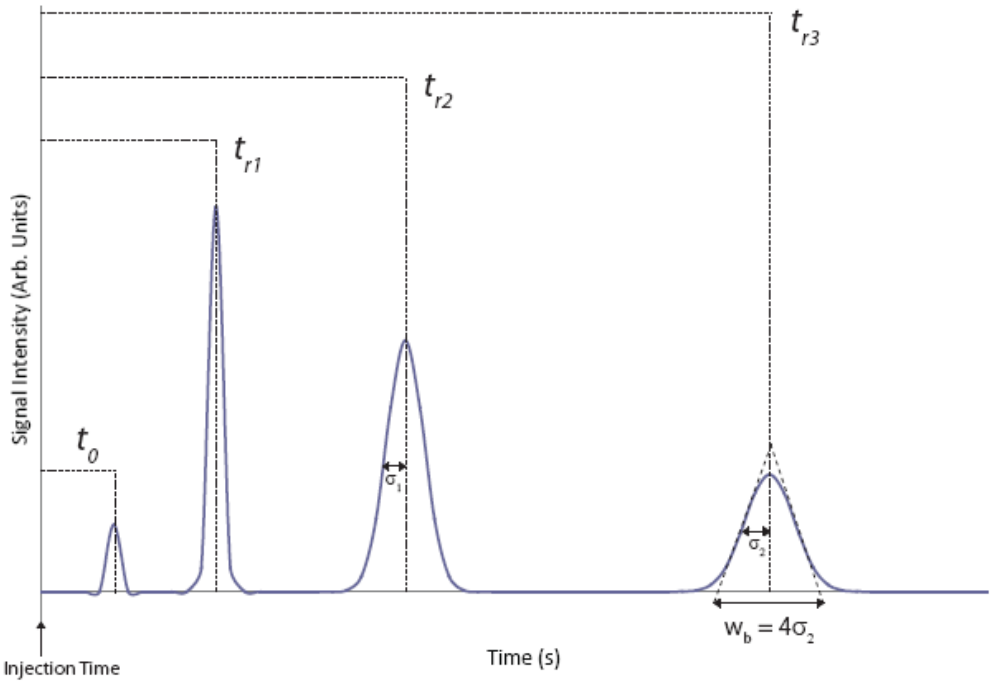

Figure 1.3 – Representative electropherogram illustrating important separation parameters. The first eluting peak corresponds to the neutral marker and t_0 reveals the value for EOF in the system.

The most important and commonly used parameter describing the quality of a separation is the separation efficiency or the number of theoretical plates (N). Efficiency is given by equation (1.15) where l is the effective capillary length.

$$N = \left(\frac{l}{\sigma}\right)^2 \tag{1.15}$$

The number of theoretical plates generated by a separation can also be related to a parameter referred to as the height equivalent of a theoretical plate (HETP or more commonly simply H) by equation (1.16).

$$H = \frac{l}{N} = \frac{\sigma^2}{l} \tag{1.16}$$

While equation (1.16) is often sufficient to describe H, a more in-depth representation that takes into account multiple sources of band broadening is given by the van Deemter equation as shown in equation (1.17).

$$H = A + \frac{B}{v} + Cv \tag{1.17}$$

The A term in equation (1.17) represents the contributions of eddy-diffusion to plate height. The second term, B/v, represents longitudinal diffusion's contributions. The final term, Cv, represents the contribution of mass transport to H.

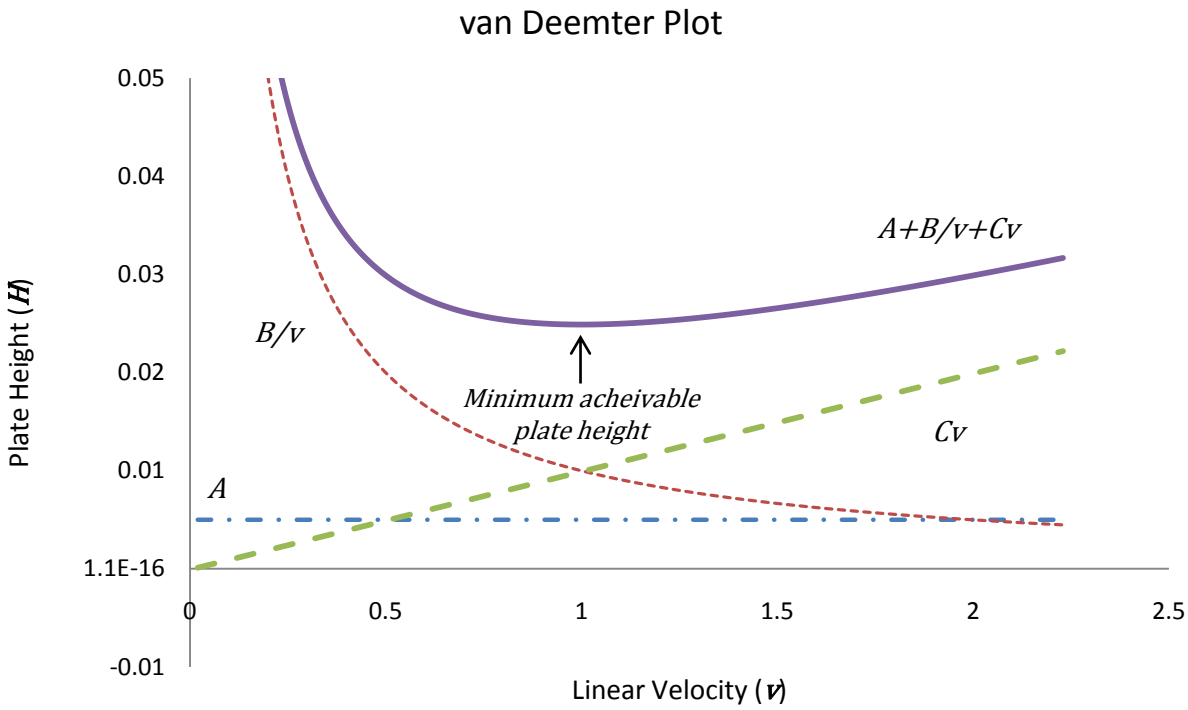

Figure 1.4 – A van Deemter plot depicting the effect of linear flow velocity on plate height (H). [A] is the constant contribution of eddy diffusion, [B/v] represents longitudinal diffusion, and [Cv] is the contribution due to mass transfer. The total contributions to plate height are shown by [$A + B/v + Cv$].

It becomes clear from Figure 1.4 that the impact of longitudinal diffusion on plate height decreases, while the effect of mass transport increases, with increasing linear flow velocity. It is possible as depicted by the total trace ($A + B/v + Cv$) to achieve an optimal linear velocity where H is minimized.[3]

1.1.3.1 Dispersion

From equation (1.15) it becomes obvious that the simplest way to maximize the efficiency of a separation is to minimize the peak variance. This is not elementary as the possible sources of variance are numerous and include molecular diffusion (σ^2_{diff}), length of injection band (σ^2_{inj}), length of detection window (σ^2_{det}), Joule heating (σ^2_{Joule}), geometry of the

channel $\left(\sigma_{geo}^2\right)$, mass transfer (σ_{MT}^2), adsorption (σ_{ads}^2), electrodispersion $\left(\sigma_{edisp}^2\right)$, and laminar flow $\left(\sigma_{flow}^2\right)$. As independent sources of dispersion, these contributors can be added to obtain the total dispersion in the system as illustrated by equation (1.18).[3]

$$\sigma_{total}^2 = \sigma_{diff}^2 + \sigma_{inj}^2 + \sigma_{det}^2 + \sigma_{Joule}^2 + \sigma_{geo}^2 + \sigma_{MT}^2 + \sigma_{ads}^2 + \sigma_{edsip}^2 + \sigma_{flow}^2 \qquad (1.18)$$

To minimize the variance associated with a separation it becomes necessary to minimize or eliminate as many terms as possible from equation (1.18). The dispersion associated with the injection plug is generally negligible in microfluidic regimes (which will be discussed later) since the gated injections traditionally used in our labs are very short. The dispersion due to injection is best described by an impulse function as indicated by equation (1.19).

$$\sigma_{inj}^2 = \frac{l_{inj}^2}{12} \qquad (1.19)$$

Dispersion due to injection only becomes an issue when performing very rapid separations.[3]

By using the appropriate objectives and spatial filters, in a laser induced fluorescence detection (LIF) setup, it becomes possible to ignore the dispersion contributions due to detection window length. The detection window length in an LIF setup is typically dictated by the diameter of the laser spot size or the spatial filter placed in front of the detector. Since the detection window length is constant and so small, this contribution to dispersion is not significant and can be omitted.[3]

If the electrical field strength applied across a capillary is too high, one can generate Joule heating which can lead to parabolic flow profiles. Joule heating is a result of the electrical energy applied to the capillary being converted to heat through the frictional drag of charged species migrating in solution. As long as the potential across the channel is kept low enough, significant Joule heating can be eliminated and radial temperature gradients leading to parabolic flow profiles can be avoided. Thus keeping the potential low enough as to prevent excessive Joule heating one can ignore the dispersion resulting from Joule heating.[3]

Dispersion due to geometric effects is the result of introducing turns into the separation channel. When travelling through a turn, particles on the inside have less ground to cover than particles travelling along the outside of the turn. This combined with the fact that the magnitude of the electrical field is higher on the inside of the turn compared to the outside of the turn results in analytes moving at a variety of velocities and thus longitudinal spreading of the analyte plug.

Elimination of geometric dispersion can be a achieved by using straight separation channels void of turns.[3]

Contributions of mass transport to dispersion only arise when the separation channels are either coated or packed with some type of stationary phase. There will be two contributions to mass transport dispersion; diffusion of analytes in the stationary phase and diffusion of analytes in the mobile phase. These relationships are shown in equations (1.20) and (1.21) where k is the capacity factor, l is the separation length, d_{st} is the thickness of the stationary phase, d_{mp} is the channel depth, D_{st} is the diffusion coefficient in the stationary phase and D_{mp} is the diffusion coefficient in the mobile phase.

$$\sigma_{st}^2 = \frac{k}{(1+k)^2} v_{eo} l \frac{2d_{st}^2}{3D_{st}^2} \tag{1.20}$$

$$\sigma_{mp}^2 = \frac{1+6k+11k^2}{96(1+k)^2} v_{eo} l \frac{d_{mp}^2}{D_{mp}} \tag{1.21}$$

Elimination of coatings or packing materials can permit the removal of mass transport contributions from the system's total dispersion.[3]

Adsorption can often be a problem in CE separations, but there are a variety of ways to minimize or prevent its effects. Solute wall interactions will most often result from either ionic or hydrophobic interactions of the analytes with the capillary surface. Positively charged analytes will be attracted towards a negatively charged surface, and large polymeric molecules such as proteins will often stick to the wall via hydrophobic interactions. The variance due to adsorption can be calculated by using equation (1.22) where k' is the capacity factor which is defined by equation (1.23) (t_r is the migration time of an adsorbed solute and t_0 is the migration time of an unadsorbed solute), D is the diffusion coefficient, r is the capillary radius, and K_d which is the first order dissociation constant.

$$\sigma_{ads}^2 = \frac{k' v_{eo} l}{(1+k')^2} \left(\frac{r^2 k'}{4D} + \frac{2}{K_d} \right) \tag{1.22}$$

$$k' = \frac{t_r - t_0}{t_0} \tag{1.23}$$

To combat these adsorption issues some common measures can be implemented. Increasing the concentration of the buffer will serve to effectively reduce the surface charge of the material in use. Optimization of the buffer pH can also reduce adsorption. Very low pH buffers will

protonate the silanol groups of a glass channel resulting in an uncharged channel wall, likewise operation at high pH will provide a negatively charged surface and often deprotonated and negatively charged analytes which will repel each other. Lastly, coating of the channel surface with polymers, surfactants, and covalent modification can be employed to prevent adsorption.[2]

Electrodispersion can be generated when differences in conductivity between the sample buffer and background electrolyte exist. Also, if the mobility of the sample ion and its buffer co-ion are dramatically different, triangular shaped peaks characteristic of electrodispersion can result. This type of variance can be largely eliminated by ensuring that the sample and background solutions are similar in composition.[3]

Variance resulting from fluid flow is generally a product of parabolic flow which can arise mainly from pressure differences and Joule heating. This dispersion can be described for rectangular channels using equation (1.24) where $\Delta P/L$ is the pressure drop along the length of the channel, d is the depth of the channel, w is the width of the channel, D is the diffusion coefficient, and η is the solution viscosity.

$$\sigma_{flow}^2 = 4\frac{(\Delta P)^2 d^6}{105 D\eta^2 L^2}\left[\frac{1}{12} - \frac{16d}{\pi^5 w} tanh\left(\frac{\pi w}{2d}\right)\right]^2 t \qquad (1.24)$$

By keeping hydrodynamic flow to a minimum by maintaining equal fluid levels in all solution reservoirs and by keeping the applied electrical potential low enough to avoid significant amounts of Joule heating, parabolic flow profiles can be all but eliminated.[3]

Since it is impossible to eliminate diffusion, optimized separations are said to be "diffusion limited" as all other contributions to variance are insignificant by comparison. While eliminating sources of band broadening is very important, one must also consider that the priority of the separation is the resolution of the individual component peaks.

1.1.3.2 Resolution

The complete resolution of adjacent individual component peaks is the primary goal of any analytical separation. The calculation that determines resolution (Equation (1.25)) uses the differences of the migration times of two adjacent peaks and their respective peak widths to assign a numerical value describing how well two peaks are separated. Resolution (R) values of 1.5 or greater are indicative of baseline resolution.[1] In the equation (1.25) below, t_1 and t_2 represent retention times of two adjacent solutes (t_2 being the solute that elutes first), w_1 and w_2

represent the baseline peak widths of two adjacent solutes (again w_2 being the solute that elutes first), and σ is the temporal peak standard deviation.

$$R = \frac{2(t_2 - t_1)}{(w_1 + w_2)} = \frac{t_2 - t_1}{4\sigma} \tag{1.25}$$

Equation (1.25) assumes that two adjacent peaks are so close together that their baseline widths are approximately equal, thus permitting the estimation that the sum of w_1 and w_2 is equal to 4σ. In Figure 1.5 the necessary parameters for the calculation of peak resolution according to equation (1.25) are shown.

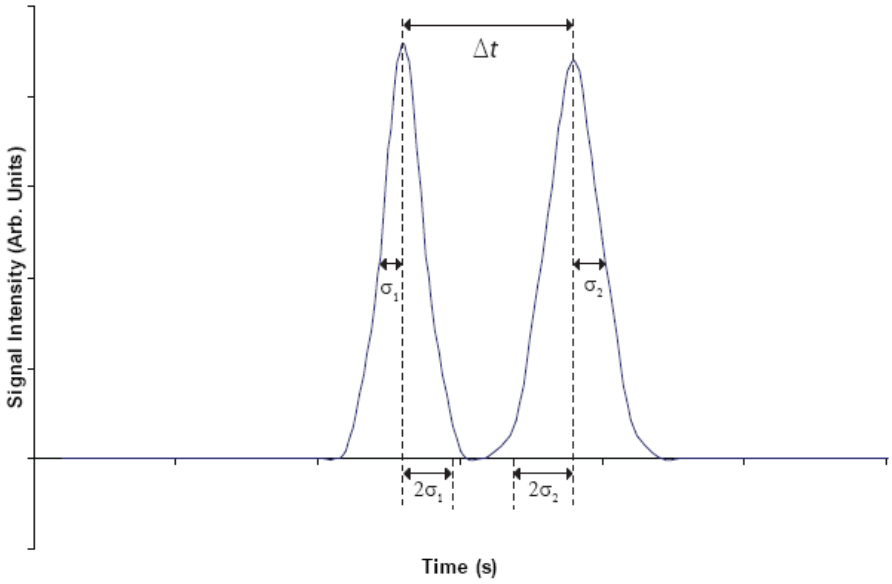

Figure 1.5 – Illustration depicting the relevant parameters for the calculation of resolution between two peaks.

Alternatively, one can predict resolution using the separation efficiency and the electrophoretic mobilities of the analytes via equation (1.26) where $\bar{\mu}$ is the average electrophoretic mobility of the two adjacent species.[2-4]

$$R = \frac{\sqrt{N}}{4}\left(\frac{\mu_2 - \mu_1}{\bar{\mu}}\right) \tag{1.26}$$

1.1.3.3 Peak Capacity

Given a desired resolution, only a limited number of peaks can be separated in a given distance, and this number of peaks is defined as the peak capacity, n_c, and is displayed in equation (1.27) where w is the average peak width, and L is the separation distance. Since the

assumption that all peaks are approximately the same width is made, w can also be written as 4σ, but in addition, the desired resolution must be defined.

$$n_c = \frac{L}{Rw} = \frac{L}{R4\sigma} \tag{1.27}$$

1.1.3.4 Micellar Electrokinetic Chromatography

In micellar electrokinetic chromatography (MEKC), a pseudo-stationary phase is employed to facilitate the separation of neutral compounds. Surfactants are added to the run buffer above their critical micelle concentration, or CMC, (for sodium dodecyl sulfate the critical micelle concentration is about 8-9 mM) resulting in the formation of micelles which are aggregates of the individually charged surfactant molecules (Figure 1.6).[2] The CMC for a surfactant will change with buffer type and pH. These essentially spherical aggregates traditionally have their charged heads on the outside interacting with the aqueous buffer while the hydrophobic tales are oriented inward away from the buffer. The separation of the neutral analytes is carried out resulting from interactions of the analyte with the micelles.

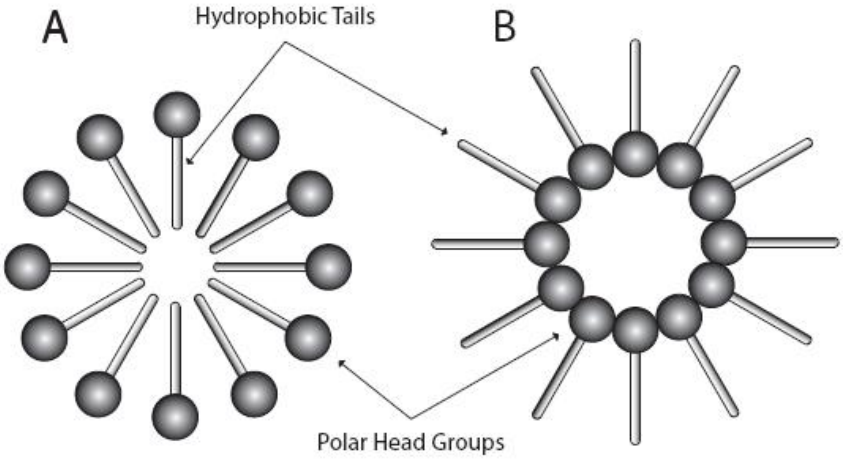

Figure 1.6 – Cross-section of a micelle in A) an aqueous environment and B) an organic environment. Typically the polar head groups will be charged.

More specifically, it is the partitioning into and out of the micelle that effectively achieves the separation of the neutral molecules.[2] The general partitioning coefficient for chromatography, K, is used to describe the ratio of the amount of an analyte found interacting with the stationary phase versus the amount of analyte that if flowing with the mobile phase.

$$K = \frac{A_{S_2}}{A_{S_1}} \approx \frac{[S]_2}{[S]_1} \tag{1.28}$$

A_{s_1} and A_{s_2}represent the activity of the solute in phase 1 and 2 respectively. When no information on activity is available or the solute is very dilute, one can approximate the partition coefficient using the concentration of the analyte in phases 1 and 2, $[S]_1$ and $[S]_2$ respectively.[2] The capacity factor, k, is given by equation (1.29) and is a ratio relating the number of moles of analyte in the micelle to the number of moles in the mobile phase, where V_{mic} and V_{aq} represent the volumes of the micellar and aqueous phases respectively.[2,8]

$$k = K\left(\frac{V_{mic}}{V_{aq}}\right) \tag{1.29}$$

The capacity factor can also be calculated directly from the migration times of the solute (t_r), EOF (t_0), and micelles (t_{mic}) as illustrated in equation (1.30). This relationship can allow for the direct calculation of the partitioning coefficient by combining equations (1.29) and (1.30) and solving for K, as illustrated in equation (1.31).

$$k = \frac{(t_r - t_0)}{t_0\left(1 - {}^{t_r}/_{t_{mic}}\right)} \tag{1.30}$$

$$K = \frac{V_{aq}(t_r - t_0)}{V_{mic}t_0\left(1 - {}^{t_r}/_{t_{mic}}\right)} \tag{1.31}$$

The stationary phases in chromatography will show different degrees of affinity for different solutes, thus the parameter α, known as the selectivity coefficient, is used. The selectivity coefficient is a ratio of the capacity factors of two components, with the solute possessing greater retention serving as the numerator and the lesser retained component as the denominator (thus α is always greater than 1) as shown in equation (1.32).[9,10]

$$\alpha = \frac{K_2}{K_1} = \frac{k_2}{k_1} = \frac{t_{r_2} - t_0}{t_{r_1} - t_0} \tag{1.32}$$

Since MEKC is more so considered a chromatographic technique as opposed to a typical free solution CE technique, the method for predicting resolution follows the relationship used for traditional chromatography using a mobile and stationary phase as depicted in equation (1.33).

$$R = \frac{\sqrt{N}}{4}\left(\frac{\alpha - 1}{\alpha}\right)\left(\frac{k_2}{1 - k_2}\right) \tag{1.33}$$

The above relationship does require one final adjustment to account for the movement of the stationary phase, which is non-existent in standard chromatographic methods. In MEKC neutral compounds must elute within a finite window. The boundaries of this elution window are dictated by the EOF in the system and the migration time of the micelles in the background electrolyte. Most commonly, micelles are moving in an opposite direction relative to the EOF, but since the magnitude of the EOF is greater than the electrophoretic velocity of the micelles, their net movement is in the direction of the EOF. Thus in MEKC the first eluted peak represents the EOF or neutral compounds that are completely excluded from the micelles and are labeled with the migration time t_0. Compounds that are contained entirely within the core of the micelles will elute last and are labeled with the migration time t_{mic}. Compounds that partition into and out of the micelles over the length of the separation will elute at some time t_r, where $t_0 < t_r < t_{mic}$ as shown in Figure 1.7.

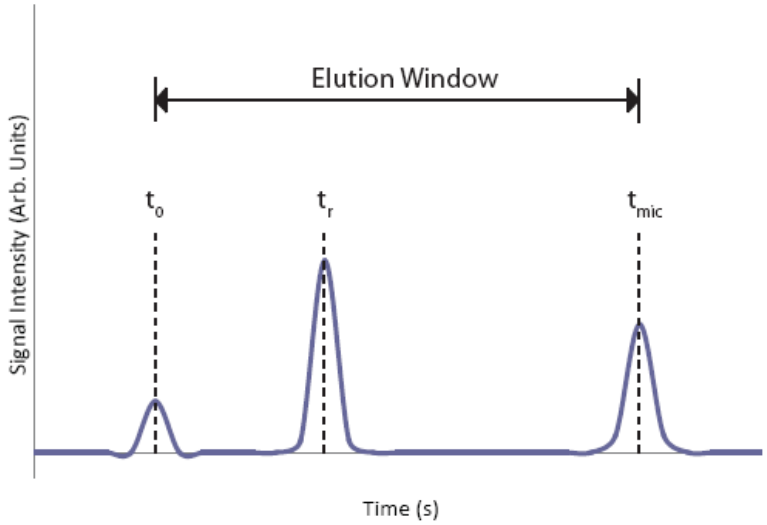

Figure 1.7 – Diagram depicting the elution window in an MEKC separation.

Due to the mobile stationary phase used in MEKC, the resolution follows the formula outlined in equation (1.34).

$$R = \left(\frac{\sqrt{N}}{4}\right)\left(\frac{\alpha - 1}{\alpha}\right)\left(\frac{k_2}{k_2 + 1}\right)\left(\frac{1 - \left[{t_0}/{t_{mic}}\right]}{1 - k_1\left[{t_0}/{t_{mic}}\right]}\right) \tag{1.34}$$

It is clear from the above relationship that independent optimization of the efficiency, selectivity, and/or capacity factor of a separation will result in improved resolution. For more complex sample mixtures with numerous components, the limited elution window in MEKC could result in insufficient peak capacity. For an MEKC separation, the peak capacity is given by equation (1.35) where it is clear that the main impact on the peak capacity in MEKC stems from the ratio of the elution times of the micelles and the excluded component.

$$n_c = 1 + \sqrt{N}\left(\frac{\ln t_{mic}}{t_0}\right) \tag{1.35}$$

Partial suppression of the EOF can be achieved with the use of organic modifiers. Organic additives will also change partitioning of analytes between the mobile and stationary phases by increasing the hydrophobicity of the mobile phase. This change in selectivity could potentially increase the buffer's ability to resolve adjacent components.[2-4,6,9]

1.1.4 Pressure Driven Flow

1.1.4.1 Flow In Open Tubes

Most of the discussion up until now has been geared towards flow through open tubes, however the tortuous path of fluid flow through packed beds or columns can be quite different. While flow through packed beds can be achieved electrokinetically (capillary electrochromatography – CEC) it is most commonly driven with applied pressure. As previously mentioned, pressure driven flow has a characteristic parabolic profile (Figure 1.2) and the velocity of the fluid in the tube, v, exhibits a dependence on its radial position (r_x) within the tube of radius r as shown be equation (1.36). The position dependent velocity of a fluid stream is denoted by v_x. Equation (1.37) gives the average velocity of fluid in the tube where P_i and P_0 represent the pressures at the inlet and outlet respectively, η is the solution viscosity, and L is the tube length.

$$v_x = 2v\left[1 - \left(\frac{r_x}{r}\right)^2\right] \tag{1.36}$$

$$v = \frac{(P_i - P_o)r^2}{8\eta L} \tag{1.37}$$

The flow profile is mathematically explained by equation (1.36) in that it takes the form of a parabola.[10] By taking equation (1.37) and multiplying by the cross-sectional area of the tube one can calculate the average volumetric flow rate, F, as depicted by equation (1.38) which is known as the Hagen-Poiseuille equation where d_c is the capillary diameter.[10]

$$F = \frac{(P_i - P_o)r^4\pi}{8\eta L} = \frac{(P_i - P_o)d_c^4\pi}{128\eta L} \tag{1.38}$$

1.1.4.2 Flow In Packed Beds

The use of packed columns is very common in the field of separations. The packing material of these columns adopts a random arrangement within the tube resulting in a complex network of fluid streams occupying the interstitial spaces between individual particles. The better a column is packed the less variation in pore diameter there will be and this results in reduced variation in path dependent fluid velocity. Darcy's Law is the relationship that describes the dependence of fluid velocity on the applied pressure gradient and is given by equation (1.39).

$$q = \frac{K_0}{\eta}\frac{P_0 - P_i}{L} \tag{1.39}$$

In the above relationship q is known as the flux density and is the fluid velocity in the column in the absence of packing. The term K_0 is the specific permeability coefficient. We can see from equations (1.37) and (1.39) that in the absence of packing K_0 is equal to $r^2/8$. Since equation (1.39) represents flow in the absence of packing it must now be related to flow through the pores of a packed column. When a column is packed only a fraction of the void volume is available to fluid as the rest of the column volume is occupied by the packing material. This fractional void volume is represented by ε, and by taking the volume occupied by packing into account, equation (1.39) becomes equation (1.40) where $\langle v \rangle$ is the average pore flow velocity.[1,10]

$$\langle v \rangle = \frac{q}{\varepsilon} = \frac{K_0 \Delta P}{\eta \varepsilon L} \tag{1.40}$$

The major weakness of Darcy's Law is its failure to describe the microscopic flow profile through the pores. Furthermore, K_0 depends on the type of packing material used and varies

widely with no clues as to the origin of the dependence. However by using what is known as the "capillaric model", some of these issues can be addressed.[1]

Due to the complicated nature of these numerous and random flow paths it is impossible to determine the exact flow profile within the packed column. It is therefore easier to treat flow through a packed bed as if fluid was flowing through a bundle of small individual tubes. Using this model permits us to find the volumetric fluid flux through each of these individual capillary elements using the Hagen-Poisseuille law outlined in equation (1.38). When implementing this model, the number of individual tube elements in a unit area will be inversely proportional to the square of the diameter of the tubes. This relationship is logical as the area of the tubes increase, the less of them that will fit into a given space and the number of tubes is proportional to $1/d_c^2$. To determine the total fluid flux as denoted by q which earlier in equation (1.39) is shown to be proportional to d_c^4, one simply multiplies the fluid flux through an individual capillary element by the number of elements in the bundle (which is proportional to $1/d_c^2$). Thus total flux is thus proportional to d_c^2. It is also useful to consider that fluid flux (and likewise velocity) are also proportional to the size of the particles used to pack the column, more specifically, their mean diameter, d_p. By rearranging equation (1.40) the particle diameter can be incorporated into the relationship that produces the average fluid velocity as depicted in equation (1.41).[1]

$$\langle v \rangle = \frac{1}{\Phi}\frac{d_p^2}{\eta}\frac{\Delta P}{L} \tag{1.41}$$

In the above equation, Φ is the flow resistance parameter and must be determined experimentally, however it is typically found to be between 500 – 1000. By simple comparison of equations (1.40) and (1.41) the specific permeability can be defined as shown below.[1]

$$K_0 = \frac{\varepsilon d_p^2}{\Phi} \tag{1.42}$$

One final consideration remains, the degree of packing. If two columns are prepared using particles of the same diameter and one is loosely packed while the other is tightly packed, a noticeable difference in flow characteristics will be observed. A loosely packed bed will result in a wider range of pore sizes which will lead to highly variable flow rated within the packed bed. This broad range of fluid velocities causes band broadening as previously described and ultimately results in poor column performance. With the compact packing materials commonly

used, the value for porosity (ε) is generally taken to be 0.4, its minimum, for randomly packed columns.[1]

Fluid passing through packed columns is often met with high amounts of viscous resistance resulting in high back pressures. Thus, it is important to factor in how the particle size chosen for a given application will affect the pressure drops across the system. The pressure drop can be found by simply rearranging equation (1.41) yielding equation (1.43) below.

$$\Delta P = \frac{\langle v \rangle \eta \Phi L}{d_p^2} \tag{1.43}$$

It becomes quickly apparent that as the diameter of the particles used to pack the column decrease, the pressure drop across the column increases rapidly. Thus, compromises between particle size, flow rate, and column length must be made for any given application.[1]

1.1.5 Flow in a Thin Layer and Paper

1.1.5.1 Thin Layer Flow

The flow that has been described up to this point is driven by some external force such as an applied voltage for CE or by some type of external pump that forces fluid through a packed bed. Thin layer chromatography is a common technique employed in many synthetic chemistry labs and promotes separations without using any type of external force to facilitate fluid flow. Fluid flow in a thin layer regime is achieved via capillarity. Capillarity is the wicking of fluids along a substrate through its empty pores. Capillary pressure, Δp as defined by equation (1.44), is responsible for promoting the movement of fluid through either paper substrates or thin layers of porous materials. The terms γ and r represent the surface tension and radius of curvature of the fluid front advancing to fill the vacant pore.

$$\Delta p = \frac{2\gamma}{r} \tag{1.44}$$

Much like packed beds, thin layer porous materials such as paper substrates involve randomly arranged materials and thus complicated arrays of flow paths. Again it is much simpler to treat flow in these types of regimes as flow through a bundle of individual capillary elements similar to the treatment for flow through a packed bed. For this model bundle of capillaries, r_c is the radius of the individual capillary tube element. If the contact angle of the fluid with the capillary wall is zero, then r_c can be simplified to simply r. Where a contact angle (θ) does exist,

however, r must be denoted by $r_c/\cos\theta$. In the presence of a contact angle the capillary pressure can be defined by equation (1.45).[1]

$$\Delta p = \frac{2\gamma \cos\theta}{r_c} \tag{1.45}$$

If we refer to the average velocity for fluid in a capillary as defined by equation (1.37), equation (1.46) can be derived by replacing $(P_i - P_0)$ with equation (1.45) and replacing L with the distance traveled by the fluid front denoted by X_f.

$$\langle v \rangle = \frac{r_c \gamma \cos\theta}{4 X_f \eta} \tag{1.46}$$

From the above relationship, it is clear that as fluid travels further into the thin layer or paper substrate the average velocity will decrease. Since velocity is the distance traveled per unit time, $\langle v \rangle$ can be replaced with dX_f/dt yielding the following equation.

$$X_f \frac{dX_f}{dt} = \frac{r_c \gamma \cos\theta}{4\eta} \tag{1.47}$$

By operating under the assumption that when the time is zero the distance traveled by the fluid front is also zero equation (1.47) can be integrated to yield a solution to the distance traveled by the fluid front in a given time given by equation (1.48).[1,4]

$$X_f = \sqrt{t\left(\frac{r_c \gamma \cos\theta}{2\eta}\right)} \tag{1.48}$$

1.1.6 Microfluidics

The development of microfluidic devices has ushered in the potential to perform chemical analyses on a size scale never before seen. Fabricated from a variety of materials including glass, poly(dimethylsiloxane) (PDMS), poly(methylmethacrylate) (PMMA), and polycarbonate as well as methods such as soft lithography, wet chemical etching, laser ablation, and injection molding, microfluidic devices present the user with a very flexible template to perform multiple experimental steps on a single substrate while at the same time consuming minimal amounts of reagents, generating minimal amounts of waste, requiring minimal amounts of sample, and demanding a minimal amount of time.[11,12] From the perspective of chemical separations, microfluidic devices offer a number of additional advantages over traditional electrophoretic regimes that employ fused silica capillary. By strategically arranging a few

simple fluidic elements in series, very precise control over fluid flow can be obtained. For example, the use of a long straight segment of channel is commonly used to perform chemical separations. The T-junction can be used as an online reactor where two different reagents meet in the center of the T where they mix at the fluidic interface and then travel down the main channel. Likewise the T-junction can also be used to dilute a sample. Finally, a cross junction can be used for valving.

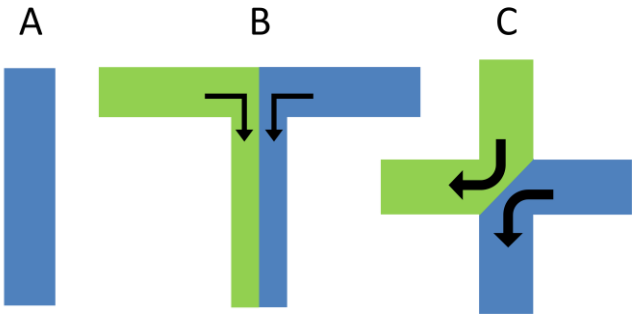

Figure 1.8 Fluidic elements composing microfluidic devices. A) straight channel segment B) T-junction C) cross junction

These simple fluidic elements are depicted in Figure 1.8. By arranging these different functional elements in series, one can construct microfluidic devices that are tailored to perform a customized analysis. The ability to manipulate fluids on a microfluidic device obviates the need for manual switching of fluid reservoirs to perform sample injections as seen with standard fused silica capillary systems, thus illustrating the potential for fully automated systems. The variety of available detection methods makes these devices very versatile and applicable to the analysis of a number of different types of compounds. Since these devices themselves have such a miniscule footprint, with the miniaturization of existing detection methods a truly portable analytical system can be realized. The high surface area to volume ratio of the channels in these devices also results in improved heat dissipation permitting the application of high electrical field strengths with minimal joule heating. The use of high field strengths allows these devices to perform high speed, high efficiency separations in a fraction of the time associated with standard CE or HPLC experiments.

The most common type of analysis performed on a microfluidic device is the analytical separation. Using electrokinetically driven fluid flow, and with the appropriate manipulation of the applied voltages, very small and reproducible injections of sample mixtures may be made

onto the separation channel. Illustrations of two different types of electrokinetic injections can be seen in Figure 1.9.

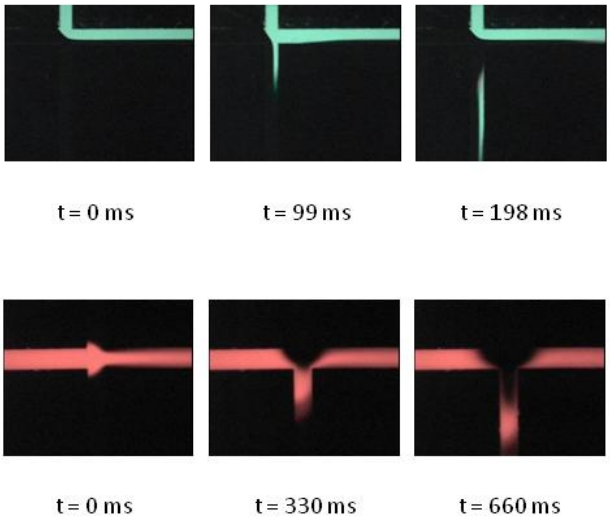

Figure 1.9 – Top: Images illustrating an electrokinetic gated injection. Bottom: Images illustrating an electrokinetic pinched injection. Listed times indicate time following the switching of applied potentials to perform injection. While potential switching for a gated injection is transient, the potential used for a pinched injection is switched and held throughout the duration of the separation.

In a situation where multiple reservoirs are the recipients of different applied voltages, solving for the electrical field strength applied to the separation column is a bit more complicated than with simple fused silica capillary systems where the field strength is simply determined by dividing the applied voltage by the length of the capillary. By treating each individual channel segment as a resistor, and using Ohm's Law (Equation (1.49)) in combination with Kirchhoff's Current Law (Equation (1.50)), the isolated electrical field strength across the separation channel may be calculated by first determining the voltage at the channel intersection.

$$V = IR \tag{1.49}$$

$$\sum_{k=1}^{n} I_k = 0 \tag{1.50}$$

Ohm's Law states that the voltage, V, is equal to the product of the current (I) and the resistance (R). Kirchhoff's current law conveys that the sum of all currents into and out of a node equals zero, with currents coming into a node or intersection carrying a positive sign, and currents

leaving the intersection being negative. With knowledge of the applied voltage and measurement of the current across the same channel, the resistances can be calculated. Once the resistances have been determined, the voltage at the channel intersection can be solved and the field strength for the separation channel can be verified.

1.1.6.1 Laminar Flow

The ability to manipulate fluids so precisely on microfluidic devices is a result of laminar flow. Laminar flow is conceptually defined as a situation where fluid movement is very ordered and regular. Individual fluid streams layer themselves together with each fluid stream having its own velocity.[13] During conditions of laminar flow, if one observes two individual fluid elements, one trailing the other, one will notice that the trailing fluid element follows a path that is identical to that established by the lead element. In situations of turbulent flow this is not the case, and sequential fluid elements will follow random, non-related paths. A term known as the Reynolds number, R_e, is a dimensionless quantity that relates viscous forces to inertial forces in the form of a simple ratio. When the R_e is sufficiently low the fluid environment is dominated by viscous forces and laminar flow is observed. At higher values for R_e, however, inertial forces can dominate resulting in turbulent flow. The Reynold's number can be calculated according to Equation (1.51), where ρ is the fluid density, v is the fluid velocity, d_c is the tube diameter, and η is the fluid viscosity.

$$R_e = \frac{\rho v d_c}{\eta} \tag{1.51}$$

For flow through an open tube Reynold's numbers below 2100 are indicative of laminar flow. As velocity through the tube increases, so do the viscous and inertial forces, but since inertial forces increase with square of velocity while viscous forces increase linearly with respect to velocity, eventually inertial forces will begin to dominate the system and turbulent flow will occur primarily in the form of eddies.[10]

For fluid flow through packed beds, the Reynold's number is calculated a little bit differently as particle diameter,d_p, is substituted for tube diameter in equation (1.51).

$$R_e = \frac{\rho v d_p}{\eta} \tag{1.52}$$

In open tube flow regimes the transition from laminar to turbulent flow is fairly well defined. This is not the case for packed tubes. Rather than a specific value for the Reynold's number that

defines the transition from laminar to turbulent flow, it is assumed that turbulent flow progressively ensues as R_e increases from 1 to 100.[10] To optimize the flow profile of fluid in a packed bed careful and uniform packing of the column with spherical particles of monodisperse size is required.

1.1.7 Conclusions

The realm of microfluidics offers the field of analytical separations a great deal of potential and a variety of solutions to many analytical problems. The main advantage of this type of analysis involves the ability to use such small amounts of sample. These volume requirements make these devices well suited for use in the analysis of dilute samples such as biological compounds. The potential to miniaturize the footprint of the analytical separation system is also quite appealing as in future these devices may lend to the construction of instrumentation tailored for application based on-site analysis. With an understanding of the fundamental properties of these devices users can begin to tailor their experiments to specific analytes developing techniques that may be applicable in other areas. The future of microfluidics at this time is limited only the imagination of the experimenter and the complexity of fabrication. Some drawbacks to microfluidic systems do exist, mainly the difficulty in generating reproducible EOF, however we hope that time reveals soltutions to this and other difficulties and sees microfluidics become a part of the mainstream branch of separation science.

Chapter 2 - Synthesis and Characterization of a Poly(dimethylsiloxane)-Poly(ethylene oxide) Block Copolymer for Fabrication of Amphiphilic Surfaces on Microfluidic Devices

The majority of this chapter is published as: Klasner, Scott A.; Metto, Eve C.; Roman, Gregory T.; Culbertson, Christopher T. *Langmuir*, **2009**, 25 (17), 10390 – 10396.

2.1 Introduction

Poly(dimethylsiloxane) has become a widely popular alternative to glass for the fabrication of microfluidic devices since its introduction by Whitesides et al. in 1998.[14] Soft photolithography using PDMS yields mechanically robust devices that are disposable, economical, and often sufficient for the analysis of simple analytes. Although PDMS has attractive features, it also suffers from a number of potential drawbacks. The surface of PDMS is extremely hydrophobic and this can lead to difficulties when trying to investigate hydrophobic analytes such as biomolecules that often adsorb to channel surfaces. While the use of aqueous buffers on these devices is prevalent, filling microchannels cast in PDMS can often prove difficult. Another characteristic of PDMS devices, compared to their glass counterparts, is that devices cast in PDMS exhibit lower electroosmotic flow (EOF) which can lengthen analysis times, leading to broader peaks, and thus reduce the overall separation efficiency.

A variety of coating techniques have been developed to manipulate the surface properties of PDMS microdevices to make them more hydrophilic and resistant to adsorption. These coating techniques fall into two main classes: dynamic and covalent. Dynamic coatings typically involve the addition of molecules to the background electrolyte which continually coat the channel walls as experiments are carried out. Some of the most frequently reported dynamic coatings include sodium dodecyl sulfate (SDS),[15-17] polyvinyl alcohol,[18] Brij 35,[19,20] methyl cellulose,[21] polyelectrolyte multilayers (PEMs),[22-24] and acrylamides.[25] Covalent modification requires the physical attachment of a desired functionality to the surfaces of the PDMS channel architectures. Some of the most popular covalent functionalities are acrylates,[26-31] acrylamides,[26,28,32] metal alkoxides,[33-35] and poly(ethylene glycols) or poly(ethylene

oxides).[26,28,29,36-39] While many of these modification techniques do achieve the desired effect, their implementation often requires many tedious and time consuming steps. It would thus be advantageous to develop a bulk material that can be readily molded using soft lithography techniques, is optically clear, has high thermal conductivity, possesses durability similar to that of PDMS, but is hydrophilic, easy to wet and provides high separation efficiencies. PDMS-PEG, or PDMS-PEO materials are known[40-43] and have been reported for use as additives in epoxy thermoset resins,[44] additives for reinforcement of chitosan materials,[45,46] and biomaterials resisting platelet adhesion.[47]

It is to this end that we report the preparation of a poly(dimethylsiloxane)-poly(ethylene oxide) block copolymer for the fabrication of novel amphiphilic microfluidic devices in this chapter. This copolymer exhibits much more hydrophilic properties compared to PDMS illustrated by reduced water contact angles as well as a similar Young's Modulus and thus similar elastomeric properties to native PDMS.

2.2 Thermally Cured PDMS – PEO Prepared by Hydrosilation

2.2.1 Experimental Section

2.2.1.1 Materials and Methods

Poly(ethylene glycol) divinyl ether (PEG-DE) was purchased from Aldrich [410195] (Milwaukee, WI). Hydride terminated poly(dimethylsiloxane), methylhydrosiloxane-dimethylsiloxane copolymer, and platinum-divinyltetramethyldisiloxane complex were obtained from Gelest (Morrisville, PA) and stored in a dessicator. Sodium borate, sodium hydroxide, hydrochloric acid, acetone, xylenes, and toluene were purchased from Fisher Scientific. Ethanol (190 proof) was supplied by AAPER Alcohol (Shelbyville, KY). Amino acids were purchased from ICN Biomedicals (Aurora, OH) and were labeled with fluorescein-5-isothiocyanate from Molecular Probes (Eugene, OR) according to the manufacturer's protocol as previously reported.[48] Poly(dimethylsiloxane) was obtained from Dow Corning (Midland, MI). All buffer solutions were prepared with distilled, deionized water (ddH_2O) from a Barnstead Nanopure System (Dubuque, IA) and filtered through 0.45 μm syringe filters supplied by the Millipore Corporation (Bedford, MA). All chemicals were used as received.

2.2.1.2 Mold Fabrication

1 × 3" (2.54 × 7.62 cm) glass slides purchased from Corning (Corning, NY) were rinsed and swabbed first with acetone and then with ethanol. Slides were next blown dry with a stream of nitrogen and placed in a 100 °C oven for 15 min for additional drying. After the slides were removed from the oven, they were allowed to cool to room temperature on a clean bench (Labconco: Kansas City, MO). Next, one of the cleaned slides was placed onto a spin-coater (Laurell Technologies: North Wales, PA) and SU-8 2005, a negative photoresist from Microchem (Newton, MA), was spun onto the slide at 1000 rpm for 30 s yielding a layer of photoresist 10 µm thick. The coated slide was soft-baked first on a 65 °C hotplate for 5 min, and then on a 110 °C hotplate for 8 min. Finally the slide was allowed to cool to room temperature for 7 min. Next the slide was placed in a UV flood exposure system (Oriel: Stratford, CT) and exposed to collimated UV light at an intensity of 45 mW/cm^2 for 6.0 s. Following exposure, the slide was hard-baked at 65 °C for 1 min followed by 110 °C for 5 min before being allowed to cool for 3 min. Next the slide was developed for 1 min in propylene glycol monomethyl ether acetate (Aldrich: Milwaukee, WI). After 1 min, the slide was immediately removed from the developing solution and gently rinsed with additional developer followed by an additional rinse with isopropanol. This produced a glass slide with complete SU-8 surface coverage. This same SU-8 coated slide was now used to cast the channel features. SU-8 2010 (a more viscous formulation) was spun onto the coated slide at 500 rpm for 10 s, followed by 1500 rpm for 30 s yielding a layer of photoresist 15 µm thick. The slide was again soft-baked at 65 °C for 5 min, then at 110 °C for 8 min before being allowed to cool to room temp for 7 min. A photomask was placed on top of the coated slide and quartz plate was placed on top of the photomask to ensure that it was pressed flat against the slide. The photomask was designed using AutoCAD LT (Autodesk, San Rafael, CA) and transferred via high-resolution printing (8000 dpi) to a transparency forming a mask (Photoplot Store: Colorado Springs, CO). Exposure was again performed for 6 s after which the slide was once again hard baked at 65 °C for 1 min and 110°C for 5 min before cooling for 3 min. A 1 min development in propylene glycol monomethyl ether acetate was repeated and the slide was immediately removed from the developing solution and gently rinsed with additional developer followed by isopropanol. This procedure resulted in SU-8 channel features 15 µm tall anchored to a layer of SU-8 which was covering the surface of the glass slide. Covering the surface of the slide with the SU-8 layer aided in the subsequent

removal of the crosslinked elastomer from the mold. The resulting positive channel mold was then gently blown dry with a stream of nitrogen and then placed in an 80 °C oven for 15 min.

2.2.1.3 Preparation of the PDMS-PEO Prepolymer

The protocol for the preparation of the PDMS-PEO prepolymer was adapted from that of Jukarainen et al.[40] To a three neck round bottom flask was added a portion of poly(ethylene glycol) divinyl ether. Based on the mass of PEG-DE added, the number of reactive vinyl equivalents was calculated and divided by 1.05 (if a 5% vinyl excess prepolymer was desired) or 1.10 (for a 10% vinyl excess prepolymer) the resulting value indicated the required number of reactive hydride equivalents on the hydride terminated PDMS. From the number of hydride equivalents required, the mass of hydride terminated PDMS was determined and added. Next the sum of the masses of the PEG-DE and hydride terminated PDMS was taken and multiplied by 0.3. The resulting value indicated the mass of toluene that was to be added to the reaction mixture to serve as the solvent.

The catalyst was prepared by taking 0.1 g of platinum-divinyltetramethyldisiloxane complex and adding it to 0.9 g of xylenes, resulting in a solution that is approximately 3250 ppm Pt. Based on the total mass of the reaction mixture, the appropriate amount of this Pt catalyst solution was added so that the final concentration of platinum in the reaction mixture was 30 ppm (assuming a density of 1 g/cm^3). The three neck flask was placed on a heating mantle and refluxed at 60 °C with gentle stirring and dry air bubbling into the mixture to prevent deactivation of the catalyst. Reaction progress was monitored via IR (Nicolet Protégé 460: Madison, WI). The disappearance of the Si-H stretch at 2125 cm^{-1} indicated complete consumption of reactive hydride groups and thus reaction completion. Total consumption of hydride groups was achieved in less than 1 h. The resulting solution was an oil with a slightly gold hue that was placed on a high vacuum line with 60 °C heat for 24 h to remove any solvent.

2.2.1.4 Crosslinking of the PDMS-PEO Prepolymer

During the prepolymer synthesis, an excess of vinyl is used resulting in a block copolymer that is vinyl-terminated. Based on the respective number of vinyl and hydride equivalents used in the prepolymer synthesis, the number of reactive vinyl groups per gram of prepolymer was determined. To cast both a molded 1" × 3" copolymer slab as well as an unmolded 1" × 3" cover plate, about 4.5 g of the prepolymer was required. The mass of

prepolymer added to a scintillation vial was recorded and used to calculate the number of reactive vinyl groups present in that aliquot. The desired equivalent excess of crosslinker to be added was chosen (either 5 or 10) and was multiplied by the number of reactive vinyl equivalents to determine the required number of hydride crosslinker equivalents. From this value, the mass of the methylhydrosiloxane-dimethylsiloxane copolymer required was determined and added to the scintillation vial containing the prepolymer. The mixture of prepolymer and crosslinker was vortexed vigorously. From the total mass of the prepolymer and crosslinker in the scintillation vial, 3250 ppm Pt catalyst solution was added to yield a mixture 30 ppm in Pt. The mixture was immediately vortexed vigorously and placed in a vacuum dessicator for about 5 min to remove bubbles. A channel architecture mold and a clean blank glass slide were placed in a 60 °C oven and the degassed polymer mixture was slowly poured over the molded and blank slides and was allowed to cure at 60 °C for 2 h. After curing, the slides were removed from the oven and the cured PDMS-PEO was carefully removed from the molded and blank slides. The two cured pieces of PDMS-PEO polymer were then brought into conformal contact sealing the channel architecture. Reservoirs could then be punched in the blank piece of the PDMS-PEO at the channel termini using a biopsy punch, taking care not to punch through both pieces of the material.

2.2.1.5 UV-Vis Measurements

Absorbance spectra of the polymers were recorded using a Hewlett-Packard 8453 diode array spectrometer. Uncured polymers were poured into disposable UV transparent plastic cuvettes (Plastibrand: Wertheim, Germany) and allowed to cure in a 60°C oven for two hours before measurement. The path length of the cuvettes was 12.5 mm.

2.2.1.6 Contact Angle Measurements

An in-house constructed stage which held a mirror at a 45° angle was used to image 5 µL droplets that had been deposited on the surface of different substrates. This stage was placed on a Nikon stereomicroscope (SMZ1500: Melville, NY) which was equipped with a Nikon digital camera (Digital Sight DS-5M) that was connected to a computer (Dell). A 5 µL droplet of water was deposited onto the surface of the various elastomeric materials and the image of the droplet that appeared on the mirror was captured using the digital camera connected to the stereomicroscope. The image capture software driving the digital camera was Nikon's ACT-2U

utility. The image of the droplet appearing on the mirror was from the side of the droplet thus permitting the measurement of the contact angle of the droplet edge with the material's surface. These contact angle measurements were performed using the angle tool in the previously mentioned ACT-2U software.

2.2.1.7 Young's Modulus Measurements

Rectangular pieces of the various polymers were subjected to stress-strain measurements. One end of the polymer piece was suspended from the ceiling with string and held with a binder clip, while the other end of the polymer section was attached to a weight. The weight was increased to the point of fracture and a section of the polymer was measured for elongation at each incremental weight increase. The elastic modulus was calculated from the stress-strain plots.[49]

2.2.1.8 Joule Heating Measurements

Polymeric microchips were cast with 1.3 cm long straight channels that were 15 μm deep. The channels were flushed with 1 M HCl, 1 M NaOH, ddH_2O, and finally 10 mM sodium borate pH 9.2 each for 1 min. A platinum electrode connected to a Bertan (Hauppauge, NY) high voltage power supply was placed in one of the reservoirs, while the other reservoir was grounded. A program written with LabVIEW (National Instruments: Austin, TX) was used for both the application of high voltages as well as the monitoring of current. Communication between the computer and high voltage power supply was achieved using National Instruments PCI-6036E and PCI-6713 I/O multifunction cards. Voltages were applied across the channel and the current was allowed to stabilize for 30 s prior to taking measurements.

Evaluation of the data points for each material was performed in a stepwise fashion. Data points were added one at a time and after the addition of each point, a linear fit was applied to the data set and the correlation coefficient was calculated. We chose 0.995 as the threshold for the correlation coefficient (values below 0.995 indicated non-linearity) since this is a commonly accepted value indicating a linear fit.[50] This data treatment allowed us to determine the linear range of each material's Joule heating curve and thus the field strengths at which Joule heating is not a significant source of band broadening.

2.2.1.9 EOF Measurements

EOF Measurements were made on both native PDMS devices as well as PDMS-PEO devices according to previously reported procedures.[34,51-53] Briefly, the channel lengths for the devices were determined by measurement with calipers. Using straight channel molded devices, the channels and reservoirs of the device were filled with 25 mM sodium borate at either pH 6 or pH 9. Once the channels were filled and free of bubbles an electrical field of 308 V/cm was applied across the length of the straight channel for a period of 60 s for the purpose of equilibration. After the device had been equilibrated, the reservoir containing the high voltage electrode was emptied of 25 mM sodium borate and filled with 50 mM sodium borate at the same pH. The electrode was replaced in the reservoir and voltage was applied. Due to electroosmotic flow the 50 mM sodium borate began migrating into the capillary replacing the 25 mM borate. The introduction of this higher conductivity buffer resulted in a corresponding increase in the observed current across this channel. The current increased to a point of plateau. At this point, the 25 mM sodium borate occupying the channel had been completely replaced by the 50 mM solution resulting in the current plateau. From the application of the voltage, the time required for the current plateau to occur along with the length of the channel and the applied electrical field strength was used to determine the electroosmotic flow of the device at those conditions as indicated by equation (2.1) where L is the length of the capillary in cm, t_p is the time taken for the current to plateau in s, and $E$is the applied electrical field strength in V/cm.

$$v_{eo} = \frac{L}{t_p E} \tag{2.1}$$

2.2.1.10 Separations

To execute electrophoretic separations of FITC labeled amino acids, the polymeric microchips were first filled with 10 mM sodium borate run buffer, pH 9.2. Samples were diluted 500-fold into the separation buffer. Electrophoretic separations using gated injections were performed using an in-house constructed high voltage power supply containing three independent power sources from EMCO (Sutter Creek, CA). Injection times were 0.08s.

The single point detection system used in this experiment is similar to that described by Jacobson et al.[54] Briefly, detection of FITC labeled amino acids was achieved using a 473 nm diode pumped solid state laser from CNI Laser (Changchun, China) with a power of 35 mW as the excitation source. The laser was reflected off a 500 nm long-pass dichroic mirror (500DRLP

Omega Optical: Brattleboro, VT) and focused into a small spot in the separation channel using a 40× objective (M40X; Creative Devices: Mechanic Station, NJ). The laser spot was focused 3 cm below the cross-intersection in the separation channel of the microdevice. The stimulated emission of the labeled analytes was collected by the same 40× objective and passed through the dichroic mirror. The emitted light was then focused onto a 400 μm pinhole for spatial filtering after which it was spectrally filtered through a 500-550 nm bandpass filter (525AF45 Omega Optical). Detection was performed with a photomultiplier tube (Hamamatsu Instruments: Bridgewater, NJ) and the signal was amplified at 100 μA/V using a low noise current preamplifier with a 100 Hz low-pass filter (Stanford Research Systems: Sunnyvale, CA). Computer sampling of the amplified signal was performed using a Dell computer equipped with a PCI-6036E I/O card from National Instruments.

The program controlling the high voltage power supply as well as data acquisition was written using LabVIEW. Analysis of all collected data was done using Igor Pro (WaveMetrics: Portland, OR).

2.2.2 Results and Discussion

2.2.2.1 Copolymer Composition Effects

The synthesis of the PDMS-PEO prepolymer was fairly straightforward. The hydrosilation reaction between the hydride terminated PDMS and the poly(ethylene glycol) divinyl ether was stoichiometric (Scheme 2.1). However, tailoring the characteristics of the crosslinked elastomeric material to produce a polymer amenable to the fabrication of microfluidic devices depended on adding the appropriate amount of crosslinker to the prepolymer mixture. We chose to make two different PDMS-PEO prepolymers, one with a 5% excess of reactive vinyl equivalents, and one with a 10% excess of reactive vinyl equivalents. The larger the excess amount of vinyl groups, the shorter the vinyl-terminated prepolymer chains. For the 5% vinyl excess prepolymer, for instance, the polymer chain should average 41 blocks in length with 21 blocks of PEO and 20 blocks of PDMS. Due to the presence of excess PEO, the prepolymer chain will have terminal PEO groups, and it is important to retain these terminal PEO groups for the subsequent crosslinking step. This 5% vinyl excess PDMS-PEO prepolymer is 35.9% PEO by weight prior to crosslinking. The 10% vinyl excess PDMS-PEO prepolymer should average 21 blocks in length with a PEO content of 36.9% by mass. Other

ratios of PEO to PDMS were examined, however none of the other formulations crosslinked into a useable material.

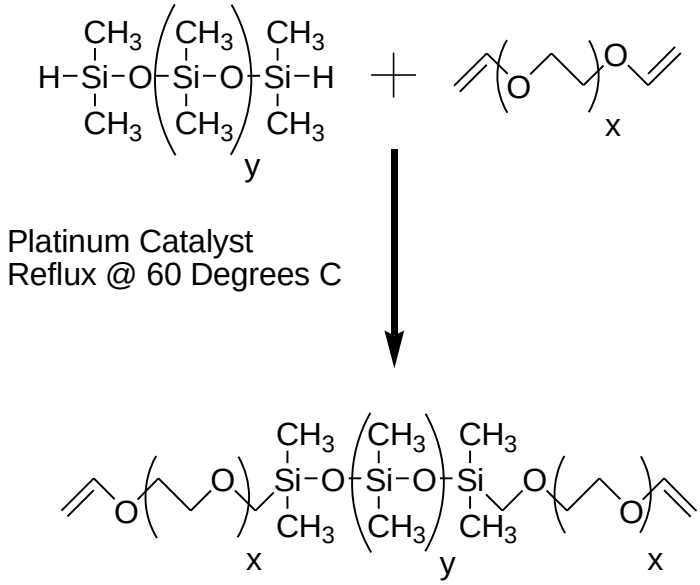

Scheme 2.1 - Reaction scheme for the preparation of vinyl terminated poly(dimethylsiloxane)-poly(ethylene oxide) block copolymer using platinum-divinyltetramethyldisiloxane complex as a catalyst. For our purposes x = 4, and y = 5.

Crosslinking of the PDMS-PEO prepolymer was achieved by mixing the vinyl-terminated prepolymer, an equivalent excess of the selected crosslinker, and the platinum catalyst solution such that the final concentration of Pt added was 30 ppm. A variety of different methylhydrosiloxane-dimethylsiloxane copolymers were examined as crosslinkers for the vinyl-terminated PDMS-PEO prepolymer. Gelest supplies these copolymers with a variety of equivalent weights ranging from 10,000 down to 135 g/equivalent. We used three different crosslinkers with equivalent weights of 490 (HMS-151), 245 (HMS-301), and 135 (HMS-501) g/equivalent. The HMS-151 produced materials of suitable durability, but the crosslinked polymers were cloudy in appearance, and optical clarity (Figure 2.1) was considered a vital property when developing polymeric microchips for use with laser induced fluorescence detection systems. The HMS-301 crosslinker was so reactive that once the prepolymer, crosslinker, and catalyst were mixed together, the material would crosslink before it could be poured onto the mold. This problem could be circumvented with the addition of an inhibitor such as tetravinyltetramethylcyclotetrasiloxane to the crosslinking step, but this crosslinker was not investigated further. The HMS-501 crosslinker showed the most promise, as it produced

materials that retained optical clarity and were durable enough to be molded into microfluidic devices (Figure 2.1). Thus the HMS-501 crosslinker was chosen for use in all PDMS-PEO device fabrication.

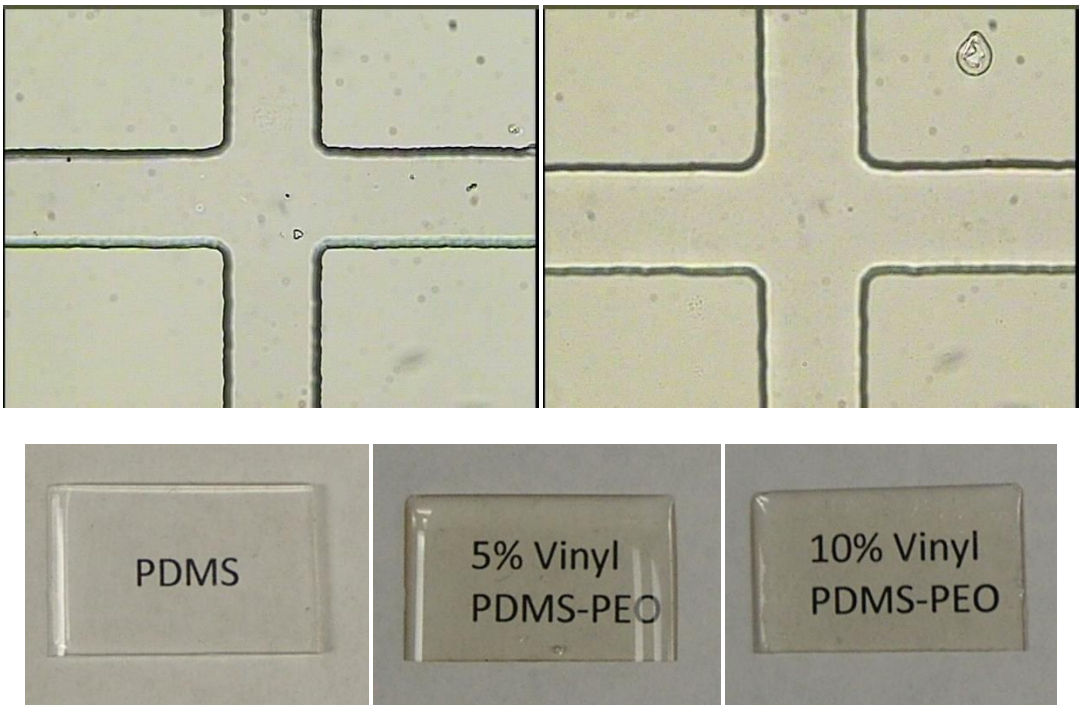

Figure 2.1 - Images of 50 µm wide, 15 µm deep molded cross channels in PDMS (top left) and 5% vinyl excess; 10-fold excess of HMS-501 crosslinker PDMS-PEO (top right). Bottom row: images comparing optical clarity of PDMS and prepared copolymers. Images captured looking through 1.5 mm thick piece of polymer laid upon a sheet of printed paper.

In order to form a material suitable for soft lithography, an equivalent excess of reactive hydride crosslinker was required for both the 5% vinyl excess and 10% vinyl excess prepolymers. The 5% vinyl excess prepolymer cured into a moldable elastomeric material when a ten-fold equivalent excess of the HMS-501 was used, while the 10% vinyl excess prepolymer only required a five-fold equivalent excess of the reactive hydride crosslinker.

2.2.2.2 UV-Vis Measurements

The absorbance spectra of the PDMS-PEO copolymers are shown in Figure 2.2. While the material is not as transparent in the UV portion of the spectrum as PDMS, PDMS-PEO does

not absorb significantly in the visible portion of the spectrum where most laser induced fluorescence measurements are made.

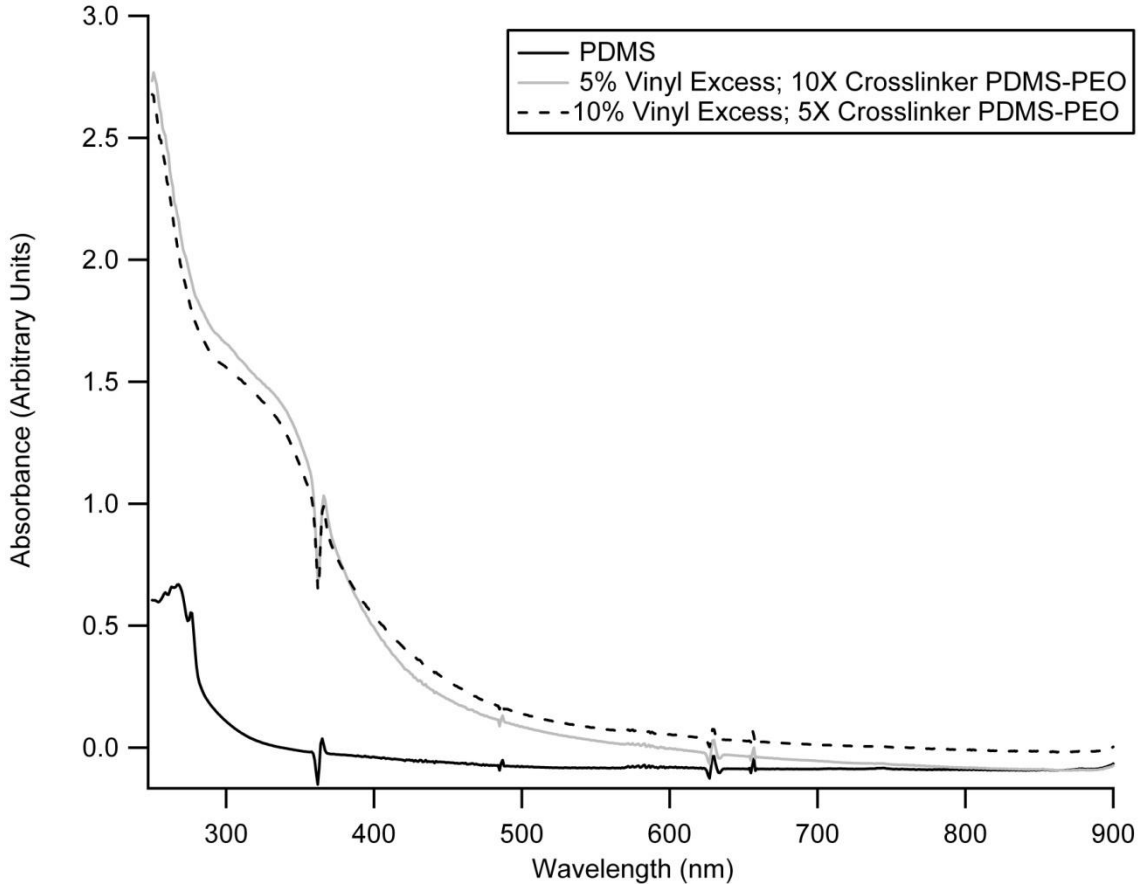

Figure 2.2 - Absorbance spectra of polymer materials across the visible wavelength range. Cuvette cell path length was 12.5 mm.

2.2.2.3 Contact Angle Analysis

The nature of the PDMS-PEO block copolymer is one of amphiphilic dynamic polymer chains. Since the copolymer is comprised of blocks of both hydrophobic PDMS and hydrophilic PEO, the material will orient its polymer chains in such a fashion as to achieve the lowest possible surface energy. When the material is exposed to an air atmosphere, the surface will be dominated by the hydrophobic PDMS blocks, but upon exposure to water the chains will reorient and the PDMS blocks will migrate back into the bulk material and be replaced at the material's surface by the more hydrophilic PEO blocks (Figure 2.3).[55]

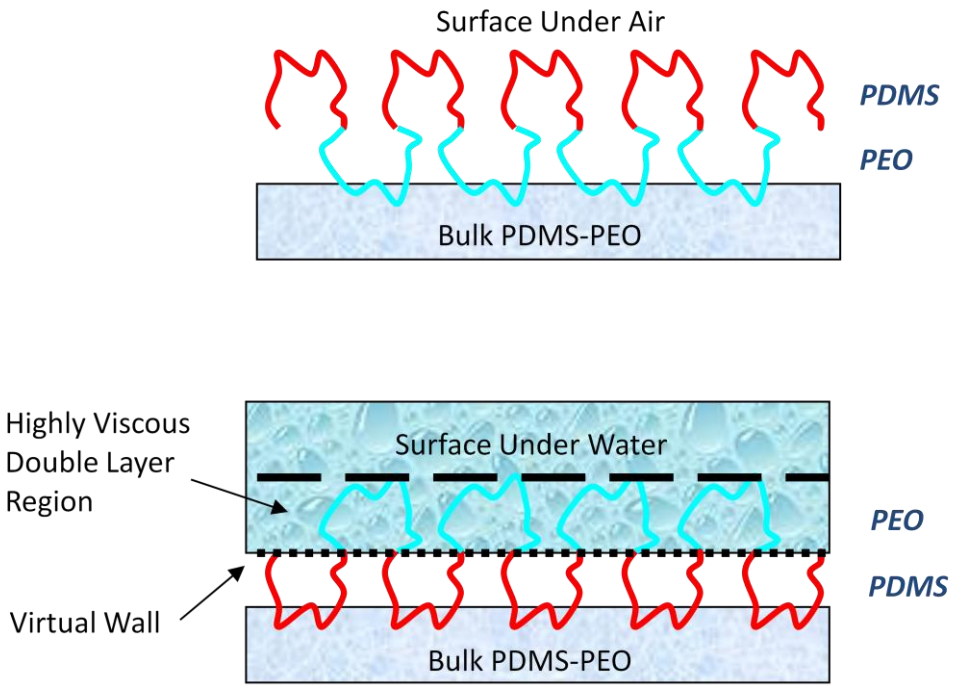

Figure 2.3 – Orientation of PDMS – PEO block copolymer chains as a function of surrounding environment. The PDMS and PEO polymer blocks are respectively oriented in a fashion minimizing the surface energy of the material. The orientation of these blocks is dictated by the environment.

This rearrangement of the polymer chains accounts for the change in contact angle with time.[55,56] The typical surface water contact angle of PDMS is approximately 110°.[57] When a droplet of water is placed on the surface of the PDMS-PEO materials, its initial contact angle is similar to that of native PDMS, however over the course of about 40 s, the droplet quickly begins to spread out and decrease to less than 70° (Figure 2.4). At equilibrium, the average water contact angle for the 5% vinyl excess material with the 10-fold excess of crosslinker was 61 ± 3° (n = 6 multiple measurements on same sample) and for the 10% vinyl excess polymer with a 5-fold excess of crosslinker was 68 ± 3° (n = 6 multiple measurements on same sample). A sample of the standard mixture of native PDMS was prepared and measured as well, yielding an average contact angle of 113 ± 4° (n = 6 multiple measurements on same sample) (Figure 2.5). Thus the PDMS-PEO copolymer possesses a contact angle that is about 40° less than that of a traditional 10 : 1 mixture of PDMS.

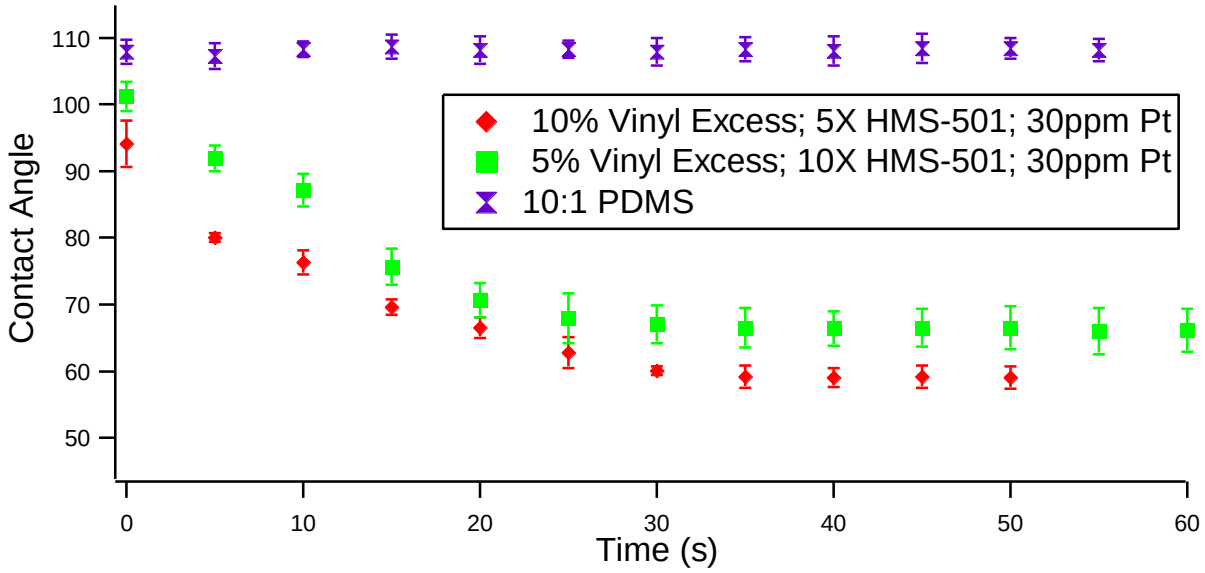

Figure 2.4 - Surface water contact angle with respect to time.

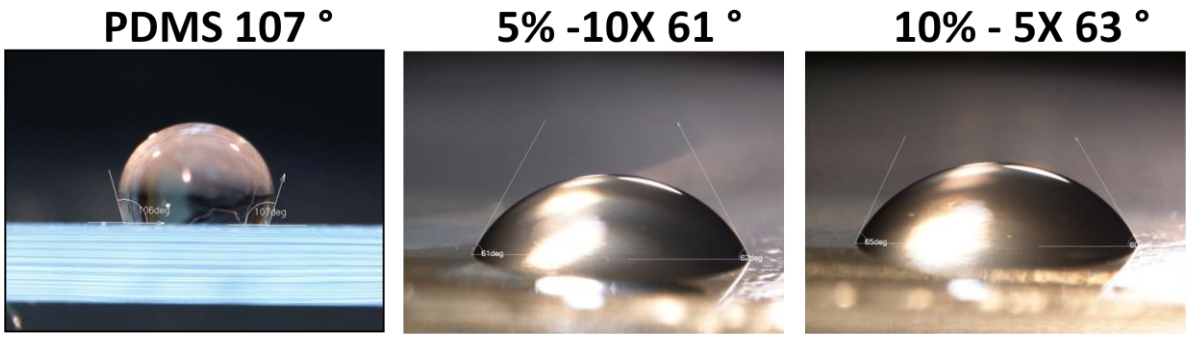

Figure 2.5 – Contact angle images of a 5 µL droplet of water on (Left) PDMS (Center) 5% vinyl excess; 10 fold equivalent excess of crosslinker PDMS – PEO (Right) 10% vinyl excess; 5 fold equivalent excess of crosslinker PDMS – PEO. The water beads up on the hydrophobic PDMS surface, while clearly spreading out on the much more hydrophilic PDMS – PEO block copolymer materials.

Small plugs of water were straddled by air within the channels of both native PDMS and PDMS-PEO microchips and the contact angle of the water with the channel walls was observed. The water plug in the PDMS channel possessed a contact angle of 95 ± 6° (n = 6) and as a result displayed convex edges. In the channels of the 5% vinyl excess PDMS-PEO microchip, the water plug had much more concave air-water interface with contact angles of 32 ± 4°.

2.2.2.4 Young's Modulus Measurements

In order to fabricate usable microfluidic devices out of an elastomeric PDMS-PEO material, it must exhibit enough mechanical strength to be successfully molded and otherwise manipulated without crumbling or tearing. Young's modulus measurements were first performed on standard 10:1 PDMS producing values of 1.91 ± 0.06 MPa. The respective Young's moduli of the 5% vinyl excess and 10% vinyl excess PDMS-PEO materials were found to be 0.94 ± 0.09 MPa and 2.6 ± 0.80 MPa. This data shows that the Young's Moduli of the PDMS-PEO copolymers are similar to that of native PDMS. Since there was a greater abundance of crosslinker present in materials cast from the 5% vinyl excess PDMS-PEO than in the 10% vinyl excess PDMS-PEO, and yet the 10% vinyl excess PDMS-PEO still exhibited a higher Young's Modulus, we believe that the driving force for the tensile modulus of the material lies in the length of the initial vinyl terminated prepolymer chains and not in the amount of crosslinker added to the prepolymer.

Often times, polymeric materials contain "fillers" to improve their mechanical robustness.[58-60] Commercial PDMS contains very small particles of precipitated SiO_2 in the elastomer base. These silica nanoparticles serve as reinforcing agents for the crosslinked material. One interesting fact to note is that the value for the Young's modulus of the crosslinked 10% vinyl excess polymer is higher than PDMS despite the fact that the PDMS elastomer is a filled polymer while the PDMS-PEO materials are un-filled.

2.2.2.5 Joule Heating Measurements

One of the most attractive features of microchip based capillary electrophoresis based systems is the higher electrical field strengths that they are able to operate under. Typically, fused silica based CE systems operate under field strengths of 300 V/cm, whereas chip based systems benefit from improved heat dissipation and thus can often operate at up to 1000 V/cm. To ensure that the PDMS-PEO chips can function under the same field strengths as their PDMS counterparts, current versus voltage curves were produced to determine the working range of the applied electrical field strength (Figure 2.6). The linear ranges for the materials were 100 – 800 V/cm, 100 – 800 V/cm, and 100 – 900 V/cm for the PDMS, 5% vinyl excess, and 10% vinyl excess polymers respectively. Both of the PDMS-PEO materials generated a linear working range at least as good as a standard PDMS chip. The block copolymer devices exhibited slightly lower currents for nearly every electric field strength examined, thus confirming that they are potential templates for high-efficiency separations.

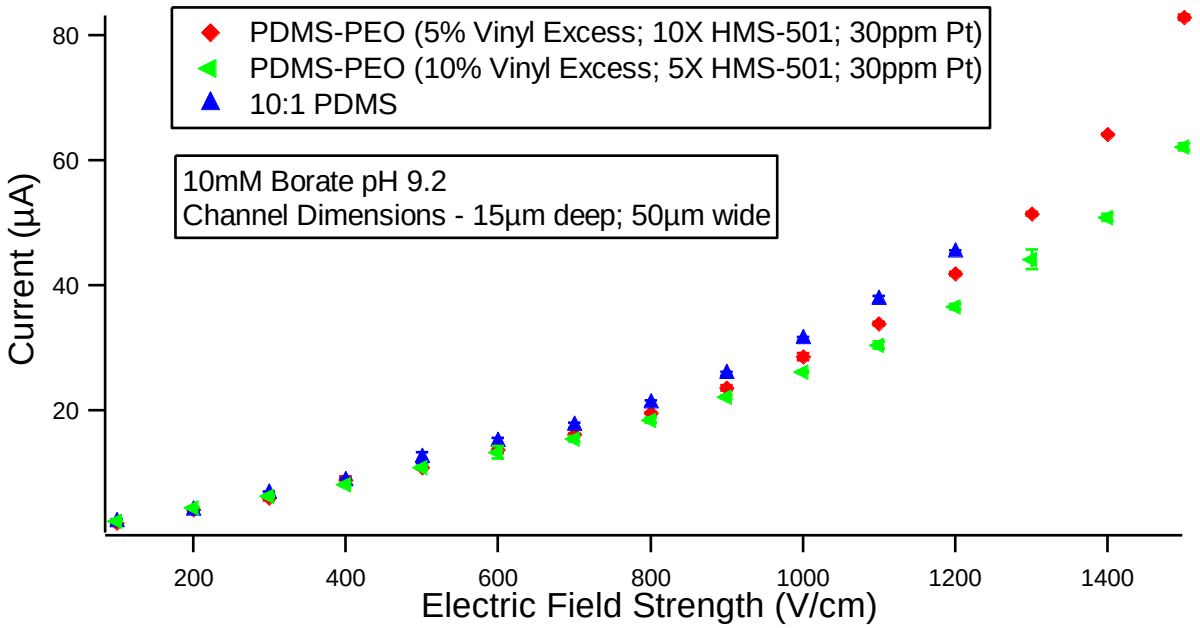

Figure 2.6 - Plot of electrical field strength applied to the microfluidic channels of different materials versus the observed current.

2.2.2.6 EOF Measurements

To generate high speed, high efficiency separations, these block copolymer devices need to possess electroosmotic flow rates on the order of native PDMS devices. EOF measurements were recorded at pH 6 and pH 9 (n = 4) for standard 10:1 PDMS as well as the 5% vinyl excess; 10-fold crosslinker and the 10% vinyl excess; 5-fold crosslinker composition PDMS-PEO devices. For PDMS, the EOF at pH 6 was determined to be $2.5 \pm 0.5\times10^{-4}$ cm^2/Vs (n = 4), while at pH 9 the EOF was recorded at $4.9 \pm 0.9\times10^{-4}$ cm^2/Vs (n = 4). A higher EOF at higher pH is generally expected as surface ionization of Si-OH groups or hydroxide ion adsorption increases with increases of pH thus increasing the overall zeta potential of a material's surface.[61] For the PDMS-PEO block copolymer EOFs of $2.5 \pm 0.7\times10^{-4}$ cm^2/Vs and $5.7 \pm 0.8\times10^{-4}$ cm^2/Vs for the 5% vinyl excess device and $1.2 \pm 0.3\times10^{-4}$ cm^2/Vs and $2.5 \pm 0.3\times10^{-4}$ cm^2/Vs for the 10% vinyl excess device at pH 6 and pH 9 respectively. Thus, under basic conditions the 5% PDMS-PEO devices have a slightly higher EOF than traditional PDMS, while the 10% vinyl excess devices exhibit an EOF slower than native PDMS (Figure 2.7). It was mentioned earlier that the 5% vinyl excess PDMS-PEO prepolymer is approximately 36% PEO by mass. When the PDMS-PEO is mixed with the 10 fold excess of PDMS based crosslinker, the percentage of PEO in the final product falls to about 30% by mass. The 10% vinyl excess PDMS-PEO prepolymer on the

other hand begins with a PEO content of approximately 39% by mass. Since only a five-fold excess of the crosslinker is used for this formulation less PDMS is imparted into the final product to achieve crosslinking and the PEO content of the crosslinked product is about 33% by mass. We can only speculate about the driving force of the EOFs observed, but we suspect it to either be a result of the different lengths of the copolymer chains, or the PEO content of the two materials studied.

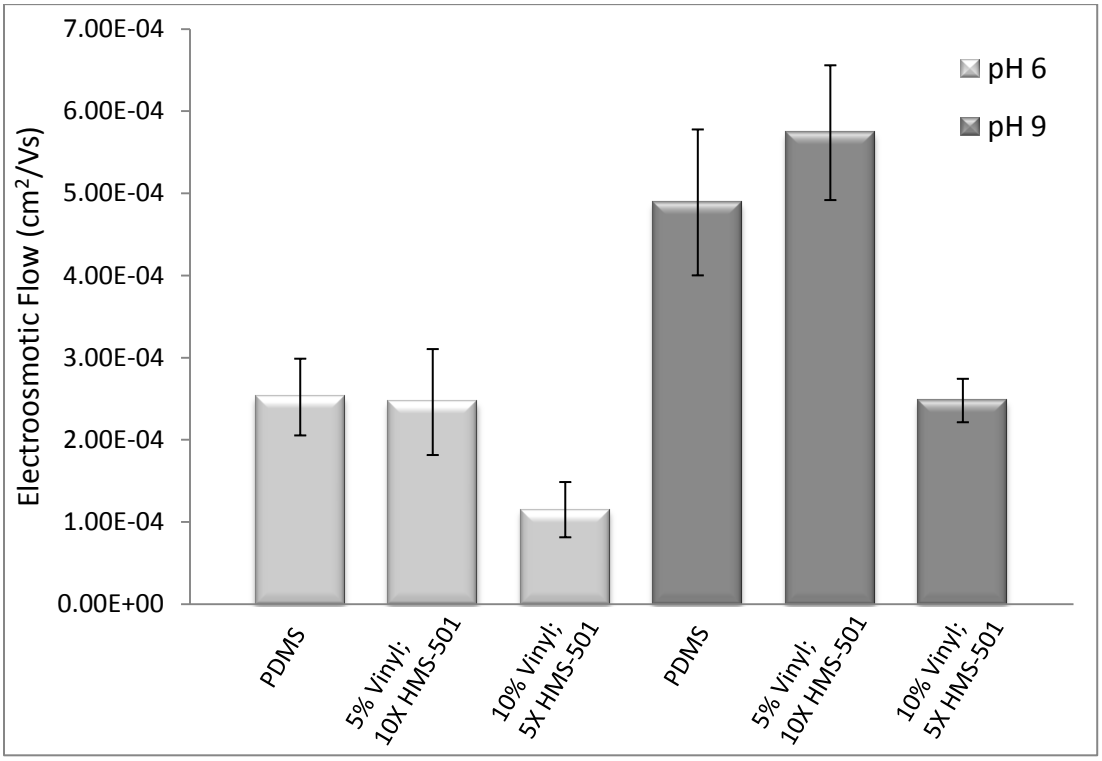

Figure 2.7 – Comparison of EOF in microchannels molded in different materials. The buffers used were 25 mM and 50 mM borate. Current was monitored as the 50 mM borate migrated into the channel (replacing the 25 mM borate) upon application of a voltage and the time taken for current stabilization dictated the EOF.

2.2.2.7 Separation and Detection

To test the viability of this material as a platform for microfluidic devices, we performed separations of fluorescently tagged amino acids. A representative separation is shown in Figure 2.8. The concentration of all of the four amino acids is 2 μM in a pH 9.0, 10 mM borate buffer. The separation distance was 3 cm and the field strength was 720 V/cm. Using a 0.08 s gated injection we can achieve an adequate separation with efficiencies similar to PDMS on these copolymer devices. The theoretical plate numbers for each analyte are shown on the

electropherogram by the corresponding peak. Our group is continuing to tailor the properties of these materials to optimize them for improved separation performance.

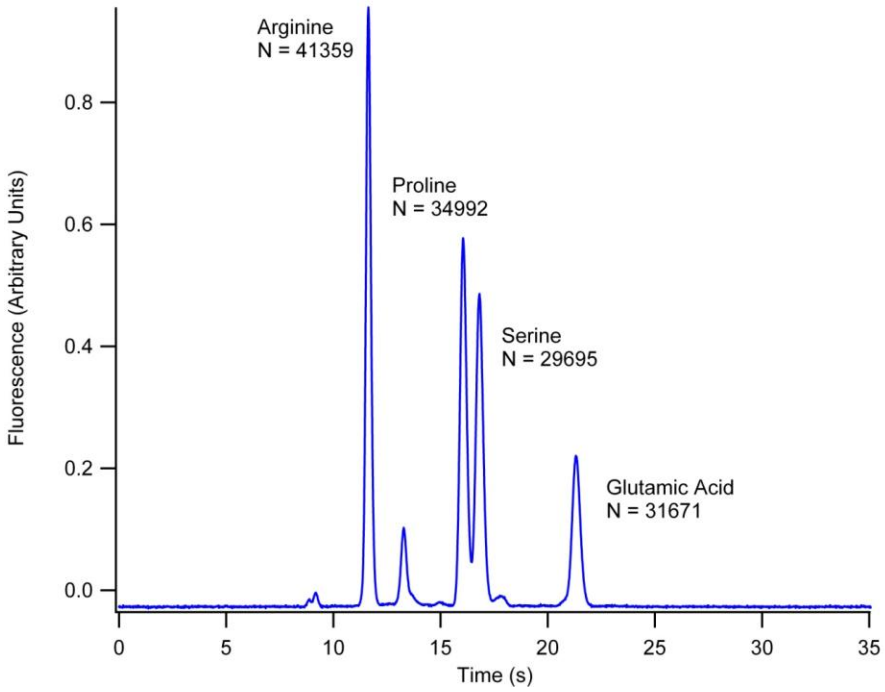

Figure 2.8 – Representative separation of selected amino acids on a 5% vinyl excess; 10X crosslinker PDMS-PEO device and their corresponding separation efficiencies (N). Separation distance was 3 cm. Separation buffer was 10 mM sodium borate pH 9.0. Electric field strength was 720 V/cm. A 0.08 s gated injection was used.

2.3 Photocurable PDMS – PEO

2.3.1 Experimental Section

2.3.1.1 Materials and Methods

Acryloxy terminated dimethylsiloxane – ethyleneoxide block copolymer (DBE-U12) as well as hexamethyldisilazane treated amorphous silicon dioxide (SIS69620) was purchased from Gelest Inc. (Morrisville, PA). The photoinitiator, 2,2'-dimethoxy-2-phenylacetophenone (DMAP) as well as the SU-8 developer, 2-(1-methoxy) propyl acetate, was purchased from Acros (Morris Plains, NJ). Tridecafluoro-1,1,2,2-tetrahydrooctyl-1-trichlorosilane was obtained from Sigma-Aldrich (St. Louis, MO). Silicon wafers with a diameter of 4 in (10.16 cm) were

supplied by Silicon Inc. (Boise, ID). SU-8 2010 was purchased from MicroChem Corp. (Newton, MA).

2.3.1.2 Mold Fabrication

To prepare the silicon wafers for SU-8 mold fabrication, a 4 in diameter silicon wafer was cut into two 1 in × 3 in silicon slides. These Si slides were then cleaned in a piranha solution for 1 h, after which time they were rinsed with ultrapure water and stored in a 100 °C oven until use. For application of photoresist to the the Si slides, a layer of SU-8 2010 was spun onto the surface of the Si slide using a commercial spincoater from Laurell Technologies (North Wales, PA). The spincoating program included two steps, the first spinning the slide at 500 rpm for 6 s, followed by a 45 s spin at 1000 rpm yielding a photoresist layer approximately 20 μm in thickness. The coated Si slide was then soft baked at 95 °C for 4 min after which time the coated substrate was placed in a UV flood exposure system (Oriel Technologies: Stratford, CT). Prior to exposure, a photomask was placed on the coated substrate and on top of the photomask was placed a 4 in × 4 in square ¼ in thick quartz plate which serves to press the photomask flat against the substrate. The photomask was designed using AutoCAD LT (Autodesk, San Rafael, CA) and transferred via high-resolution printing (8000 dpi) to a transparency forming a mask (Photoplot Store: Colorado Springs, CO). The exposure was carried out for 5.5 s at an intensity of 45 mW/cm^2 (or alternately, a total UV dosage of 247.5 mJ/cm^2). Following exposure, the substrate was hard baked at 95 °C for 4 min. The substrate was then allowed to cool at room temperature for 1 min prior to immersion in the development solution. After cooling, the Si slide was placed in the SU-8 developer, 2-(1-methoxy) propyl acetate, for 3.5 – 4 min where all uncrosslinked (unexposed) SU-8 was removed. The patterned slide was removed from the development bath, rinsed with isopropanol, and dried with a gentle stream of nitrogen.

To facilitate removal of cured elastomer from the SU-8 mold, the mold was then placed in a vacuum chamber with a petri dish containing 100 μL of tridecafluoro-1,1,2,2-tetrahydrooctyl-1-trichlorosilane spotted onto its surface. Vacuum was applied to the chamber and the tridecafluoro-1,1,2,2-tetrahydrooctyl-1-trichlorosilane vapor was allowed to react with the silicon. The mold remained in this passivation chamber overnight resulting in fluorination of the exposed silicon.

2.3.1.3 Photocurable PDMS – PEO Copolymer Preparation

The commercially available acryloxy terminated dimethylsiloxane – ethyleneoxide block copolymers were rendered photoactive with the addition of DMAP. The photoinitiator was mixed with the copolymers so that its final concentration was 0.1% (w/w). This process was simplified by the fact that DMAP was soluble in the neat copolymers, thus no additional solvents were required. Following the addition of DMAP, the optional addition of hexamethyldisilazane treated amorphous silicon dioxide (to serve as filler) can be carried out. Silicon dioxide particles were added in concentrations of 5 – 20% (w/w) to investigate their ability to reinforce the material. The copolymer-photoinitiator mixture was vortexed vigorously for 20 s. Vortexing introduces numerous bubbles into the copolymer that must be removed prior to chip casting. To this end, the polymer mixture was placed in a sonicator (Branson Ultrasonics: Danbury, CT) and degassed for 5 min. To remove the remaining bubbles, the polymer mixture was then placed in a vacuum dessicator for 1 h. Once all visible bubbles were removed, the photoactive polymer was now ready for casting.

2.3.1.4 Crosslinking of the Photoactive PDMS – PEO

It is known that polymerization of acrylate monomers is inhibited by oxygen, thus a simple containment system was constructed to locally create a nitrogen rich (oxygen depleted) environment as shown in Figure 2.9. The mold was placed in the flood exposure system and the photoactive PDMS – PEO was poured onto the mold until it was covered. A plastic container containing one open side was used to cover the polymer covered mold. This plastic shroud had three holes cut in it: one allowed the insertion of a segment of tygon tubing that was connected to a nitrogen cylinder, a second hole was located in the wall of the plastic cover opposite the tygon tubing entrance to serve as a vent allowing gas to escape, and a final hole was cut into the top of the plastic cover allowing the UV light to access the polymer on the mold (this light access porthole must have dimensions larger than the substrate to be exposed thus ensuring the entire surface of the mold receives the appropriate dose of UV light) (Figure 2.9). A quartz plate is placed over this UV light porthole to create a soft seal to contain the nitrogen while permitting transmittance of the UV light. After everything was assembled as shown in Figure 2.9, the nitrogen cylinder was opened permitting the flow of nitrogen into the container at about 10 -15 psi. The nitrogen was allowed to purge the container for 60 s after which time the UV system shutter was opened exposing the polymer to 45 mW/cm^2 UV light for 10 s (total UV dose of 450 mJ/cm^2). Following exposure, the nitrogen was turned off and the cured elastomer could be

removed from the mold. This process was repeated for a featureless piece of photocurable PDMS – PEO. The molded and featureless pieces of PDMS – PEO could then be brought into conformal contact creating an enclosed channel network. Access to the channels was achieved by punching holes at the channel termini in the molded piece of the PDMS – PEO using a biopsy punch.

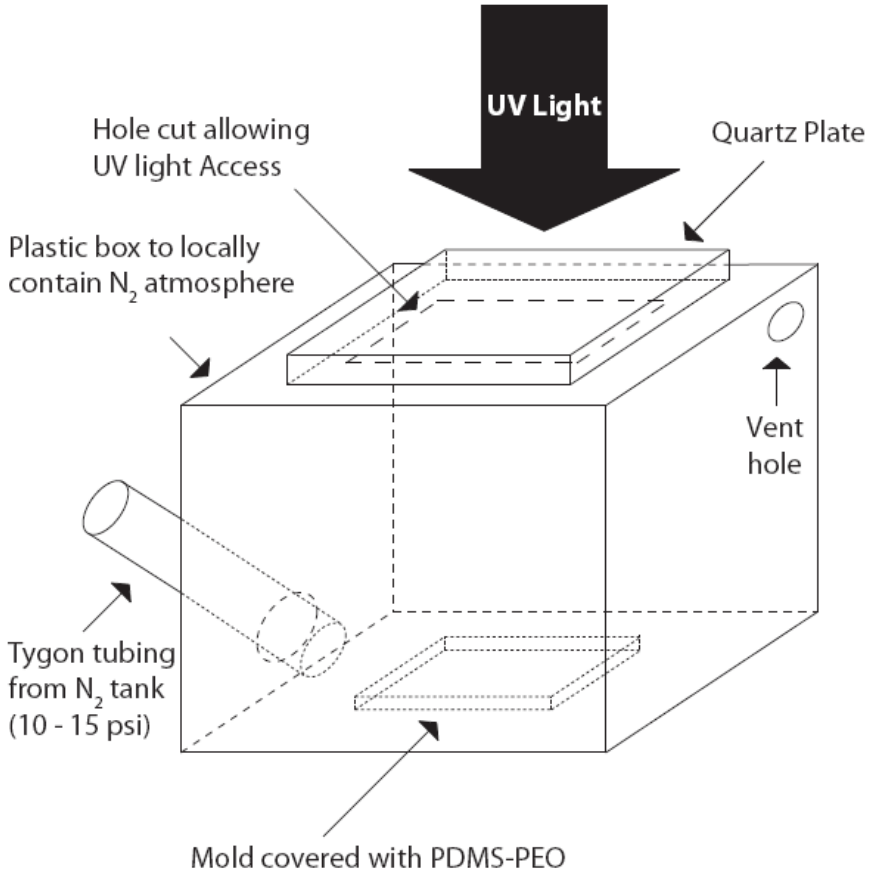

Figure 2.9 – Setup for exposure / crosslinking of photoactive PDMS – PEO.

Irreversible sealing of PDMS – PEO chips could be achieved by placing the assembled PDMS – PEO device back into the nitrogen chamber (following the punching of reservoirs) and performing a second 10 s exposure in the nitrogen rich environment. Following the initial 10 s exposure, enough residual acrylate groups are present to permit the subsequent crosslinking of the two layers together.

2.3.1.5 Contact Angle Measurements

Contact angle analysis was performed in the same fashion as with the thermally cured PDMS – PEO.

2.3.2 Results and Discussion

2.3.2.1 Copolymer Composition Effects

Initially the appropriate dose of UV light required to crosslink the photoactive PDMS – PEO had to be determined. To this end, small amounts of photoactive copolymer were exposed to different doses of UV light. Initially, a 5 s exposure at 45 mW/cm^2 resulted in a partially cured elastomer. Increasing the exposure time to 10 s appeared to further the crosslinking and durability of the material. Increasing the exposure time beyond 10 s didn't appear to have any additional effect on the material, so an exposure time of 10 s was established.

The use of the tridecafluoro-1,1,2,2-tetrahydrooctyl-1-trichlorosilane greatly facilitated the removal of the photocured elastomer from the mold. In many instances, the elastomer would spontaneously release from the mold if allowed to rest for a few minutes following exposure. This decreased the opportunity to crack or tear the material upon manual removal from the mold. The photocured elastomer appeared to retain molded features just as well as the thermally cured PDMS – PEO, and an image of a molded cross is shown below in Figure 2.10.

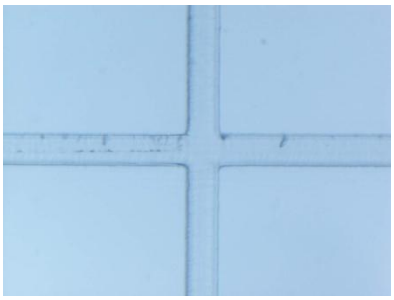

Figure 2.10 – Molded cross channel pattern cast in photocurable PDMS – PEO. Channel width is 50 μm and channel depth is 15 μm.

The crosslinked photoactive PDMS – PEO was not as durable as native PDMS, and readily crumbled when exposed to shear, however the material could be stretched and was still fairly elastic, so attempts to reinforce the material and decrease its susceptibility to shear were made.

Using hexamethyldisilazane treated amorphous silicon dioxide as a filler, photoactive polymer mixtures of PDMS – PEO were prepared containing 3%, 5%, 7% and 10% SiO_2 (w/w). These materials were crosslinked in the same manner as the materials void of SiO_2 filler, but as the amount of SiO_2 in the polymer increased, so did the viscosity. This increased viscosity made removal of bubbles more difficult and decreased the overall user friendliness of the

uncrosslinked material. Once the materials were crosslinked into elastomeric slabs a few other general observations were made. The rigidity of the material increased with increasing SiO_2 content, the conformal contact strength decreased with increasing SiO_2 content, and diffraction of light increased with increasing SiO_2 content. It was thus determined that minimizing or even eliminating the SiO_2 filler would leave a material better suited for the fabrication of microfluidic devices. In general both this photoactive PDMS – PEO as well as the thermally cured PDMS – PEO exhibited a much lower degree of conformal adhesion relative to native PDMS. The advantage of the photoactive PDMS – PEO over the thermally cured formulation, however is in its ability to easily form irreversible seals between two slabs as previously mentioned, and its overall speed of fabrication.

One of the major drawbacks of this material however is its autofluorescence. An ideal material for the fabrication of microfluidic devices will exhibit no native fluorescence as this will inhibit the use of fluorescence based detection methods that are commonly used in conjunction with microfluidics. The source of the fluorescence in this material is hypothesized to be the inhibitors added to the polymer by the supplier to prevent the polymerization of the polymer during shipping and prolonged storage. These acryloxy terminated dimethylsiloxane – ethyleneoxide block copolymers contain methyl hydroquinone at 670 ppm to prevent polymerization during storage.

Due to the native fluorescence of this material, we did not examine its properties beyond water contact angle, as it is currently incompatible with the detection methods currently being used in our lab. Upon the development of an easy method for the removal of the inhibitors from the commercial PDMS – PEO copolymer it will be necessary to revisit this material and characterize its other properties relevant to elastomeric mircrofluidic substrates. Removal of these inhibitors could potentially be achieved by using a traditional silica gel column, but if the tendency of the polymer to spontaneously react in the absence of inhibitors was high, it may be necessary to attempt the extraction of the inhibitors after the crosslinking of the polymer. Solvent based extractions of low molecular weight oligomers from PDMS has been reported[62] however attempting these types of extractions on thermally cured PDMS-PEO materials resulted in extensive cracking of the material upon its removal from the solvent system. Assuming the native fluorescence of this material could be eliminated, it could be an even better alternative to

native PDMS than the thermally cured PDMS – PEO due to the ease of fabrication of photocurable devices.

2.3.2.2 Contact Angle Measurments

Contact angle measurements were performed on the photocurable PDMS – PEO as well. The photocurable PDMS – PEO should follow the same model as the thermally cured PDMS – PEO as far as the dynamic nature of the polymer chains. In addition to the PEO groups in the polymer chain, the acrylate group itself should contribute to the hydrophilic character of the elastomer as it contains an oxygen rich ester group (Figure 2.11).

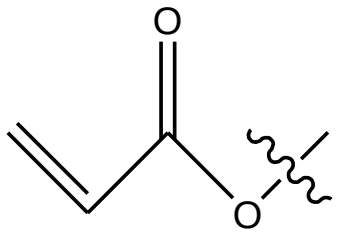

Figure 2.11 – Terminal acryloxy functional group found on photoactive PDMS – PEO block copolymers.

The water contact angle of our photocurable PDMS – PEO was determined to be 75 ± 5° (N = 6) (Figure 2.12) and exhibited a similar change with time as the thermally cured PDMS-PEO. This contact angle is slightly higher than the contact angles for the two different thermally cured PDMS – PEO formulations who had average contact angles of 61° and 68°. This increased contact angle could be a result of the composition of the commercial polymer. Since the acryloxy terminated dimethylsiloxane – ethyleneoxide block copolymer that was purchased from Gelest was said to be 30 – 35% ethylene oxide by mass, an ethylene oxide weight percent on the lower end of the 30 – 35% range would result in a higher water contact angle. This would also discount the original theory of the acryloxy functionality of the prepolymer being a significant contributor to the hydrophilic character of the bulk material.

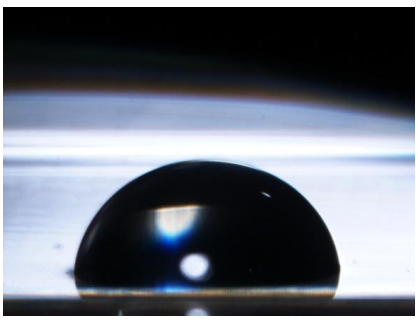

Figure 2.12 – 5 μL droplet of water on the surface of photocurable PDMS – PEO. Image was one of many used to determine the water contact angle of photocurable PDMS – PEO elastomer.

2.4 Conclusion

We have presented a strategy for the preparation of a poly(dimethylsiloxane)-poly(ethylene oxide) block copolymer for use in the fabrication of microfluidic devices. This material allows for the incorporation of hydrophilic functional groups directly into the bulk material of the microfluidic device obviating the need for any further functionalization. The material possesses an amphiphilic nature and displays water contact angles much lower than traditional PDMS. The crosslinked copolymer also exhibits sufficient mechanical durability to be used as an alternative to PDMS. For the thermally cured polymer, enclosure of patterned channels was achieved by bringing the molded polymer slab into conformal contact with an unpatterned slab. The adhesion between the two pieces of the cured polymer was not as strong as native PDMS, but was sufficient to successfully perform high speed separations. For the optically cured materials, a simple method for irreversible sealing was developed. Microchannels molded into thermally cured PDMS-PEO materials also tolerated electrical field strengths similar to those used on PDMS devices, and EOF measurements confirmed that the magnitude of EOF is also acceptable for application to high speed high efficiency chemical separations. PDMS-PEO, like PDMS absorbs most organics, however different formulations are currently under investigation which display improved solvent resistance. Removal of inhibitors from the optically cured materials would eliminate problematic autofluorescence and greatly simplify fabrication of PDMS-PEO microfluidic devices. These materials with their amphiphilic nature could potentially be useful for examining hydrophobic analytes such as biomolecules which typically adhere to standard PDMS chips due to the hydrophobic nature of PDMS and may be useful for other applications as well.

Chapter 3 - Covalent Labeling and Analysis of Ecdysteroids by Micellar Electrokinetic Chromatography with Laser Induced Fluorescence Detection

3.1 Introduction

The process of metamorphosis has intrigued entomologists for a very long time. The transformation of an insect larva into a pupa, and subsequently into an adult is accompanied by an array of physical changes. These changes are governed by a certain class of chemical compounds known as ecdysteroids. Ecdysone, the most common ecdysteroid, was first isolated and subsequently named by Peter Karlson in 1954.[63] These compounds are steroid hormones secreted by insects and they serve to control and or initiate molting, metamorphosis, and the reproductive cycle.[64]

As insects grow they need to shed their cuticle periodically to allow for the growth of a new and larger one. The actual trigger for the initiation of the molting process is still in question, but in some insects molting is triggered by abdominal stretching or by reaching a critical size. Molting cycles begin with the release of prothoracicotropic hormone by the brain which initiates the prothoracic gland to begin ecdysone synthesis. Once ecdysone is synthesized it is immediately released into the insect's blood, known as hemolymph, where carrier proteins deliver the hormones to their target tissues.[64] Exactly what role the carrier proteins serve is yet unknown, but they are believed to increase the carrying capacity of the hemolymph and also believed to help the steroids penetrate cell walls. Once ecdysone reaches its target tissues it is then converted to its functional form 20-hydroxyecdysone (also known as β-ecdysone or ecdysterone) by the fat body and epidermal cells. As the levels of ecdysone in the hemolymph begin to rise, known as the "Preparatory Phase", a pattern of DNA and RNA synthesis begins in the epidermal cells.[64] Nucleotide synthesis is also accompanied by an array of cytoplasmic changes. As ecdysone levels continue to rise, apolysis (separation of the cuticle from the epidermis) occurs. Once ecdysone levels plateau, the deposition of the epicuticle occurs, and as ecdysone levels begin to fall towards the end of the molting process, the insect deposits its exocuticle.

While ecdysone is responsible for all of these physical changes it also can affect insect behavior. The first release of ecdysone typically causes the insect to stop feeding and "void its gut contents", as well as causing the insect to enter into the "wandering phase" where it moves away from food in search of a site for pupation.[64]

While ecdysteroids are found in all classes of arthropods, many can be found in plants as well. Despite the fact that often times the chemical structure of the ecdysteroids found in plants matches identically with an ecdysteroid from an insect, convention classifies the compounds differently. Typically, these hormones are referred to as ecdysteroids when found in insects and phytoecdysteroids when found in plants. The function of phytoecdysteroids in plants is still a topic of debate, but the most commonly held belief is that they serve as a chemical defense agent against predatory insects. This defensive theory most likely stems from the belief that consumption of these steroids could have detrimental effects on the insects that employ these hormones for regulatory purposes.[63]

Following the discovery of ecdysteroids in plants, many of these compounds became readily available in a relatively large supply and this initiated the testing of the pharmacological effects of these compounds.[63] It was quickly learned that these chemicals are non-toxic to mammals, and it was also noted that these phytoecdysteroids possessed a variety of rather beneficial effects. Phytoecdysteroids, while believed to serve as a defense against insects, are today commonly included in plant extracts sold as health supplements in many drug and health food stores.[65] Thus these molecules possess commercial implications in addition to scientific interest.

In insects, ecdysteroids circulate in the hemolymph at concentrations ranging from 10 to 3000 ng/mL, and since insects are generally very small, only a few hundreds of nL to a few μL of hemolymph may be extracted from a single insect without causing severe damage. With only a few microliters of hemolymph to analyze, analyte concentrations fall below the detection limits of UV and electrochemical detection methods, and a new detection scheme must be developed that is capable of identifying picograms of analyte. In the past, the issue of a lack of techniques with sufficient limits of detection was circumvented by; pooling the hemolymph from a number of insects, by using whole-insect homogenates, or by drawing hemolymph from a single large insect (at least 100 mg body weight).[64] If one looks at ecdysone for example, with a molecular weight of 464 g/mol, and assumes that it is present in the hemolymph at 1500 ng/mL, this

translates to a concentration of about 3 µM. If 5 µL of hemolymph is extracted from a large insect, then one obtains a total of approximately 15 pmol of ecdysone, well above the reported limits of fluorescence detection (10^{-17}-10^{-20} mol).[66]

In addition to ecdysone and 20-hydroxyecdysone, one might expect a number of other ecdysteroids to be present in the hemolymph, and these will mainly be metabolites of the two aforementioned ecdysteroids (20,26-hydroxyecdysone and 26-hydroxyecdysone). In order to identify these other steroids and to more accurately quantify their respective concentrations, it will be necessary to employ a separation of these steroidal compounds. This particular class of compounds will require a very high efficiency separation such as capillary electrophoresis, CE, because in many instances two ecdysteroids will differ structurally by as little as one atom, as is the case with ecdysone and 20-hydroxyecdysone. However, standard CE will not be enough, as it is only suited for the separation of charged analytes. The methods of covalent modification that will be discussed later involve neutral tags bonded to neutral analytes. Micellar electrokinetic chromatography (MEKC), as previously described, is a type of CE involving the addition of surfactants to the run buffer. These surfactant molecules aggregate to form micelles. It is the interaction of the analyte molecules with these charged micelles that allows MEKC to separate out neutral compounds. The analysis of ecdysteroids using HPLC has been reported.[67-69] In addition separation was achieved by MEKC, using standard fused silica capillary regimes with either UV or fluorescence detection.[70-73] The detection limits involved with these two methods are simply too low to permit analysis on the single insect level.

Given the major implications of these steroids in insects, plants, and mammals alike, a facile, sensitive, and precise method of analysis would prove incredibly useful to entomologists, botanists, and pharmacologists. Ecdysteroids themselves do not contain a good chromophore or fluorophore, but with the development of a method for the covalent labeling of ecdysteroids with a fluorescent tag, one could make these compounds a candidate for fluorescent detection which carries the potential for analyses on the individual insect level. Once labeled, these compounds can be separated for identification and quantification potentially providing an abundance of information on individual insects.

3.2 Experimental Section

3.2.1 Materials and Methods

Ecdysone and 20-hydroxyecdysone were obtained from the Alexis Corporation (San Diego, CA), BODIPY® FL Hydrazide, fluorescein-5-thiosemicarbazide and AlexaFluor 488 hydroxylamine were purchased from Invitrogen (Carlsbad, CA). Ethanol was supplied by Aaper (Shelbyville, KY). Seventh Generation liquid dish soap was purchased at a local supermarket. Acetonitrile, 2-cyclohexen-1-one, sodium borohydride, sodium cholate, sodium dodecyl sulfate, trifluoroacetic acid were purchased from Sigma Aldrich (St. Louis, MO). Anhydrous magnesium sulfate, sodium hydroxide, hydrochloric acid, methanol, sodium borate, tetrahydrofuran, dimethylformamide we supplied by Fisher Scientific. Fused silica capillary was purchased from Polymicro Technologies (Phoenix, AZ).

3.2.2 Fluorescein-5-thiosemicarbazide Labeling

α-Ecdysone was received in a 5 mg package and was diluted with 1 mL of ethanol resulting in a sample that was 10.8 mM. The fluorescein-5-thiosemicarbazide solution was prepared by dissolving 5 mg in 1 mL of dimethylformamide (DMF) resulting in stock solution that was approximately 11.9 mM. Labeling of α-ecdysone was carried out using a 1:1 mole ratio of the label to the hormone by adding 92.6 μL of the α-ecdysone stock and 84 μL of the label stock to 823.4 μL of buffer. The buffer being used was 10 mM sodium borate pH 9 containing 50 mM SDS. A label blank was also prepared by adding 84 μL of the label stock and 92.6 μL of ethanol to 823.4 μL of buffer. The two solutions were incubated in a -20° C freezer for 2 h. Following incubation, 100 μM and 10 μM solutions were prepared by dilution into the borate – SDS run buffer. These solutions were used for electrophoretic separations.

Electrophoretic separations were performed using the same experimental setup described in section 2.2.1.10 with one major change. A length of fused silica capillary was used in place of the polymeric microchip. The separation conditions for these samples were as follows: the length of the fused silica capillary was 30 cm with an inner diameter of 25 μm; the effective separation distance was 15 cm; the applied voltage was 10 kV producing an electrical field strength of 333 V/cm; 10 s electrokinetic injections were performed at 10 kV; the data acquisition rate was 25 Hz.

3.2.3 BODIPY® FL Hydrazide

A variety of conditions were used in the establishment and optimization of a reliable labeling protocol, and as such, all of the specific labeling conditions used will be presented and their respective results will refer back to the section number corresponding to their preparation.

3.2.3.1 Initial Labeling Method

A 1 μg/mL BODIPY® FL hydrazide stock solution was prepared in ethanol (according to Katayama et al. this solution was good for three hours).[74] A 0.08% (v/v) solution of trifluoroacetic acid (TFA) in ethanol was prepared (83 μL TFA in 99.917 mL ethanol). Stock solutions of progesterone, α-ecdysone, and 20-hydroxyecdysone were prepared in ethanol. Next, 200 μL of both the BODIPY FL hydrazide stock solution and the 0.08% TFA stock solution were added to four different microcentrifuge tubes. A different steroid solution was added to each of three different tubes such that the final concentration of the steroid in the labeling cocktail was 1 ng/mL, and also leaving one tube to serve as a label blank. The resulting molar ratios for BODIPY® FL hydrazide to steroids were: 241:1 for progesterone, 357:1 for α-ecdysone, and 369:1 for 20-hydroxyecdysone. All sample mixtures were then vortexed and allowed to incubate in the dark for 15 h at room temperature. Following this incubation period, the samples were placed in a vacuum dessicator in order to remove ethanol until only about 50 μL of solution remained. To the remaining 50 μL of sample, 800 μL of separation buffer was added. The separation buffer consisted of 50 mM sodium borate pH 9.2, 25 mM SDS, 25 mM sodium cholate, and 10% isopropanol (v/v). This run buffer was chosen based on previous work by Santagati et al. who performed MEKC on ecdysteroids with UV detection.[71] Electrophoretic separions of these samples were then performed.

3.2.3.2 Labeling Without TFA – Heat Incubation – 200-Fold label Excess – Separation in Phosphate Buffer

Stock solutions of progesterone, α-ecdysone, and 20-hydroxyecdysone were prepared in ethanol at a concentration of 5 mg/mL. Dilution of these hormone stocks was carried out by adding 2 μL of the stock solution to 998 μL of ethanol (referred to as "steroid stock B"). To 100 μL of each steroid stock B solution was added the appropriate amount of 0.5 mg/mL (1.63 mM) BODIPY® FL hydrazide in ethanol to produce a molar ratio of 200:1 label to steroid for each

analyte. A blank was also prepared using a similar concentration of label void of any steroids. For the progesterone solution the concentrations were 3.18 μM and 636 μM for the progesterone and label respectively; the concentrations were 2.15 μM and 430 μM for α-ecdysone and label respectively; and the concentrations for 20-hydroxyecdysone and BODIPY® FL hydrazide were 2.08 μM and 416 μM respectively. The blank contained label at a concentration of 500 μM. The three labeling solutions as well as the blank were incubated on a block heater at 50 – 60 °C for 1 h after which they were immediately placed in a vacuum dessicator where vacuum was applied until the effective solution volume reduced to approximately 20 μL. The samples were then reconstituted to 1 mL with run buffer. The run buffer used in this instance was 10 mM sodium phosphate pH 6.8 containing 50 mM SDS and 10% acetonitrile (v/v) prior to analysis.

3.2.3.3 Labeling without TFA – Heat Incubation – Equimolar Label and Steroid – Seventh Generation™ Buffer

All methanol used in this experiment was of HPLC grade to ensure no carbonyl bearing impurities may be present in the solvent. Stock solutions of progesterone and BODIPY® FL hydrazide were prepared in methanol at concentrations of 12.7 mM and 16 mM respectively. In the derivatization tube, the label and steroid were present in roughly equuimolar concentrations. For the samples containing steroid, 10 μL of the progesterone stock and 10 μL of the BODIPY® FL hydrazide stock were added to 980 μL of methanol. For the label blank, 10 μL of BODIPY® FL hydrazide stock and 990 μL of methanol were used. All solutions were vortexed and placed in a block heater and covered to incubate in the dark for 12 h at 60 °C. Samples were then diluted into the run buffer. The run buffer chosen for this experiment was an environmentally friendly micellar buffer reported by Hoeman et al.[75] The buffer contained 10 mM sodium borate pH 9.1 with 5% Seventh Generation™ liquid dish soap by weight. Serial dilutions were carried out yielding samples where the final concentration of tag and steroid in the mixtures was 16 μM and 13 μM respectively. All separations were run in positive polarity mode.

3.2.3.4 Labeling without TFA – Heat Incubation – Equimolar Label and Steroid – Borate Buffer with THF

The labeling reaction was carried out exactly as describe in section 3.2.3.3, however the additional analyte 20-hydroxyecdysone was incorporated. In addition, following the 12 h

incubation period, the sample vials were placed in a vacuum dessicator and evaporated to dryness. Next, the samples were reconstituted in 100 μL of THF. For dilution of the samples into the separation buffer, 10 μL of the label mixture dissolved in THF was added to 990 μL of the separation buffer. The separation buffer consisted of 10 mM sodium borate pH 9.1 containing 50 mM SDS with 30% THF (v/v). These mixtures were serially diluted to generate the samples for separation. Separations were performed on a segment of fused silica capillary under positive polarity.

3.2.3.5 Labeling with TFA – Heat Incubation – 10-Fold Label Excess – Separation in Borate Buffer – Sodium Borohydride

A 70 μM stock solution of progesterone and a 1.4 mM stock solution of BODIPY® FL hydrazide were prepared in methanol. For the labeling reaction, 71.4 μL of the progesterone stock solution and 31.25 μL of the BODIPY® FL hydrazide stock were added to a microcentrifuge tube. The resulting concentrations of each analyte were 48.7 μM and 487 μM for the label respectively. The label was prepared by adding 71.4 μL of methanol and 31.25 μL of the label stock to a microcentrifuge tube. Both the sample and the blank were placed in a 50 - 60 °C block heater for 1 h. Dilution of the two incubated samples in the separation buffer was achieved my mixing 10 μL of the incubated samples with 990 μL of the separation buffer, resulting in a blank containing BODIPY FL hydrazide at a concentration of 4.87 μM and a hormone sample containing progesterone at a concentraton of 487 nM and BODIPY FL hydrazide at 4.87 μM. The separation buffer used in this experiment was 10 mM sodium borate pH 9.2 containing 50 mM SDS and 10% methanol by volume. Additional samples were prepared with this protocol with one change: during the 1 h incubation in the block heater, after the first 30 min approximately 1 mg of sodium borohydride was added to each of the microcentrifuge tubes after which the remaining 30 min of incubation in the block heater was carried out. Dilution of samples containing sodium borohydride was carried out in the same manner as samples not containing sodium borohydride.

3.2.3.6 Labeling with TFA – Heat Incubation - 10-Fold Label Excess – Separation in 7th Generation Buffer – Addition of Magnesium Sulfate

All methanol used in this experiment was of HPLC grade to ensure no carbonyl bearing impurities may be present in the solvent. Stock solutions of 20-hydroxyecdysone and BODIPY® FL hydrazide were prepared in methanol at concentrations of 210 μM and 1.6 mM respectively. Two sets of labeling reactions were prepeared, one where the label was in a 10-fold molar excess over the steroid as well as a set where the label and steroid were present in equal concentrations. For the samples containing an equal ratio of tag and steroid, 190 μL of the 20-hydroxyecdysone stock and 25 μL of the BODIPY® FL hydrazide stock were added to 80 μL of 1% TFA in methanol (v/v) and 705 μL methanol. For the preparation of the samples containing a 10-fold molar excess of the label over the steroid, 190 μL of the steroid stock solution and 250 μL of the BODIPY® FL hydrazide stock solution were added to 80 μL of 1% TFA in methanol (v/v) and 480 μL of methanol. The label blanks for both sets of samples were prepared by substituting 190 μL of methanol for the 190 μL of steroid stock solution. Following the mixing of all the labeling solutions, approximately 5 mg of anhydrous magnesium sulfate ($MgSO_4$) was added to each microcentrifuge tube to serve as a water scavenger. All solutions were vortexed and placed in the dark to incubate for 12 h. Following the 12 h incubation period, 2 – 3 mg of $NaBH_4$ was added to each of the vials to reduce the C = N bond to a C – N bond forming a stable amine much less susceptible to hydrolysis. Following addition of $NaBH_4$ solutions were again placed in the dark for 1 h. Next all samples were filtered through a 0.45 μM Millex-LCR PTFE syringe filter (Millipore: Billerica, MA) to remove all $MgSO_4$ and $NaBH_4$ solids. Samples were then diluted into the run buffer. The run buffer chosen for this experiment was the same environmentally friendly micellar buffer reported by Hoeman et al.[75] The buffer contained 10 mM sodium borate pH 9.1 with 5% Seventh Generation™ liquid dish soap. Dilution of the samples was carried out as follows; 50 μL of a labeling cocktail was added to 950 μL of buffer. The final concentrations of tag and steroid in the equimolar mixtures was 2 μM, while in the 10-fold label excess mixture the concentration of fluorophore was 10 times higher at 20 μM with the concentration of steroid remaining at 2 μM. All separations were run in positive polarity mode.

3.2.4 Capillary Conditioning

Prior to performing analytical separations both glass microfluidic chips as well as standard fused silica capillary were subjected to thorough cleaning and conditioning treatments.

3.2.4.1 Microfluidic Device Preparation

To clean and condition glass microfluidic devices, the channels and reservoirs were first filled with a 1:1 mixture of 1 M sodium hydroxide and methanol. Vacuum was applied to one reservoir for 60 s after which the fluid in the reservoir was emptied and then replenished with fresh fluid. This process was repeated for the three remaining reservoirs. Next the fluid in the reservoirs was replaced with ultrapure water, and the same method used with the 1:1 NaOH : methanol solution was employed. Finally, the water in the reservoirs was replaced with the selected separation buffer and the same method used with the 1:1 NaOH : methanol was repeated a final time.

3.2.4.2 Fused Silica Capillary Preparation

For the conditioning of fused silica capillaries, one end of the capillary was connected to a syringe via luer lock fittings from Upchurch Scientific (Oak Harbor, WA) while the other end was left open to drain into a waste container. Initially, a syringe containing 1:1 1 M sodium hydroxide and methanol was connected to the capillary and placed into a syringe pump. Fluid was pumped through the capillary at a rate of 10 μL/min for 5 min. After 5 min, the syringe containing the sodium hydroxide / methanol mix was swapped for one with ultrapure water. Pumping at 10 μL/min recommenced for 5 min. Finally the syringe containing water was replaced with one containing the selected buffer. The buffer was then pumped through the capillary for 5 min at a rate of 10 μL/min. At this time, all syringes and Upchurch fittings were removed from the capillary, and the open ends of the buffer filled capillary were placed in 1 mL microcentrifuge tubes (Eppendorf: Hauppauge, NY) containing 1 mL of the same buffer used to condition the capillary. A Pt electrode was inserted into the reservoir containing the capillary inlet, and a Pt ground wire was inserted into the capillary outlet reservoir. High voltage was applied across the capillary (using the same electrical field strength that would be used for subsequent separations) for 10 min and the current was monitored on an analog ammeter that had been connected in series with the Pt ground wire. The application of voltage served to stabilize the EOF in the capillary.

3.3 Results and Discussion

3.3.1 Fluorescein-5-thiosemicarbazide Labeling

Our initial attempts to fluorescently derivatize the ecdysteroids involved the use of fluorescein-5-thiosemicarbazide, a common commercial fluorophore, which can be coupled with aldehydes and ketones to form a Schiff base, which follows a general formula of R_1R_2–C=N–R_3. Early experiments quickly revealed what appeared to be rapid decomposition of the fluorophore over the course of a few separations. The separations of the samples containing only the label and not the ecdysteroid (referred to as the "label blank") are shown in Figure 3.1. The major peaks in the label blank appear as a doublet of roughly equal amplitude in the first separation. However, over the course of a few separations, it can be clearly seen that the amplitude of the faster eluting of the two peaks begins to diminish as subsequent separations are performed. This is most likely due to the decomposition of the fluorophore possibly as a result of hydrolysis.

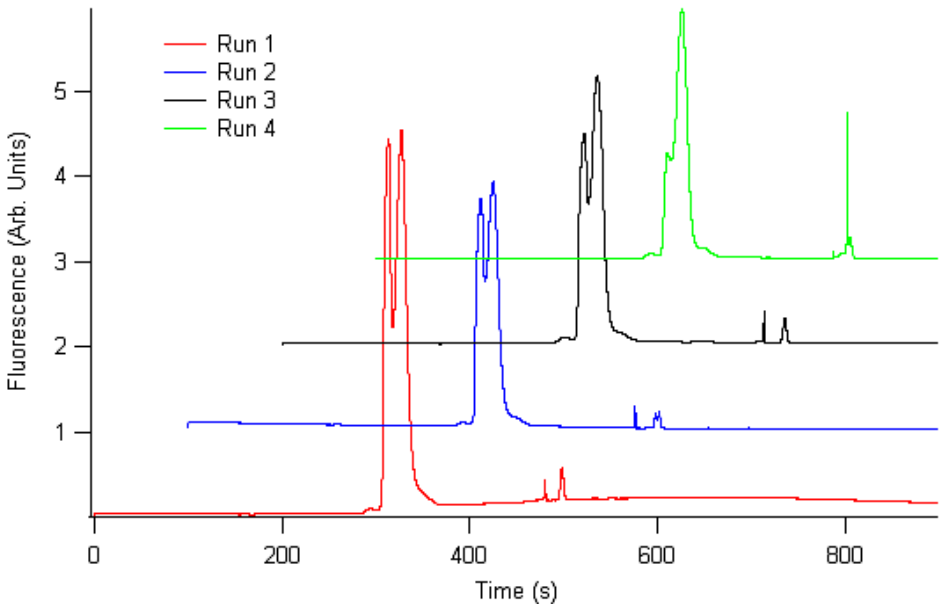

Figure 3.1 – Electropherograms of fluorescein-5-thiosemicarbazide in 10 mM sodium borate pH 9 with 50 mM SDS. Electrical field strength: 333 V/cm, Separation length: 15 cm, Concentration of fluorescein-5-thiosemicarbazide: 10 µM.

Separations of the ecdysone / fluorescein-5-thiosemicarbazide mixtures were performed to determine if any successful labeling of the analyte had occurred, keeping in mind the poor performance of the fluorophore. These separations are shown in Figure 3.2. From this data no discernable additional peaks that could be attributed to a labeled ecdysone adduct can be seen. There are also notable changes in the shape of the major peaks over the course of a few runs

likely due to decomposition of the fluorophore as previously described. The two early eluting peaks in Run 3 are carryover from the previous run.

Due to what is suspected to be the rapid decomposition of this fluourophore it was determined not to be a viable option for use as a tag and was not pursued further. It would, however be interesting to identify exactly what the cause of the disappearing peak was, and how that impacted the possible linking of the tag to the ecdysone.

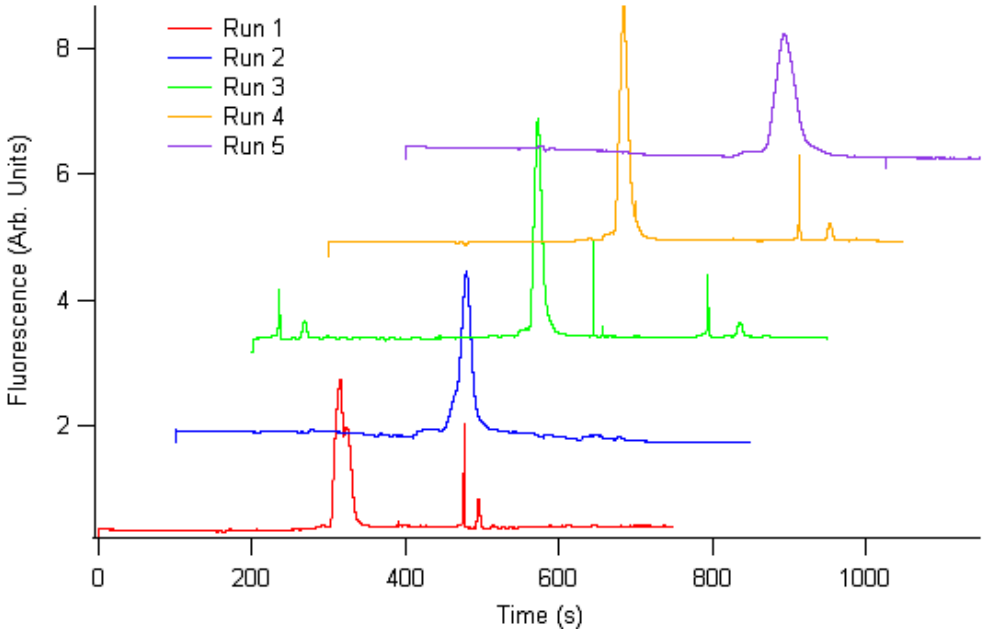

Figure 3.2 – Electropheregrams of 1:1 mixtures of α-ecdysone and fluorescein-5-thiosemicarbazide in 10 mM sodium borate pH 9 with 50 mM SDS. Electrical field strength: 333 V/cm, Separation length: 15 cm, Concentration of fluorescein-5-thiosemicarbazide and α-ecdysone: 10 µM.

3.3.2 BODIPY® FL Hydrazide

BODIPY® FL hydrazide is a proprietary fluorophore supplied by Invitrogen Figure 3.3. It reacts with aldehydes and ketones, much like the fluorescein-5-thiosemicarbazide, forming the previously described Schiff base. The derivatives formed by the reaction of this label with ketones and aldehydes are known to be subject to hydrolysis, however Invitrogen claims that the linked adduct can be reduced to a more stable amine by using sodium borohydride. Initial labeling protocols were based on those reported by Katayama et al. who reported the use of

BODIPY® FL hydrazide as a fluorescent tag for progesterone and 17-hydroxyprogesterone for HPLC analysis with fluorescence detection.[74]

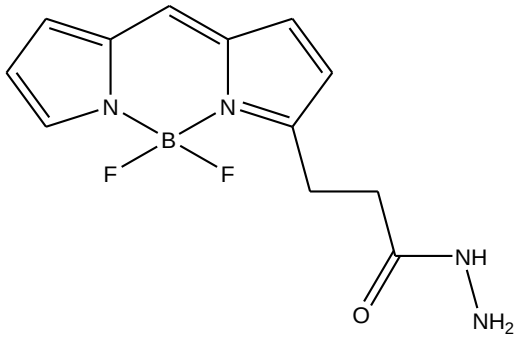

Figure 3.3 – Molecular structure of BODIPY® FL hydrazide.

Since the reagents involved (α-ecdysone, 20-hydroxyecdysone, BODIPY® FL hydrazide) are all quite expensive (5 mg > $100.00), progesterone and 17-hydroxyprogesterone were chosen for use as model compounds to validate the proposed derivatization method as these compounds are much more affordable and possess the same target functional group, the α,β-unsauturated ketone, or enone, as shown in Figure 3.4.

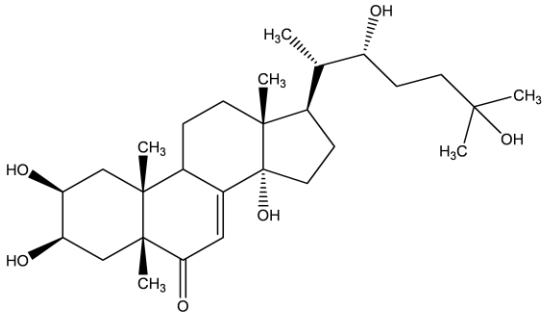

α-Ecdysone

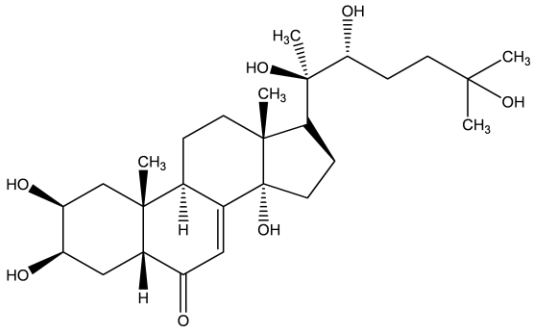

20-Hydroxyecdysone

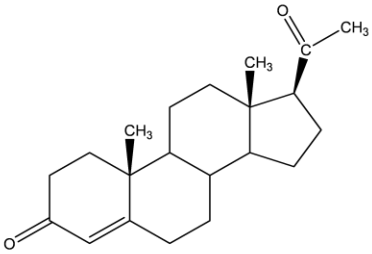

Progesterone

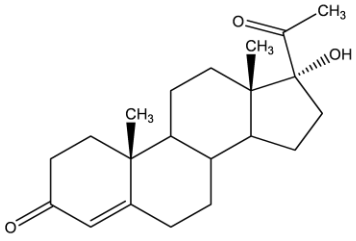

17-Hydroxyprogesterone

Figure 3.4 – Molecular structures of ecdysteroids (top) and abundant model hormones (bottom) possessing a similar functional group, the α,β-unsaturated ketone which can be covalently linked to BODIPY® FL hydrazide.

Immediately one can see that the model hormones, progesterone and 17-hydroxyprogesterone, possess both a ketone and an α,β-unsaturated ketone, and thus will be subject to derivatization at two different locales. This means that for both of the model hormones used, each will potentially form three different adducts depending on where on the molecule derivatization occurs: modification at the ketone, modification at the α,β-unsaturated ketone, or modification at both positions.

3.3.2.1 Initial Labeling Method

Initial labeling methodologies were based on those reported by Katayama et al.[74] According to their work with labeling of progesterone and 17-hydroxyprogesterone, at a molar ratio of about 100:1 dye to hormone, the detector reached a maximum response signal and plateaued. Thus, a molar ratio of at least 200:1 BODIPY® FL hydrazide to steroid was initially used. Labeling was performed according to the method described in section 3.2.3.1.

Following the 15 h incubation period, microchip based electrophoretic separations were performed on these samples. The resulting electropherograms are shown in Figure 3.5.

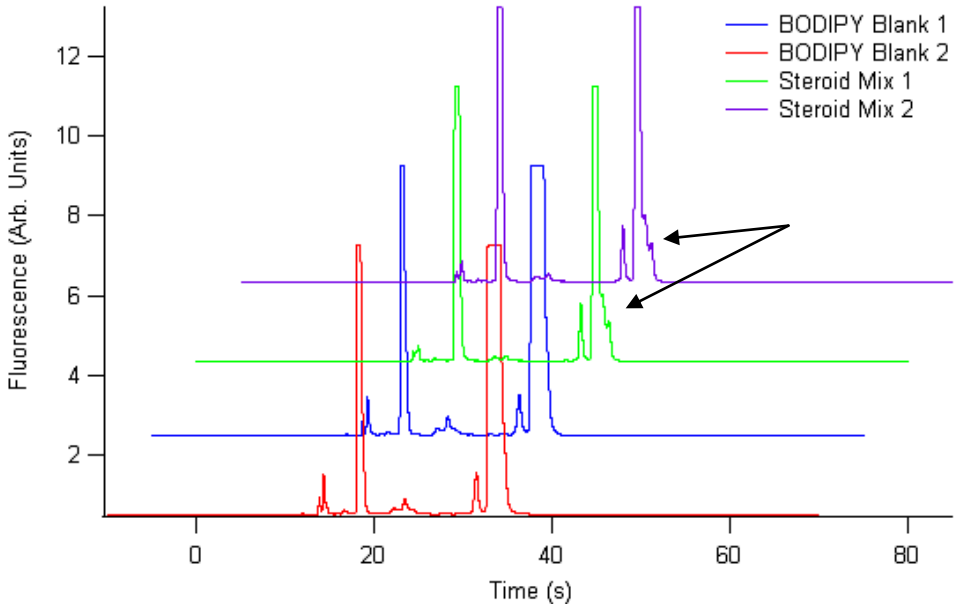

Figure 3.5 – Representative electropherograms of chip based separations of BODIPY FL hydrazide, and a mixture of BODIPY® FL hydrazide, progesterone, 17-

hydroxyprogesterone, and α-ecdysone. Separation buffer was 50 mM sodium borate pH 9.2 with 25 mM SDS, 25 mM sodium cholate, and 10% isopropanol (v/v). A 0.06 s gated injection was used with a separation length of 2.75 cm.

Looking at the separations of the BODIPY® FL hydrazide blank, multiple peaks are clearly seen. These multiple peaks could represent degradation products of the fluorophore, as according to Katayama et al., the labeling solutions prepared with this fluorophore are only good for 3 h, but the labeling reaction itself is carried out for 15 h.[74] Presently the source of these multiple peaks is not definitively known. It also does not appear that any new peaks due to labeled steroids appear in the mixed steroid sample runs, however, a shoulder does appear in the major peak eluting at about 35 s (indicated by arrows). These could be labeled steroids, or additional degradation of the label. With so many peaks appearing in the label blank it is difficult to tell. It should also be noted that the concentrations of the steroids were 2.15 nM, 2.08 nM, and 3.18 nM for α-ecdysone, 20-hydroxyecdysone, and progesterone. These concentrations were probably too low for proof of concept experiments and would undoubtedly make detection of labeled adducts difficult in the midst of such a large excess of label. Two options were initially available to determine if these are labeled adducts: changing the buffer selectivity or reducing the excess of label used in the labeling reaction. Changing the buffer selectivity could aid in the resolution of the minor peaks from the major peak at 35 s, while reduction in the molar excess of the label over the steroids would reduce the amplitude and width of this free label peak and minimize its overshadowing of smaller peaks in its immediate vicinity.

3.3.2.2 Labeling Without TFA – Heat Incubation – 200-Fold Label Excess – Separation in Phosphate Buffer

A few changes were made to the initial labeling and separations methods. After many discussions with organic chemistry faculty, it was decided that TFA should not be necessary to facilitate reaction of the α,β-unsaturated ketone with BODIPY® FL hydrazide, and as such, TFA was removed from the method. Also, due to the question of the lifetime of the label, instead of a 15 h incubation of the fluorophore with the steroids at room temperature, 1 h incubation at 50 – 60 °C in a block heater was employed. The molar ratio of label to steroids was maintained at 200:1, however the concentration of the steroids was increased from nM levels to μM (the corresponding concentration of label had to be increased as well). Finally there was concern that

any labeled derivatives could undergo base hydrolysis as a result of the high pH separation buffer, thus the buffer was changed to a pH 6.8, 10 mM phosphate buffer containing 50 mM SDS and 10% acetonitrile by volume. The details of this protocol were previously outlined in section 3.2.3.2. Equal parts of all three steroid solutions were mixed and were used for on-chip electrophoretic separations along with the blank sample. The results are shown in Figure 3.6.

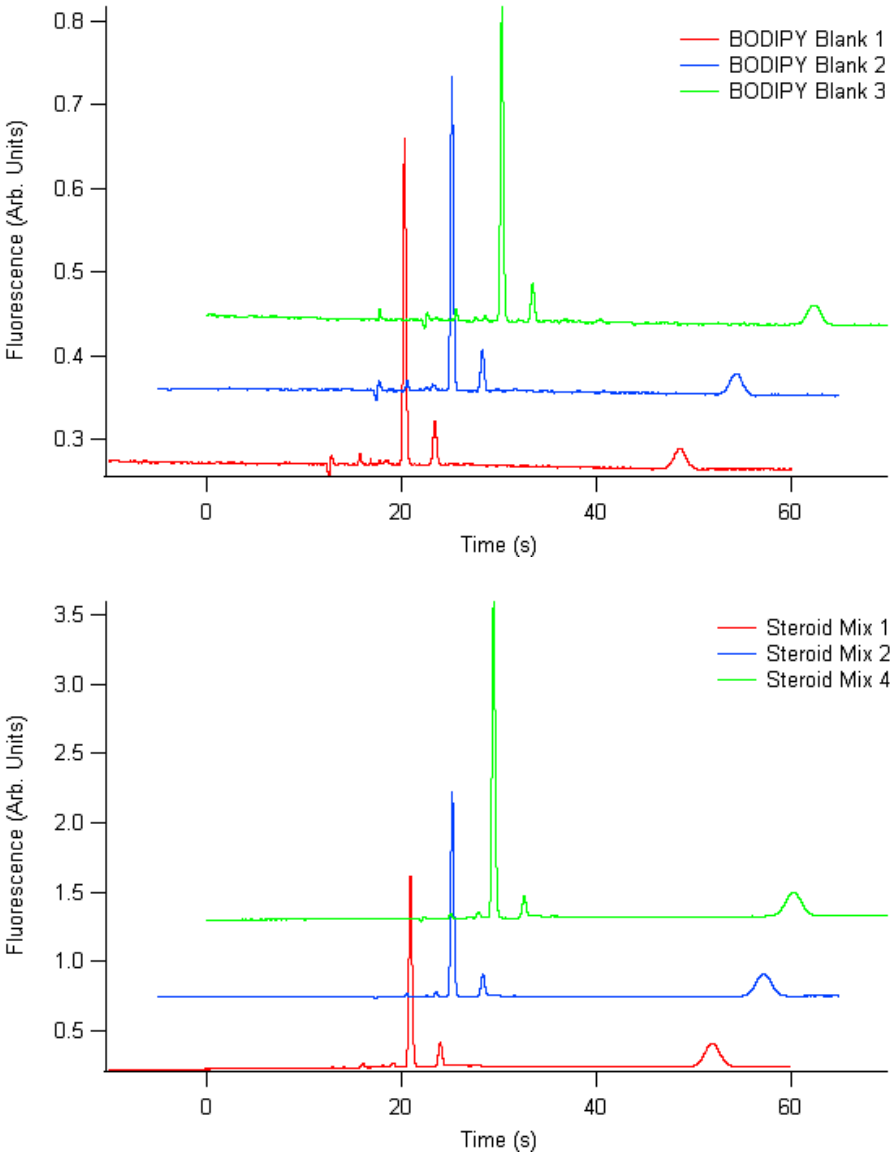

Figure 3.6 – Separations of BODIPY FL hydrazide (TOP) and BODIPY FL hydrazide labeled progesterone, ecdysone, and 20-hydroxyecdysone (BOTTOM). The buffer was 10 mM sodium phosphate pH 6.8 containing 50 mM SDS and 10% acetonitrile (v/v). 0.1 s

gated injection was used. Concentration of label blank, progesterone, α-ecdysone, and 20-hydroxyecdysone are 500 μM, 1.06 μM, 0.72 μM, and 0.69 μM respectively.

These separations illustrate an apparent decreased degradation of the BODIPY® FL hydrazide label as only one major peak appears in the label blank. Some additional minor peaks remain, however these results were obtained with relatively low sensitivity since the concentration of the label was still so high and it was very easy to saturate the detector. While the corresponding concentration of steroids were also increased, to maintain the 200:1 label to steroid ratio, it is conceivable that any peaks corresponding to a labeled analyte could still be overlapped with the dominant label peak as no new peaks appear in the electropherograms of the steroid mixture.

3.3.2.3 Labeling without TFA – Heat Incubation – Equimolar Label and Steroid – Seventh Generation™ Buffer

As has been discussed, with the use of a 200-fold molar excess of fluorophore over the steroid molecule, it is conceivable that the large peaks corresponding to the high concentration of label could easily overshadow any minor peaks resulting from the successful labeling of a steroid. Keeping this in mind, focus was shifted to the labeling of progesterone as it is a much more abundant and economical alternative to ecdysteroids. The separation buffer was also changed to an environmentally friendly buffer developed by Hoeman et al. that uses a commercially available liquid dish soap manufactured by Seventh Generation™.[75] This buffer uses a combination of neutral, anionic, and cationic surfactant molecules and has been shown to produce separations of amino acids with high resolution.[75]

It was observed that following the labeling incubation period, some insoluble residue had precipitated in the vial containing the steroid. If the tagged steroid is insoluble in methanol, it would make detection impossible if it has crashed out of solution. NMR analysis was performed on the residue; however reliable NMR spectra were unattainable as a result of too dilute samples. It is not clear at this time whether the observed residue represents a single compound or a mixture of several. Separations of the remaining supernatant liquid samples are shown in Figure 3.7. While no new peaks are observed in the trace for the sample containing the progesterone, the major peak eluting at approximately 340 s has increased in amplitude dramatically over the minor peak eluting at the same time in the label blank (indicated by arrows). It is therefore

suspected that the major peak in the progesterone trace does in fact represent a fluorescently labeled derivative. There remains, however, the question of the two peaks in the blank trace that elute between 100 and 200 s that have disappeared in the progesterone trace. It is at this time unclear why 5 peaks are observed in the trace for the label blank, while only 1 major and 1 minor peak are observed in the sample containing the progesterone. If the two peaks between 100 and 200 s in the trace for the blank represent decomposition products of the fluorescent tag that are still chemically able to react with progesterone, it would make sense that these two peaks would show up elsewhere on the trace for the sample with progesterone, but since they have disappeared completely it is difficult to determine what these two peaks represent.

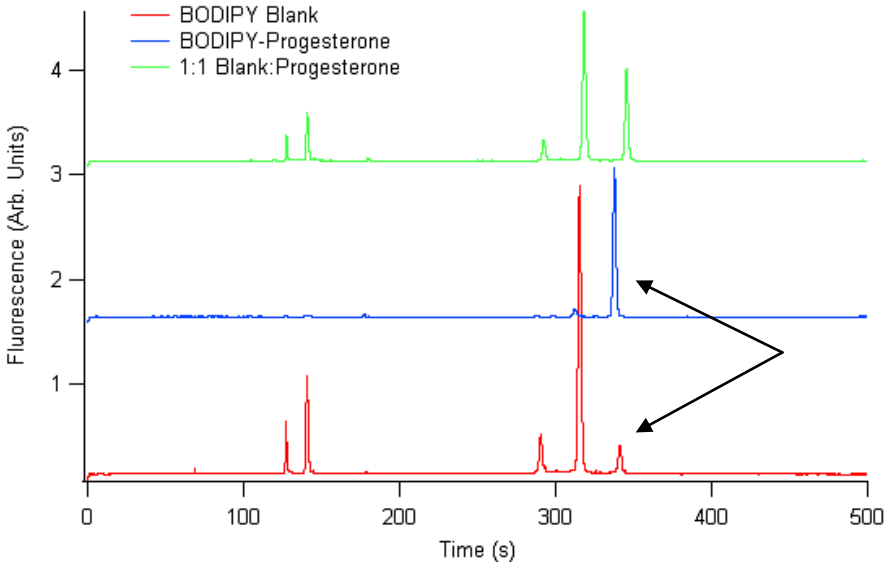

Figure 3.7 – Separations of BODIPY FL hydrazide labeled progesterone. Labeling performed with roughly equimolar concentrations of fluorophore and steroid. Separations conditions were as follows: total capillary length – 40 cm; inner diameter – 50 µm; separation distance – 20 cm; 1 s electrokinetic injection at 175 V/cm; separation electric field strength – 300 V/cm. Separation buffer consisted of 10 mM sodium borate pH 9.1 with 5% Seventh Generation™ liquid dish soap (w/w).

To more confidently identify the peak suspected to be labeled progesterone in Figure 3.7, as well as investigating the ability of these labeling conditions to tag an enone a different analyte, 2-cyclohexene-1-one was used instead of progesterone (Figure 3.8).

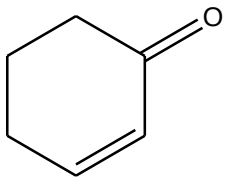

Figure 3.8 – Structure of 2-cyclohexene-1-one

If the increase in peak amplitude observed in the progesterone trace of Figure 3.7 is in fact due to labeled progesterone, by employing this new analyte, successful labeling should result in a migration time shift of this peak. Labeling of 2-cyclohexene-1-one was carried out in the same fashion as that for progesterone, and the final concentrations of 2-cyclohexene-1-one and BODIPY FL hydrazide in the samples was 22.9 μM and 1.6 μM respectively, thus the analyte was in excess of the tag. As seen in Figure 3.9, a shoulder appears to have developed on the peak eluting at approximately 375 s in the sample with the 2-cyclohexene-1-one. It is reasonable that a peak corresponding to labeled 2-cyclohexene-1-one would fail to be fully resolved from the peak corresponding to the free dye as the dye molecule in this case has a molecular mass more than three times that of the analyte molecule, thus a tagged derivative would be similar in mass and size to that of the free label. Also, if the partitioning coefficient of the free dye and dye-2-cylcolehene-1-one complex are similar, both molecules will elute at similar times as they will spend similar amounts of time in the micelles present in the buffer.

It is difficult to identify these peaks based on migration time alone but, at this time it is suspected that the successful labeling of both progesterone (Figure 3.7) and 2-cyclohexene-1-one (Figure 3.9) were carried out since no shoulder was observed in the progesterone sample as with the sample containing 2-cyclohexene-1-one.

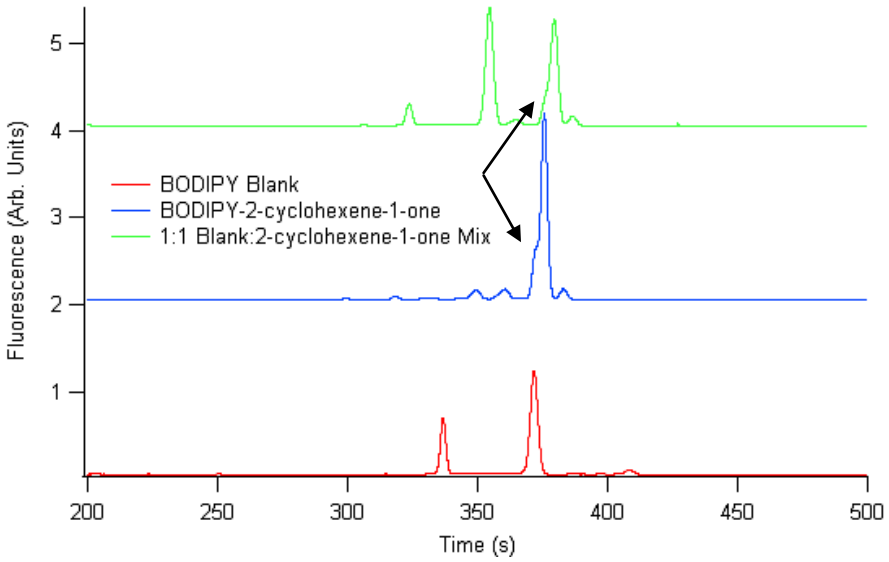

Figure 3.9 – Separation of BODIPY® FL hydrazide and 2-cyclohexene-1-one labeling mixtures. Separation conditions: 40 cm long capillary, 50 µm inner diameter; 20 cm separation; 1 s electrokinetic injection at 175 V/cm; separation electric field strength – 300 V/cm. Separation buffer consisted of 10 mM sodium borate pH 9.1 with 5% Seventh Generation™ liquid dish soap (w/w).

3.3.2.4 Labeling without TFA – Heat Incubation – Equimolar Label and Steroid – Borate Buffer with THF

As previously described, during this labeling procedure, an insoluble residue was formed following the period of sample incubation. If this residue is actually the fluorescently tagged derivative of interest it is vital that it be solubilized and included in the separated samples. To this end an additional step was introduced during sample preparation. Following labeling, the microcentrifuge tubes were placed in a vacuum dessicator and evaporated to dryness. The remaining residue was then dissolved in 100 µL of THF. In an effort to keep everything in solution THF was incorporated into the separation buffer as well. Separations of these samples dissolved in THF and separated in this modified buffer are shown in Figure 3.10.

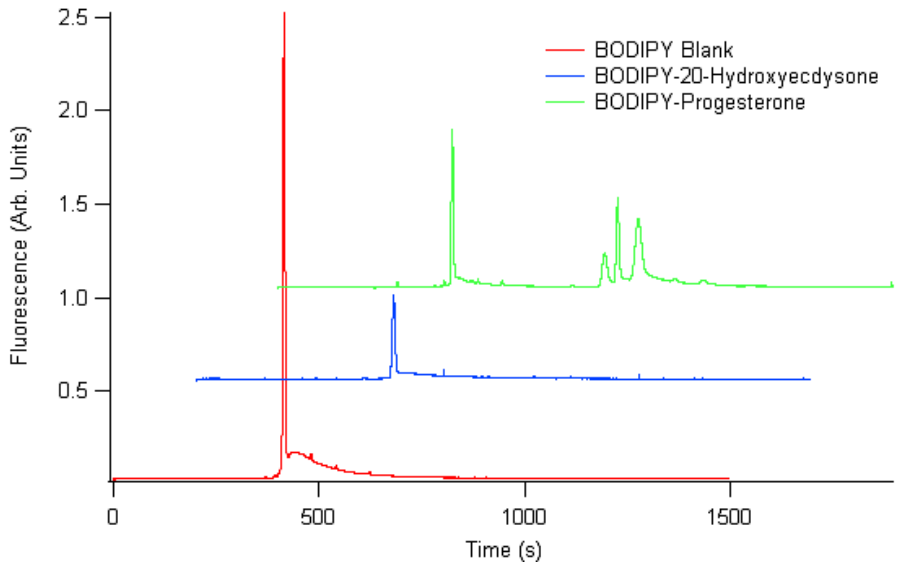

Figure 3.10 – Separations of BODIPY FL hydrazide labeled progesterone and 20-hydroxyecdysone in buffer composed of 10 mM sodium borate pH 9.2 with 50 mM SDS and 30% THF (v/v). Separation conditions: 40 cm capillary with inner diameter of 25 µm; 20 cm separation; 1 s electrokinetic injection at 375 V/cm; separation at 375 V/cm.

The data presented in Figure 3.10 displays both optimistic and contradictory results. Looking at the separation of the sample containing the 20-hydroxyecdysone, no additional peaks are observed when compared to the blank; however the sample containing progesterone shows three new distinct peaks. The appearance of three peaks would be reasonable assuming both carbonyls on the progesterone molecule underwent derivatization. This would produce three distinct derivatives: one peak corresponding to labeling at the ketone, one corresponding to labeling at the enone, and one corresponding to labeling at both sites. If this is the case, then our buffer system is capable of successfully resolving all three of the progesterone derivative peaks. One questions remains: if the α,β-unsaturated ketone on the progesterone molecule was successfully derivatized using this protocol, why then does the α,β-unsaturated ketone on the 20-hydroxyecdysone still fail to react with the fluorescent tag? The answer to this question is still under investigation.

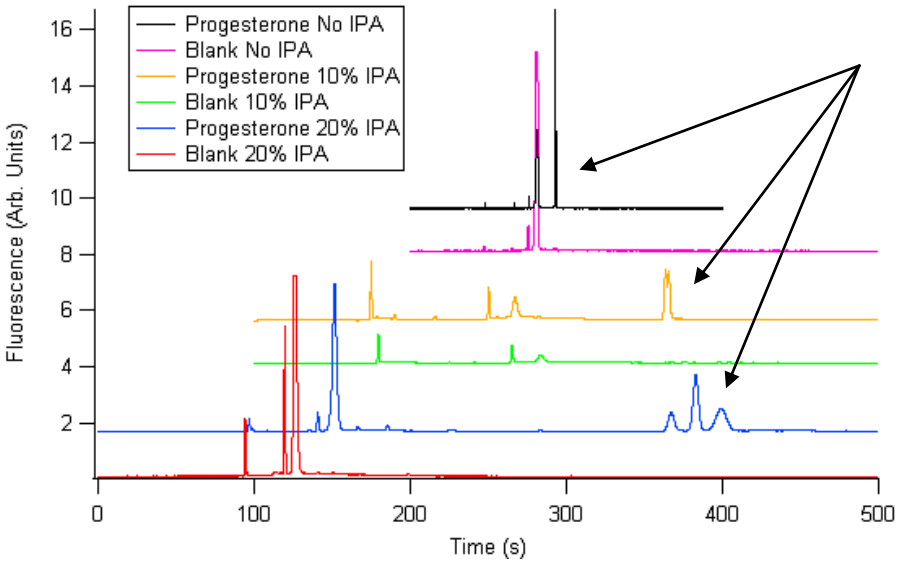

Figure 3.11 – Electropherograms of BODIPY® FL hydrazide labeled progesterone. Separation buffer consisted of 10 mM sodium borate pH 9.1 containing 25 mM SDS and 25 mM SC with either 0%, 10%, or 20% isopropanol (v/v) as indicated in legend. Arrows indicate labeled progesterone peaks. Separation conditions: 40 cm segment of 25 µm inner diameter capillary; 20 cm separation distance; 1 s electrokinetic injection at 500 V/cm; separation under positive polarity at 500 V/cm; DAQ rate of 10 Hz.

In an effort to quantify the amount of progesterone present in the sample, new buffer systems were investigated that would permit the successful resolution of the labeled progesterone peak from that of the unbound fluorophore, but whose selectivity was not so great as to resolve the three different peaks corresponding to the site dependent labeled progesterone. The buffer used for these separations involved a mixed micelle systems using both SDS as well as sodium cholate (SC). In Figure 3.11 the effect of isopropanol as an organic modifier in the buffer can be observed. As isopropanol concentration increases so does peak resolution and as a result, separation time, however by eliminating isopropanol from the buffer entirely, successful separation of the tagged progesterone from the unbound dye is achieved, and the multiply labeled products appear as a single sharp peak thus permitting quantification.

Using a mixed micelle buffer containing both SDS and SC produces a single sharp peak which corresponds to all three labeled progesterone derivatives. Since it is already known that this single sharp peak is actually three overlapping peaks, it is questionable if it is still possible to quantify progesterone from an unresolved and completely overlapped trio of peaks. Using serial

dilutions, a number of samples containing different concentrations of labeled progesterone were prepared and used for separations. Five separations were performed at each concentration and a calibration curve was prepared relating concentration to both the peak amplitude and peak area for the samples. Each of these separations is shown in Figure 3.12. As can be seen in these separations, good migration time reproducibility was achieved. From each set of separations average peak heights and areas were calculated and used to form calibration curves for concentration determination. All of this data is presented in Table 3.1 and the calibration curves can be found in Figure 3.13.

Using both peak amplitudes as well as peak areas yield very linear curves over the concentration ranges examined. These results appear to convey that it is possible to quantify multiply labeled analytes that elute as three distinct peaks by condensing them into a single sharp peak. According to Katayama et al. the clinically relevant levels for progesterone in women's serum falls between the range of 10 ng/mL to 200 ng/mL (31.8 nM to 636 nM), which puts this scheme for the labeling and analysis of progesterone in the clinical range.[74]

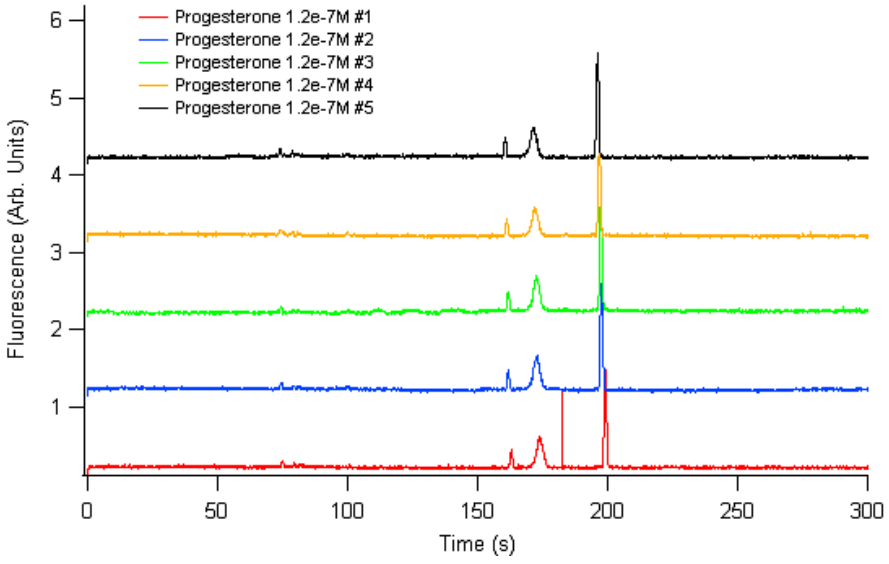

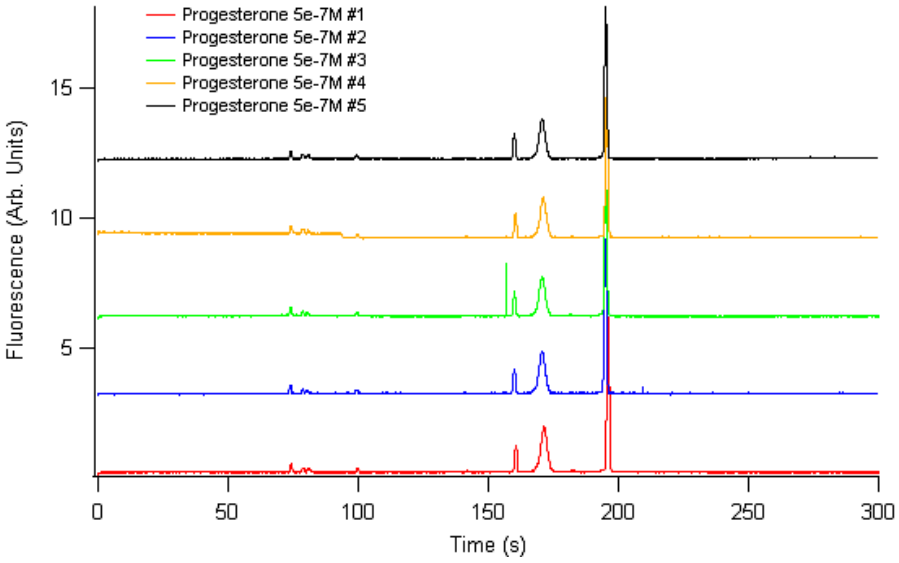
Progesterone 5e-7M #1
Progesterone 5e-7M #2
Progesterone 5e-7M #3
Progesterone 5e-7M #4
Progesterone 5e-7M #5
Fluorescence (Arb. Units)
15
10
5
0
50
100
150
200
250
300
Time (s)

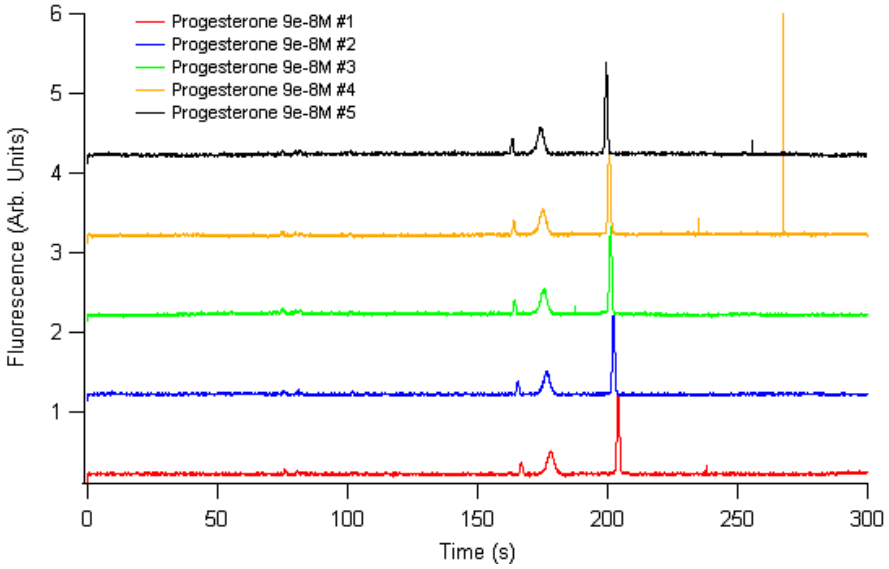
Progesterone 9e-8M #1
Progesterone 9e-8M #2
Progesterone 9e-8M #3
Progesterone 9e-8M #4
Progesterone 9e-8M #5
Fluorescence (Arb. Units)
6
5
4
3
2
1
0
50
100
150
200
250
300
Time (s)

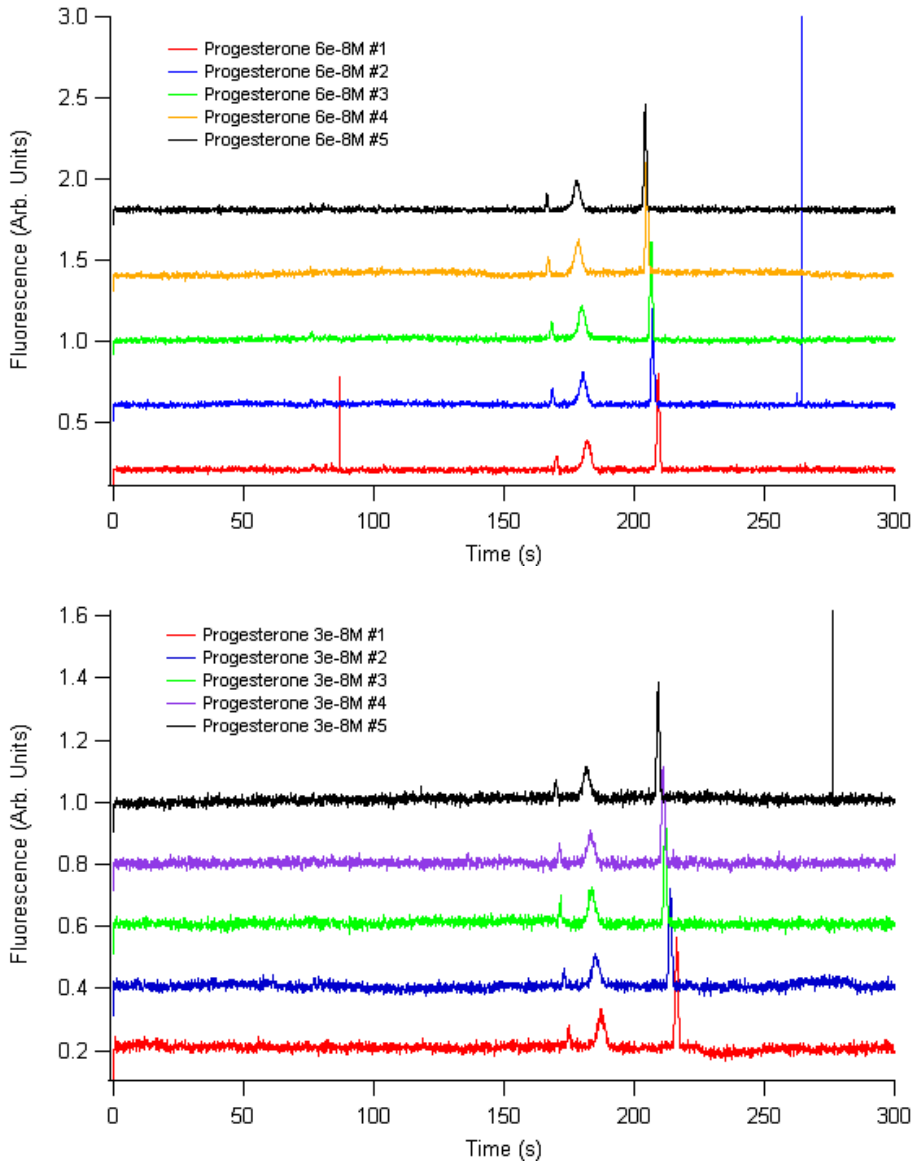

Figure 3.12 – Separations of BODIPY® FL hydrazide labeled progesterone at various concentrations. Separation buffer was 10 mM sodium borate pH 9.1 containing 25 mM SDS and 25 mM SC. Separation conditions for each graph: 40 cm capillary segment with an inner diameter of 25 µm; 20 cm separation distance; 1 s electrokinetic injection at 500 V/cm; separation under positive polarity at 500 V/cm; DAQ rate of 10 Hz.

3.00E-8M Run Data	Peak Area	Plate Number	K1 (Amplitude)	K2 (Migration Time)	K3 ($\sigma_t\sqrt{2}$)
Run 1	0.40827337	186775	0.32539	216.33	0.7079
Run 2	0.455802106	155647	0.335399	213.892	0.766725
Run 3	0.374436905	217458	0.328708	211.917	0.642678
Run 4	0.815304157	91397	0.465896	211.06	0.987315
Run 5	0.414196826	189317	0.343774	209.141	0.679765
	0.493602673	168118.7812	0.3598334		
	0.182145262	48149.80749	0.059706276		

6.00E-8M Run Data	Peak Area	Plate Number	K1 (Amplitude)	K2 (Migration Time)	K3 ($\sigma_t\sqrt{2}$)
Run 1	0.820594174	161451	0.628932	209.149	0.736122
Run 2	0.750652436	178465	0.611051	207.037	0.693085
Run 3	0.805442055	170231	0.642063	206.484	0.707753
Run 4	0.806963835	198022	0.69969	204.746	0.650689
Run 5	0.855905111	169999	0.689698	204.127	0.700151
	0.807911522	175633.8684	0.6542868		
	0.037913828	13886.40128	0.038655612		

9.00E-8M Run Data	Peak Area	Plate Number	K1 (Amplitude)	K2 (Migration Time)	K3 ($\sigma_t\sqrt{2}$)
Run 1	1.340921374	159233	1.04626	204.028	0.723084
Run 2	1.28080938	175513	1.05862	202.213	0.682605
Run 3	1.575590096	150178	1.21178	201.017	0.733575
Run 4	1.474183599	161591	1.17869	200.572	0.70563
Run 5	1.41349782	181445	1.20459	199.406	0.662035
	1.417000454	165591.8455	1.139988		
	0.114857401	12686.38874	0.080980004		

1.20E-7M Run Data	Peak Area	Plate Number	K1 (Amplitude)	K2 (Migration Time)	K3 ($\sigma_t\sqrt{2}$)
Run 1	1.674470993	165823	1.36653	199.063	0.691327
Run 2	1.767690057	169635	1.47024	197.554	0.678333
Run 3	1.95664464	168527	1.62372	197.354	0.67987
Run 4	1.573975423	180311	1.35514	196.759	0.655298
Run 5	1.679393003	177199	1.43837	196.075	0.658729
	1.730434823	172298.9262	1.4508		
	0.143853741	6153.465183	0.108034732		

5.00E-7M Run Data	Peak Area	Plate Number	K1 (Amplitude)	K2 (Migration Time)	K3 ($\sigma_t\sqrt{2}$)
Run 1	8.605791039	156299	6.92749	195.931	0.700874
Run 2	6.721784526	200431	6.16025	194.885	0.615618
Run 3	6.316716947	187024	5.58716	195.056	0.63786
Run 4	6.366343002	208954	5.94126	195.41	0.604556
Run 5	6.569585339	190532	5.86434	195.08	0.632039
	6.916044171	188648	6.0961		
	0.958433553	20024	0.507945027		

Concentration	Peak Amplitude Average	Peak Amplitude Std. Dev.	Peak Area Avg.	Peak Area Std. Dev.
3.00E-08	0.3598334	0.059706276	0.493602673	0.182145262
6.00E-08	0.6542868	0.038655612	0.807911522	0.037913828
9.00E-08	1.139988	0.080980004	1.417000454	0.114857401
1.20E-07	1.4508	0.108034732	1.730434823	0.143853741
5.00E-07	6.0961	0.507945027	6.916044171	0.958433553

Table 3.1 – Peak amplitudes, areas, and plate numbers for each individual BODIPY® FL hydrazide labeled progesterone separation performed in Figure 3.12. Data residing in yellow cells are averages while the data residing in green cells are the corresponding standard deviations.

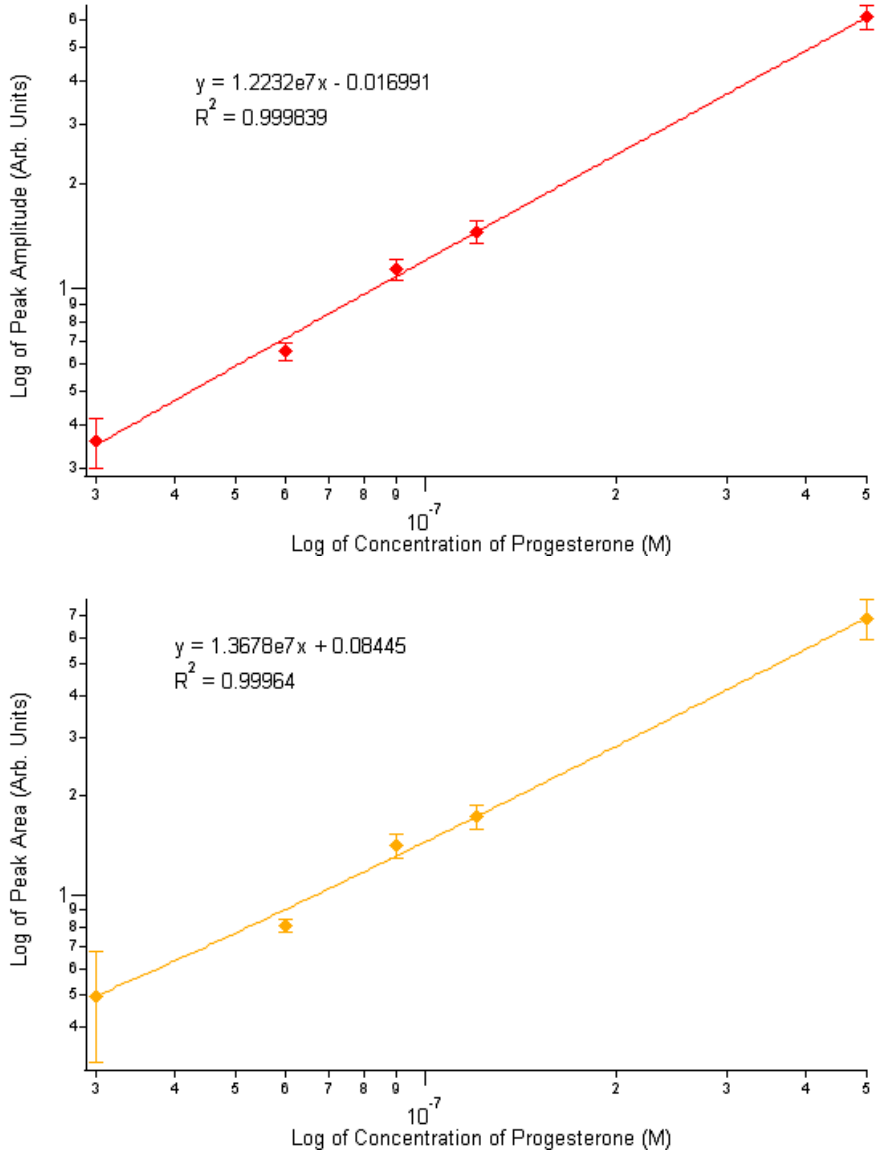

Figure 3.13 – (TOP) Calibration curve for fluorescently labeled progesterone calculated using peak amplitude. (BOTTOM) Calibration curve for fluorescently labeled progesterone calculated using peak area.

While the data for the quantification of progesterone looks very good, this assay falls short in practice, because real samples are bound to contain multiple steroids, as well as their

metabolites. One common metabolite of progesterone is 17-hydroxy progesterone (Figure 3.4) and as shown in Figure 3.14, when a sample mixture contains both progesterone and 17-hydroxyprogesterone, when implementing a buffer similar to the one used for the quantification of progesterone, peaks corresponding to labeled progesterone and 17-hydroxyprogesterone are completely overlapped. The presence of overlapped peaks is confirmed by the addition of isopropanol to the sample buffer which begins to resolve the two sets of multiply labeled derivatives as shown in Figure 3.15.

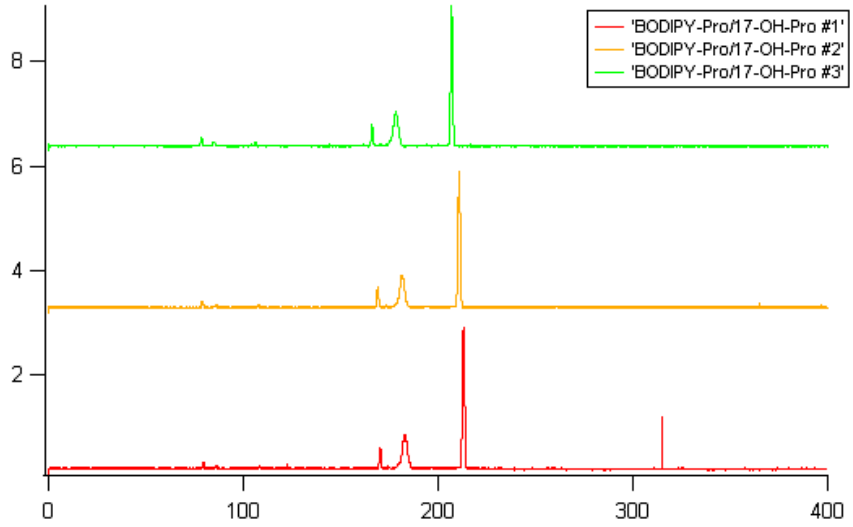

\

Figure 3.14 – Electrophoretic separations of BODIPY® FL hydrazide labeled progesterone and 17-hydroxyprogesterone. Separation buffer consisted of 10 mM sodium borate pH 9.1 with 25 mM SDS, 25 mM SC, and 2 mM β-cyclodextrin. Separation conditions: 40 cm capillary, 20 cm separation distance, 25 μm inner diameter, 4 s electrokinetic injection at 125 V/cm, Separation field strength of 500 V/cm.

Optimally, a buffer that exhibited a high enough selectivity to separate labeled progesterone from labeled 17-hydroxyprogesterone while still keeping the multiply labeled derivatives of each analyte condensed in a single peak would be necessary for the development of a quantitative assay for the detection of progesterone and its metabolites. This would be a very difficult task as a very high selectivity buffer would be required to separate the two steroid molecules since they only differ by a single oxygen atom. A buffer capable of this degree of resolution would also most likely be capable of separating the multiply labeled derivatives, which is undesirable. Of all the buffer systems we examined, we were never able to completely

resolve all of the peaks corresponding to the multiply labeled derivatives. Some of the peaks corresponding to progesterone would always overlap peaks assigned to one of the 17-hydroxyprogesterone derivatives.

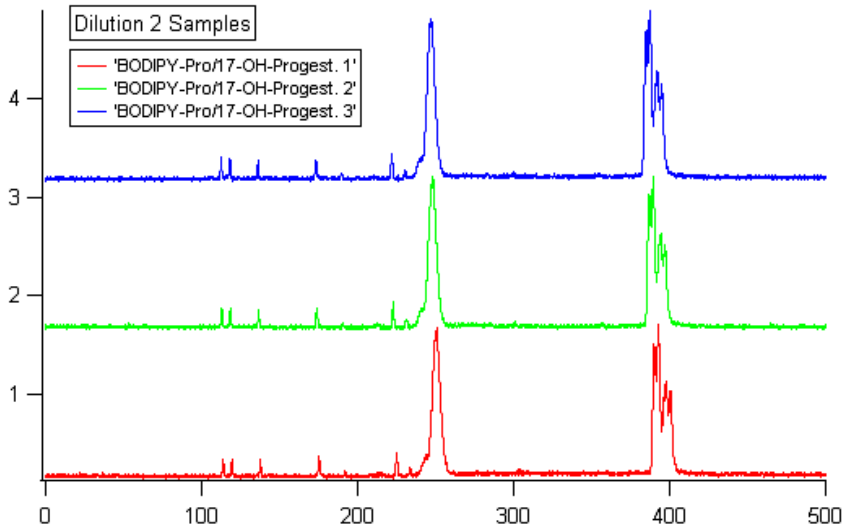

Figure 3.15 – Electrophoretic separations of BODIPY® FL hydrazide labeled progesterone and 17-hydroxyprogesterone. Separation buffer consisted of 10 mM sodium borate pH 9.1 with 25 mM SDS, 25 mM SC, and 10% isopropanol (v/v). Separation conditions: 40 cm capillary, 20 cm separation distance, 25 μm inner diameter, 4 s electrokinetic injection at 125 V/cm, Separation field strength of 500 V/cm.

3.3.2.5 Labeling with TFA – Heat Incubation – 10-Fold Label Excess – Separation in Borate Buffer

In this experiment, labeling was performed using only a 10-fold molar excess of the BODIPY® FL hydrazide over progesterone in order to shrink the peaks corresponding to unbound label. Also, after further consultation of literature, it was decided to proceed by using trifluoroacetic acid as a catalyst as its use to form derivatives with steroids and other hydrazones had been reported.[74,76] Separations were performed using a length of fused silica capillary and resulting electropherograms are shown in Figure 3.16. It is obvious that there are still numerous peaks due to the label itself, but one new small peak does appear in the separation of the sample containing progesterone as indicated by the arrow. This new peak could be due to fluorescently labeled progesterone, and since it is not completely resolved from one of the peaks

corresponding unbound label is only visible due to the reduction from 200 to 10 fold molar excess of the label during the derivatization process.

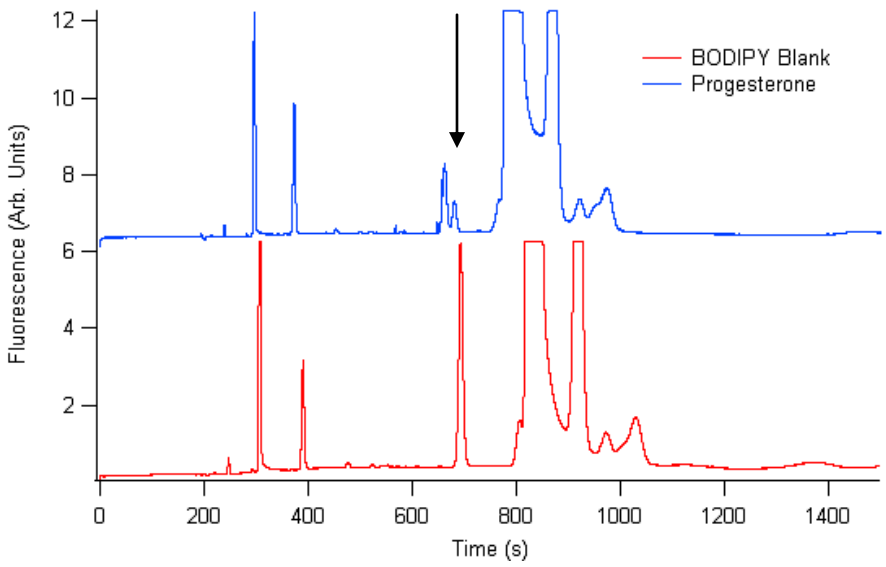

Figure 3.16 – Electrophoretic separation of BODIPY® FL hydrazide and progesterone. Separation performed in a 38 cm segment of 50 µm inner diameter fused silica capillary. The separation distance was 12.5 cm with an electrical field strength of 158 V/cm. Electrokinetic injections were performed for 3 s at 158 V/cm under negative polarity. Concentration of progesterone was 487 nm; concentration of BODIPY® FL hydrazide was 4.87 µM in both traces.

In an attempt to clean up the BODIPY® FL hydrazide traces a small amount of sodium borohydride was added to the labeling cocktails midway through their incubation on the block heater. These samples were then separated in the same manner as those in Figure 3.16. The goal of adding the sodium borohydride was two-fold. First, since the labeled adduct could potentially be destroyed via hydrolysis, the sodium borohydride will reduce the C = N bond to a single C – N bond forming a stable amine linkage. Secondly, the sodium borohydride could partially reduce some of the C = C bonds in the unbound label resulting in the formation of fewer decomposition products and thus fewer peaks in the electropherogram. Upon the addition of $NaBH_4$, our labeling cocktails began bubbling vigorously and the initially deeply yellow solutions turned clear. After the full incubation period, the samples with the sodium borohydride had regained some of their yellow color, but it was still noticeably lighter in color than prior to the $NaBH_4$ addition. The suspicion as to what was happening to the BODIPY FL hydrazide

during the disappearance and reappearance of its color, is that initially complete reduction of the molecule occurs resulting in the solution's clarity, and after all of the $NaBH_4$ has been consumed, the fluorophore is slowly re-oxidized by atmospheric oxygen resulting in the reappearance of the solution's yellow color. Separations of the samples containing sodium borohydride are shown in Figure 3.17.

.

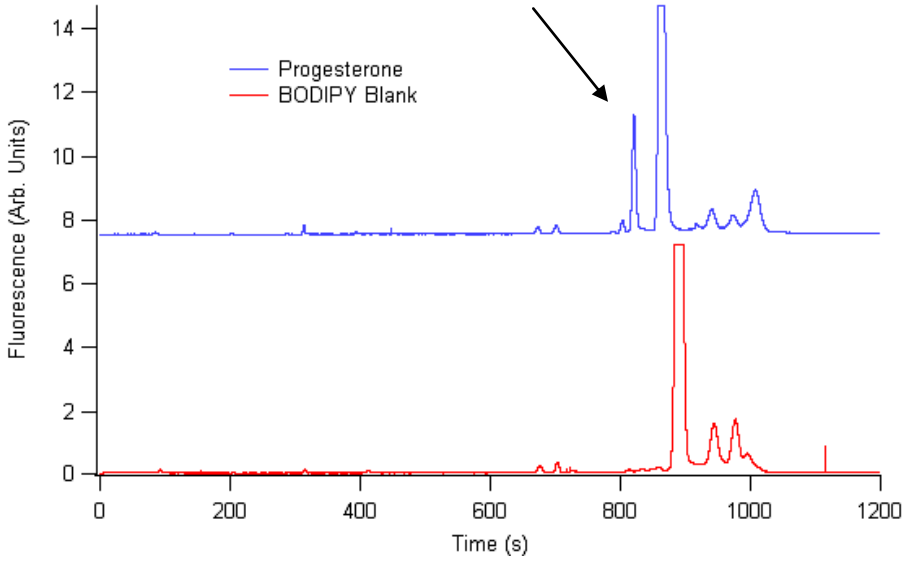

Figure 3.17 – Electrophoretic separation of BODIPY® FL hydrazide and progesterone using sodium borohydride in the labeling solution. Separation performed in a 40 cm segment of 50 µm inner diameter fused silica capillary. The separation distance was 20 cm with an electrical field strength of 250 V/cm under negative polarity. Electrokinetic injections were performed for 3 s at 250 V/cm. Concentration of progesterone was 700 nm; concentration of BODIPY® FL hydrazide was 7.0 µM in both traces.

From the traces in Figure 3.17 the appearance of the labeled progesterone peak at just over 800 s is evident (indicated by arrow). It must also be noted that even though the concentration of BODIPY FL hydrazide is higher in these separations when compared to those in Figure 3.16, the magnitude of the signal for the free label is much lower. This is most likely due to the fact that upon addition of the sodium borohydride, some the free label being reduced does not, with atmospheric oxygen, reoxidise to a fluorescent molecule. This theory is further supported by the color change of the solution observed upon addition of sodium borohydride to the labeling cocktail.

To examine the feasibility of labeling steroid molecules when fluorophore was in short supply, labeling reactions were performed using the same methods described in section 3.2.3.3 with the addition of sodium borohydride, except an excess of the steroid was used. For these derivatization reactions the labeling cocktail contained progesterone and BODIPY FL hydrazide at 11 mM and 490 μM respectively.

Using these conditions, progesterone was in a 23-fold molar excess over the fluorophore. In addition to the differences in the relative concentrations of the steroid and fluorophore, two different buffers were employed as well. The same buffer that was used to perfrom the separations illustrated in Figure 3.16 and was used, as was that same buffer containing 20% methanol by volume. Separations of the mixtures containing an excess of steroid are shown in Figure 3.18.

Labeling reactions using an excess of progesterone over the fluorophore were successfully executed acquiring valuable information. The fact that the labeling reaction can be performed without using a large excess of BODIPY® FL hydrazide is important. This will permit separations of solutions with more dilute concentrations of fluorophore thus diminishing the appearance of large peaks corresponding to unbound reagent. Incorporating lower concentrations of fluorophore should dramatically simplify the process of resolving peaks that represent labeled adducts from peaks corresponding to free label. Using a buffer with a higher concentration of methanol also appears to result in improved peak resolution.

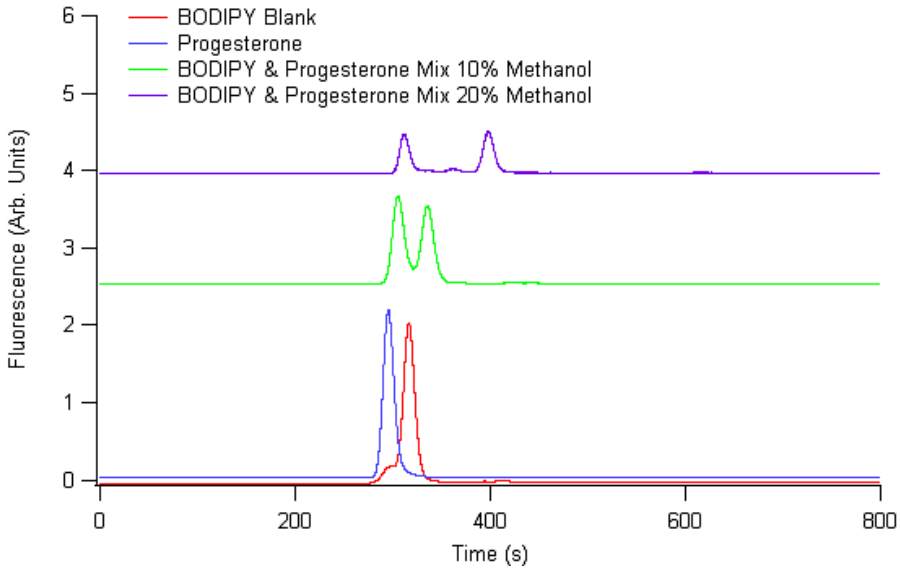

Figure 3.18 – Electropherograms of BODIPY FL hydrazide and progesterone where labeling reactions were performed in an excess of steroid. Separation buffer consisted of 10 mM sodium borate pH 9.2 containing 50 mM SDS and either 10% or 20% methanol by volume as indicated. Separations performed using a 40 cm segment of 50 μm inner diameter fused silica capillary with a separation distance of 20 cm. Separation field strength was 375 V/cm under negative polarity. Electrokinetic injections were performed for 3 s at 375 V/cm. The concentrations of progesterone and BODIPY FL hydrazide are 147 μM and 6.5 μM respectively.

With the knowledge that using a higher concentration of the steroid over the label in the derivatization mixture yields successful labeling for progesterone and electropherograms with minimal peaks corresponding to unbound dye, this same methodology was next applied to 20-hydroxyecdysone. Fresh derivatization solutions were prepared using ratios of fluorophore to hormone of 1:10, 1:1, 10:1, and 100:1. Samples were prepared both with and without using $NaBH_4$ to reduce the carbon to nitrogen double bond. The results of these separations are shown in Figure 3.19.

The data presented in Figure 3.19 show the appearance of a new peak in the green trace (indicated by arrow) corresponding to the sample where labeling was performed using a 10-fold molar excess of the ecdysteroid over the tag with a sodium borohydride reduction step. This could be a result of successful labeling of the 20-hydroxyecdysone. The absence of this peak in the black trace could indicate that without the reduction step, the labeled adduct is quickly hydrolyzed back to unlabeled analyte and free fluorophore. The labeling mixtures using equimolar or greater concentrations of the BODIPY® FL hydrazide did not reveal any new peaks in their electropherograms (data not shown).

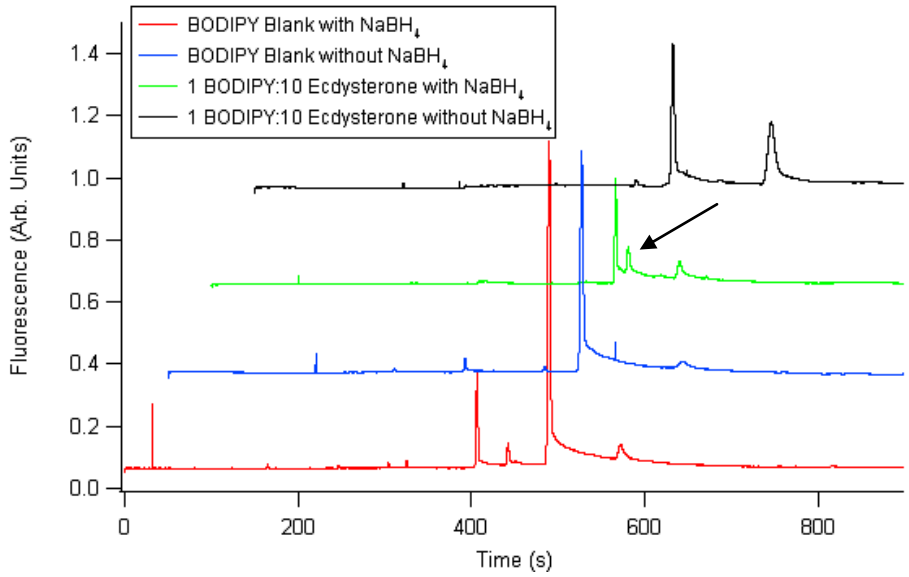

Figure 3.19 – Electropherograms of 20-hydroxyecdysone and BODIPY® FL hydrazide labeling mixtures with and without $NaBH_4$. Separation buffer was 10 mM sodium borate pH 9.2 with 50 mM SDS and 20% HPLC grade methanol (v/v). Separation conditions: 40 cm capillary with an inner diameter of 25 µm; separation distance of 20 cm; 1 s electrokinetic injection at 500 V/cm; separation field strength of 500 V/cm (positive polarity); 25 Hz DAQ rate.

In an attempt to better resolve the peaks in Figure 3.19, those samples were separated in a buffer containing THF as opposed to methanol. Those separations are shown in Figure 3.20. The THF buffer offers a different selectivity and the minor peak that is suspected to represent fluorescently labeled 20-hydroxyecdysone now elutes before the major peak corresponding to free label. Despite the different selectivity, peak resolution is not improved. If the labeling under these conditions is successful, it will make accurate quantitation of ecdysteroids difficult, as the steroid must be in excess over the fluorescent tag.

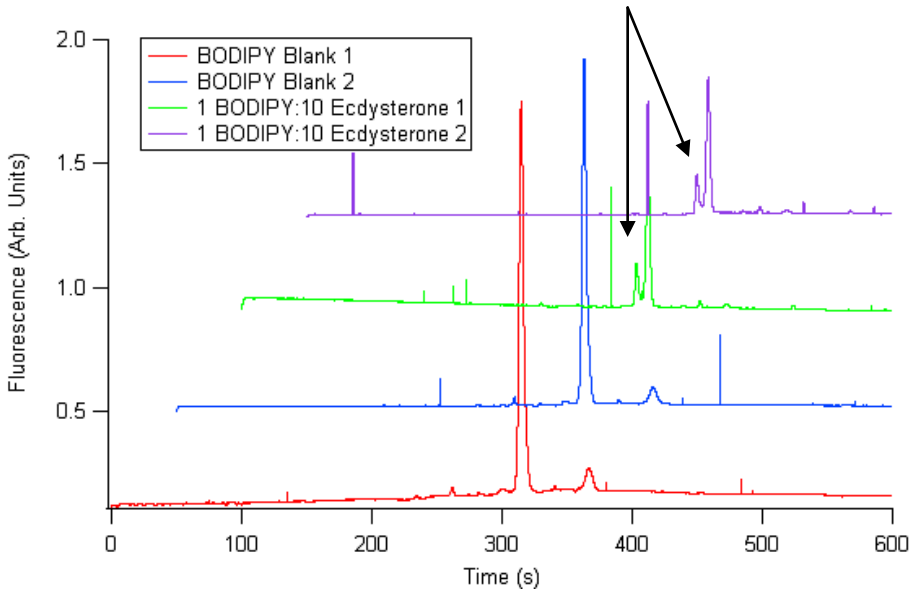

Figure 3.20 – Electropherograms of BODIPY® FL hydrazide labeled ecdysterone samples. Ecdysteroid was present in the labeling cocktail in a 10-fold molar excess over the fluorophore. Separation buffer was 70% 10 mM sodium borate pH 9.2 containing 50 mM SDS (v/v) and 30% THF (v/v). Separation conditions: 40 cm capillary segment with an inner diameter of 25 µm; 20 cm separation; 1 s electrokinetic injection at 500 V/cm; separation field strength of 500 V/cm (positive polarity); 25 Hz DAQ rate.

Now knowing that using a higher concentration of the steroid over the label in the derivatization mixture yields successful labeling for progesterone and, we suspect, 20-hydroxyecdysone, as wells as fewer peaks corresponding to unbound dye, this same methodology was next applied to α-ecdysone. Fresh derivatization mixtures were prepared using an excess of steroid over label. The concentrations of progesterone and BODIPY FL hydrazide were 11 mM and 490 µM respectively. The concentrations of α-ecdysone and BODIPY FL hydrazide were 1.7 mM and 400 µM respectively. The blank contained BODIPY FL hydrazide at a concentration of 490 µM. Separations of these samples are shown in Figure 3.21.

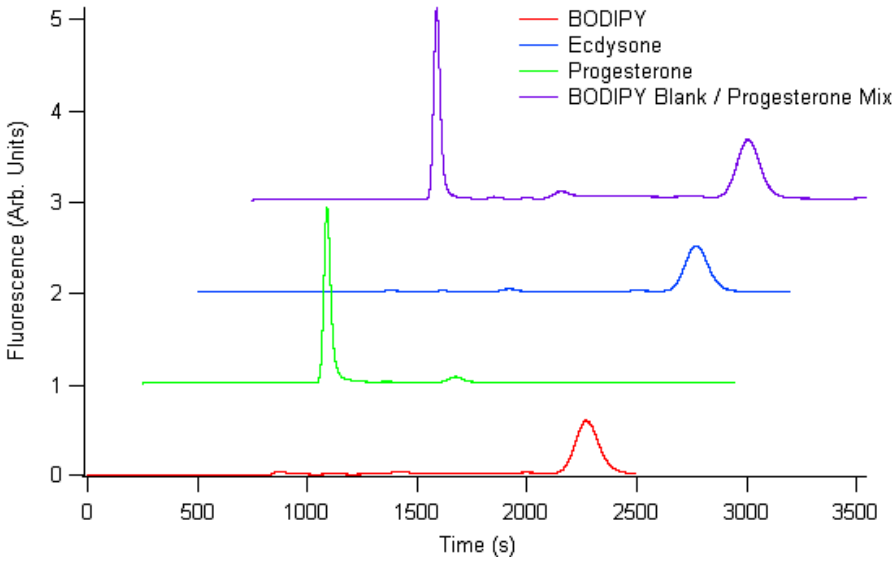

Figure 3.21 – Separations of progesterone and α-ecdysone labeled with BODIPY® FL hydrazide. Steroids present in the derivatization mixture in excess of label. Separation buffer was 10 mM sodium borate pH 9.2 containing 50 mM SDS and 20% methanol by volume.

Immediately, it can be seen from the above separations that while the labeling of the progesterone was successful, the labeling of the α-ecdysone failed. Since the progesterone molecule contains both a ketone and an α,β-unsaturated ketone, it is possible that the fluorescent tag is targeting the ketone and not the enone which would explain successful derivatization of progesterone and not the ecdysteroid. This type of labeling would further explain why only one peak has been observed for the fluorescently tagged progesterone. The BODIPY® FL hydrazide should tag both the ketone and enone on progesterone, and if both of these sites are viable targets the formation of three distinctly different labeled products is observed as in Figure 3.10. It is therefore suspected that these labeling conditions are only conducive to the labeling of the ketone group on the progesterone; however this cannot be confirmed as separation in buffers containing isopropanol or THF were the only systems to successfully resolve the multiple derivatives, and these buffers were not investigated with these samples, so while only one peak for labeled progesterone is observed, it may actually be three entirely overlapped peaks, as we have already demonstrated that it is possible to collapse the trio of multiply labeled derivative peaks into a single peak by altering the separation buffer. It is also useful to note that these samples were only incubated for 1 h at 60 °C instead of the 12 h at 60 °C used for the samples that yielded

multiple peaks. This shortened incubation time was chosen for the preservation of the label's integrity, but in the process we may have sacrificed the necessary time required for tagging at the enone.

3.3.2.6 Labeling with TFA – Heat Incubation - 10-Fold Label Excess – Separation in 7th Generation Buffer – Addition of Magnesium Sulfate

It is possible that the failure of the enone to label even in the presence of excess steroid could be a result of the system equilibrium. The reaction of a hydrazide with a ketone or enone produces water as a byproduct, thus the elimination of water from the labeling mixture could be used to help drive the equilibrium to the products side. To this end, small amounts of magnesium sulfate were added to the labeling mixture to serve as a water scavenger thus helping to shift the equilibrium to favoring the production of a labeled derivative. As it has already been shown in, Figure 3.18, and Figure 3.21, a 200-fold excess of the fluorophore is not necessary for successful labeling of progesterone, thus tagging of the ecdysteroid was attempted using both an equimolar mixture of the label and steroid as well as a 10-fold molar excess of the label over the steroid. Electropherograms from these separations are shown in Figure 3.22.

From these separations, no new peaks are observed in either the equimolar labeling mixtures or the samples containing a 10-fold molar excess of the fluorophore. It appears that maintaining a water free environment does not ensure a product favored equilibrium. These results also further confirm those seen in Figure 3.21 where the labeling of α-ecdysone is unsuccessful despite the ability to label progesterone under the same conditions. This data conveys that the enone groups on the ecdysteroids possess significantly lower reactivity than the ketones present on progesterone. The lack of enone reactivity could stem from the resonance stabilization of the carbonyl group by the nearby alkene group.

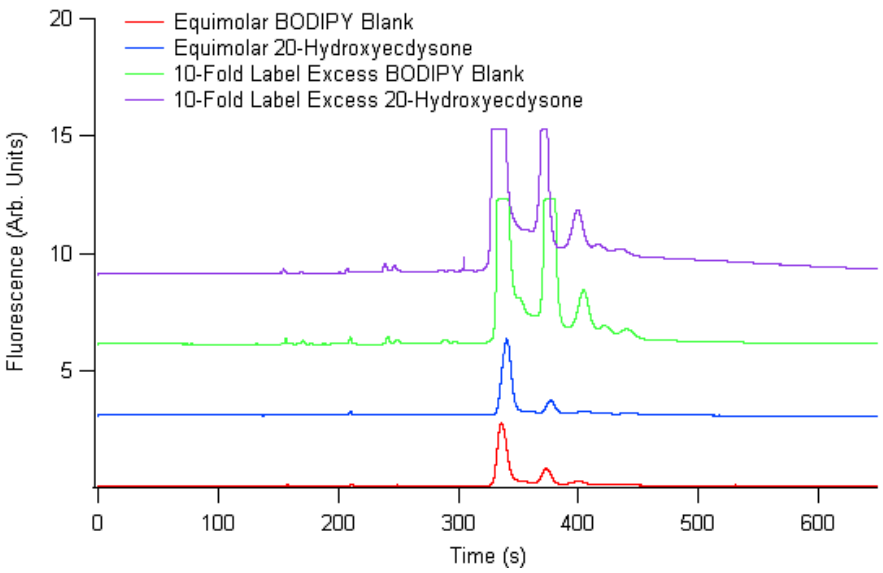

Figure 3.22 – Electropherograms of equimolar and 10-fold molar excess of label mixtures of BODIPY® FL hydrazide and 20-hydroxyecdysone. Anhydrous $MgSO_4$ was added to the labeling mixture as a water scavenger to help push the equilibrium towards the formation of the labeled products. Separation conditions are as follows: total capillary length was 40 cm; separation distance was 20 cm; inner diameter was 50 µm; electrokinetic injections of 1 s were performed at 125 V/cm; separations performed at 250 V/cm; data acquisition rate was 25 Hz.

3.4 Conclusions

At present, the analysis of ecdysteroids by electrophoresis with fluorescence detection is still under investigation. Successful labeling and quantitation of the model steroid progesterone was achieved, but due to a difference in the reactivity of the functional groups on progesterone versus the corresponding enone on the ecdysteroid molecules, a reliable method for fluorescent labeling was not developed. Failure to reliably tag these ecdysteroids with a fluorophore limits their analysis to detection methods where the sensitivity is simply too low for analysis at the single insect level. Some of the results with progesterone presented in this chapter paint an optimistic picture for the feasibility of tagging these insect hormones, however in practice they fail to result in a successful approach to labeling when applied to the ecdysteroids. A more practical limitation to this project stems from the very high cost of the reagents. Both the BODIPY® FL hydrazide as well as the ecdysteroids cost more than $100.00 for just a few mg.

These financial burdens made repeat trials difficult to perform, and with the limited total mass of insect hormones available, higher concentration labeling solutions were difficult to prepare. The success with the labeling of both the ketone and the enone on the progesterone molecule perpetuates optimism regarding the possibility of labeling these ecdysteroids with a similar method. With the constant introduction of new commercial fluorescent tags, perhaps a new label will be developed making the labeling of the enone more reliable, as is necessary when working with low concentrations. Alternatively, the development of a more efficient synthetic pathway with high yields could increase the affordability and availability of artificially prepared ecdysteroids, making multiple iterations and procedure development much more cost effective.

Chapter 4 - Micro-Immunoaffinity Purification of Insect Serine Protease Inhibitors

4.1 Introduction

Global cases of malaria amount to 350-500 million annually of which over 1 million result in death. Most of these deaths occur in sub-Saharan Africa.[4] Mosquitoes of the species *Anopheles gambiae* are the leading source of malaria transmission in this region.[77] *Plasmodium falciparum* is the protozoan parasite responsible for malaria, and its transmission by *Anopheles gambiae* is highly efficient. This species of mosquito is highly anthropophilic which increases the likelihood of transmission of the parasite to humans.[77] As treatments and preventative measures for malaria continue to develop, new difficulties arise as the parasite begins to become resistant to current drugs and the transmission vectors resistant to insecticides.[77] Current investigations focus on disrupting the development of *Plasmodium falciparum* within its host and thus preventing transmission to humans. This involves a careful examination of the immune response of *Anopheles gambiae* and an understanding of how the parasite is able to develop in vivo and how the insect subsequently transmits it to humans.

4.1.1 Propogation of Malaria

Plasmodium falciparum sexual reproduction occurs within its host mosquito. When a mosquito ingests a blood meal containing the parasitic gametocytes, the gametocytes make their way to the midgut of the insect where gametogenesis (cell division) occurs. The resulting gametes are fertilized producing a zygote. Following meiosis, the zygote matures into an ookinete which is capable of transversing the midgut epithelial tissue. The formation of the ookinete within the insect occurs within about 1 day of the insect's ingestion of the parasite, and the ookinete will take up residence in the outer lining of the gut wall forming an oocyst.[77] The oocyst will reside here and produce sporozoites which after a period of about two weeks from the time of parasite ingestion, are released into the mosquito's hemocoel. Once the sporozoites have invaded the insect's circulatory system they are able to gain access to the salivary glands. The sporozoites will penetrate the salivary gland epithelial tissue which results in their mixing with the insect's saliva. Once in the saliva, these sporozoites will be transmitted to the next host fed

upon by the mosquito.[77] Successful transmission of the Plasmodium falciparum parasite implies an ability to overcome or subvert the host mosquito's immune system.[77]

4.1.2 Serpins

The life cycle of the malaria parasite within its host mosquito involves its residence in a variety of internal organs as well as the transversal of multiple epithelial tissues which expose the parasite to numerous opportunities for defeat by immune response. Some immune responses in insects are regulated by serine protease inhibitors, or "serpins".[78]

Serpins are proteins of 350 to 500 residues in length (~50 kDa) whose most common function is the inhibition of serine proteases. Proteins belonging to the superfamily of serpins are classified both by their structure as well as the mechanism of their inhibitory action.[79,80] The tertiary structure of a serpin is defined by the presence of a reaction center loop (RCL) near the C-terminus; a result of the folding of 3 β-sheets and 7-9 α-helices.[78] The RCL is ultimately responsible for the specificity of the serpin for its target protease, and the alteration of a single residue in the protein encoding gene can result in the targeting of a completely different substrate.[81] Serpins will generally adopt one of two conformations; one with the RCL completely inserted into the protein, and one where the RCL is primarily exposed.[81] By transitioning from the RCL exposed to the RCL inserted conformation, serpins are able to trap their target protease allowing them to act as covalent suicide inhibitors.[81] Conformation transformation is initiated through the reaction of the active serine residue on the protease with the RCL of the serpin. This indicates that the proteases are active before they will interact with the serpin. Cleavage of the scissile bond of the RCL leads to dramatic conformational changes in which the RCL moves approximately 70 Å to the opposite end of the serpin dragging with it the bound protease (Figure 4.1). The change in conformation does not dramatically affect the serpin, however it can lead to a greater than 35 % loss in native protease structure.[82] The loss in function of the protease is a result of the shifting of the serine from the active site as well as disturbance of the reactive site geometry. The structural disruption prevents the release of the protease and results in its deactivation.[82] When the RCL is cleaved, the subsequent conformational change leads to an incorporation of the RCL into the A β-sheet in the core of the protein while the rest of the molecule maintains a structure very similar to that of the un-cleaved state.[81] Incorporation of the RCL into the A β-sheet also results in the repositioning of the target

protease to the distal end of the serpin, with simultaneous distortion of the protease active site. The trapping and distortion of the target protease renders it inactive.[78,81] More than 500 serpins have been identified, and most operate as proteinase inhibitors, however evolution has led to some serpins serving other biological roles such as hormone transport, regulators of blood pressure, and storage proteins.[78,79,83] Coincidently, in *Maduca sexta*, the hormone 20-hydroxyecdysone serves to negatively regulate expression of serpin-1.[81]

The ability to isolate and analyze serpins specific to *A. gambiae* will lead to a better understanding of how they function in conjunction with the insect's life cycle and immune response and hopefully shed light on how the malaria parasite is able to escape destruction within its host mosquito.

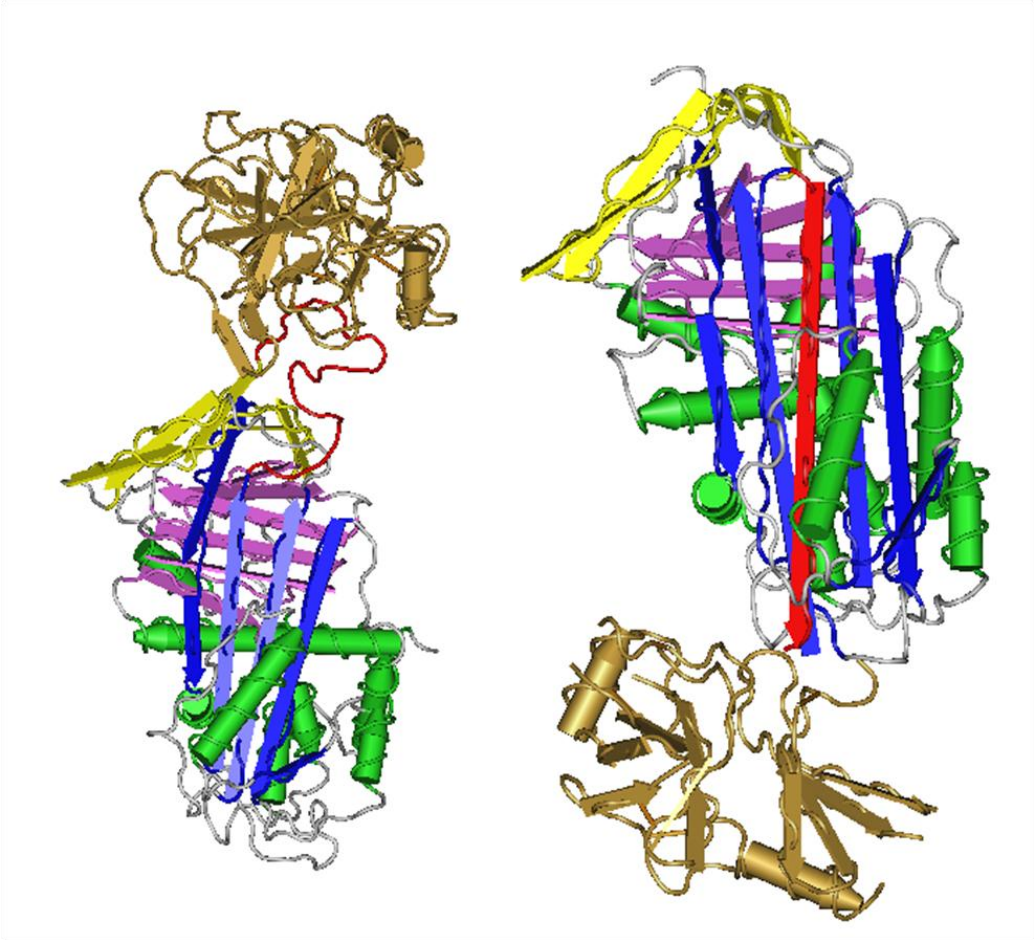

Figure 4.1 – Left: Non-covalent interaction of insect Serpin1K and mutated inactive rat trypsin (1K9O) with the reactive center loop depicted in red. Right: Covalent complex between antitrypsin and inactive trypsin (1EZX). The protease has cleaved the RCL (red)

which has inserted itself into the A β-sheet of the serpin. Upon cleavage the protease is dragged to the opposite pole of the serpin where it is covalently trapped and structurally deformed leading to inactivation. Image was prepared using Cn3D 4.1.

4.2 Insect Immune Response

The immune system of insects is regulated by genetically encoded physiological responses to different types of foreign molecules. Since insects don't produce antibodies, they rely on innate rather than acquired immunity to fend off invading substances and pathogens.[84] The innate immune response of insects can be divided into two segments, cellular reaction and humoral reaction. The cellular responses are dominated by phagocytosis while humoral responses involve 4 distinct steps: recognition, modulation, activation, and replenishment.[77,84] Most of what is known about the immune response of insects is based on research performed on *Manduca sexta* as its large size permit the collection of larger volumes of hemolymph and thus a greater number of the molecules that the insect releases in response to an immune challenge.[77,85]

4.2.1 Cellular Immune Reactions

Found in the hemolymph of invertebrates, hemocytes are responsible for the phagocytosis of foreign microbes. In addition to phagocytosis, which occurs predominantly at low concentrations of invading microbes, hemocytes can form aggregates around invading microbes trapping them within what is known as a nodule when these microbes appear in higher concentrations.[84,85]

4.2.2 Humoral Immune Reactions

The initiation of the humoral immune response in insects first requires the recognition of the foreign invader within the insect. The cell walls of many foreign microorganisms contain components not native to the insect such as lipopolysaccharides, peptidoglycans, and β-1,3-glycans.[77,84] The detection of these molecules stimulates the production and release of "effector molecules" which initiate the activation of different serine proteases.[77,84] The molecules responsible for microbe recognition are called pattern recognition receptors (PRR) and include peptidoglycan recognition proteins (PGRP), which participate in the synthesis of antimicrobial peptides, initiation of the proPO cascade resulting in melanization, and phagocytosis of $Gram^-$ bacteria; C-type lectins or immunolectins (IML) which bind lipopolysaccharides and encourage

phagocytosis, nodule formation, and stimulate the activation of proPO; and thioester containing proteins (TEP) which bind the surface of bacteria promoting phagocytosis.[77,85,86] The most important proteolytic cascade in terms of the species *Anopheles gambiae* is the conversion of inactive proPO to PO which promotes melanization. The result of successful and efficient melanotic encapsulation of *Plasmodium falciparum* would be a mosquito that self-prevents the propogation and transmission of the malaria parasite.[77]

Phenoloxidase (PO) is an enzyme that performs a number of functions in arthropods. It is secreted in an inactive form known as prophenoloxidase (proPO), and once cleaved at a specific site it becomes active and contributes to the healing of wounds, the synthesis of melanin, the synthesis of quinones which are used to repair the arthropod cuticle, and the killing of invading microbes through encapsulation. More specifically, monophenols are hydroxylated by PO to *o*-diphenols resembling dopamine. These o-diphenols are then oxidized to quinones. These quinones will udergo subsequent reactions and polymerization resulting ultimately in the deposition of melanin on the surface of foreign microbes.[80,81,86] The activation of phenoloxidase is the result of certain proteases present in the insect hemolymph.[81,85] When this process of proPO activation is impeded by serine protease inhibitors, immune response pathways that ultimately lead to the killing of the malaria parasite are blocked. Understanding how *Plasmodium falciparum* is able to use these serpins to circumvent the mosquito's immune system thus requires an understanding of the structure and function of the mosquito serpins themselves. This is no trivial endeavor as mosquitoes themselves are very small yielding only a few nL of serpin containing hemolymph per insect. Therefore the development of a method able of isolating and purifying these serpins could help to provide biochemists and etymologists with invaluable information and ultimately insights on how to stimulate the immune system of mosquitoes to attack and/or kill the malaria parasite and thus minimize or prevent transmission of the parasite to humans.

4.3 Immunoaffinity Chromatography

Immunoaffinity chromatography is just one particular area within the broader scope of affinity chromatography. This type of separation technique exploits the tendencies of some molecules to form strong, non-covalent, reversible interactions. Some of the molecular pairs typically examined using affinity chromatography are antibodies and antigens, enzymes and

substrates, and ligands and receptors.[10] This technique is most commonly applied to biomolecule analysis and more specifically, protein analysis, as some of the more prevalent chromatographic methods lack the required specificity.

Immunoaffinity chromatography (IAC) specifically focuses on interactions between antibodies and their antigens. In IAC the molecule that will be used to capture the desired analyte is more commonly an antibody (as opposed to its target protein however the opposite experiment can also be performed and used to isolate antibodies) and is also referred to as the affinant.[10] Initially the antibody must first be immobilized onto a solid support, typically small beads, whose composition can be any number of materials such as porous glass, agarose, polystyrene, or polyacrylamide. Once the affinant is secured onto the support, binding of the target molecule can be performed. The binding process can either be performed using a tube based format where the insoluble support to which the antibody has been linked can be mixed with the solution containing the target antigen and then isolation of the bound antigen is achieved using centrifugation, or in a column flow through format where the antibody linked beads form a packed bed within a column and the antigen containing solution flows through this bed which retains the target molecule and discards the concomitant solution.[10] For our purposes we will focus on the column flow through format. In order to maximize the surface coverage of the antibodies on the solid support, the pH as well as the ionic strength of the binding solution should be optimized.[10] The pH and ionic strength is also important when the antigen containing solution is flowed past the antibody bed, as binding of the antigen to the antibody will be affected as well. Once the antigens have been retained on the column bed, they can be released via application of a different buffer with altered pH and ionic strength.[6,10]

4.3.1 Antibodies

Antibodies are proteins consisting of two light chains of identical amino acid sequence as well as two heavy amino acid chains, again, with identical sequence as shown in Figure 4.2. The light chains are composed of approximately 210 amino acid residues while the heavy chains are larger with the number of amino acids usually falling between 450 – 575.[87] There are two different types of light chains, κ, and λ, and five known classes of heavy chains, α, δ, ε, γ, and μ, and either light chain may combine with any of the heavy chain varieties to form the anitibody.[88] These light and heavy chains are held together with the disulfide bonds formed between cysteine

residues forming the tertiary structure of the antibody. Ultimately the class or isotype of the antibody is determined by which type of heavy chain is present resulting in either IgA, IgD, IgE, IgG, or IgM antibodies.[87,88]

Both the light and heavy chains can be broken down in to subunits called domains. Domains are typically 100 – 200 amino acids long, and the variable domains (V) tend to be slightly longer than the constant (C) ones.[87] The COOH-terminal of both the light and heavy chains possesses a conserved amino acid sequence specific to that antibody's class. For example, all IgGs will have the same sequence at the COOH-terminus. It is at the NH_2-terminus of the heavy and light chains where amino acid sequence variability arises, and it is variations in this sequence that lends to the extensive variety of binding site structures adopted by antibodies and ultimately results in the number of binding specificities that are exhibited by different antibodies.[87] Not all residues in the variable region exhibit the same likelihood of variability. Some amino acids are much more likely to vary and are labeled "hypervariable".[88,89] It is these hypervariable regions, or complementarity determining regions (CDRs) , of both the heavy and light chains that comprise the binding site for the non-covalent attachment of the antigen's corresponding binding site or epitope.[88,89]

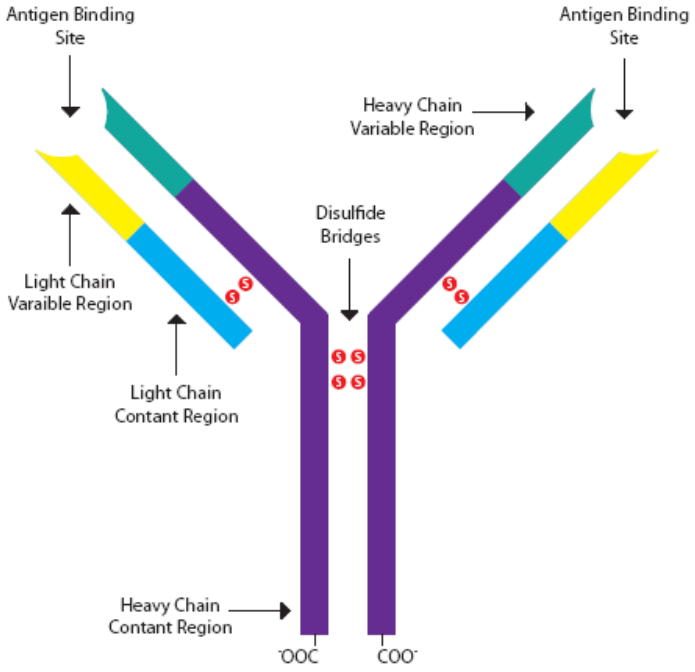

Figure 4.2 – General structure of a divalent (capable of binding two molecules of antigen) antibody

4.3.1.1 Antibody – Antigen Affinity

Specifically binding a target molecule forming an antibody-antigen complex is by far the most important function of an antibody. It is these antibody-antigen complexes that are recognized by the immune system and result in the subsequent destruction or sequestering of foreign pathogens and molecules. The binding of an antigen's epitope by an antibody is a result of common intermolecular forces such as hydrogen bonding, ionic bonding, Van der Waals interactions, and hydrophobic interactions.[88] Just as there are attractive forces between antibodies and their antigen likewise are there repulsive forces between antibodies and molecules not in possession of the appropriate epitope. These repulsive forces are driven by steric factors resulting from the shape of the electron clouds on the antibody binding site and the proposed epitope of a foreign molecule. The less the shape of the electron cloud on the potential epitope complements that possessed by the antibody binding site, the stronger these repulsive forces will be. It is therefore the repulsive forces that permit the antibody to prevent the binding of inappropriate target molecules.[88]

The quantitative measurement of an antibody's affinity for its corresponding antigen is given by the association constant K which possesses the units of L/mol.[90] The calculation of the association constant stems from an equilibrium interaction between bound and unbound antigen in the presence of binding sites of equal affinity for the antigen. The association constant represents an average affinity as most binding sites exhibit slightly varied affinities towards one antigen.[90] According to the Law of Mass Action, the rate of formation of the antibody-antigen complex is directly proportional to the individual concentrations of both the antibody and antigen and thus equals $k_a[Ab][Ag]$. Likewise, the rate of dissociation of the assembled antibody antigen complex is $k_d[AbAg]$. With the system at equilibrium both processes are occurring simultaneously and thus the rates of association and dissociation are equal as shown in equation (4.1).

$$k_a[Ab][Ag] = k_d[AbAg] \tag{4.1}$$

The relationship depicted above can be rearranged to provide the overall association constant for the antibody-antigen binding event as shown in equation (4.2).

$$\frac{k_a}{k_d} = \frac{[AbAg]}{[Ab][Ag]} = K \tag{4.2}$$

Experimental determination of the association constant is far from trivial due to the inevitable heterogeneity of a population of antibodies' affinity for an antigen. The source of the heterogeneous affinity is a reflection of the cells that produced those antibodies. The cells that produce antibodies will have immunoglobulins on their surface. These immunoglobulins are receptors for the antigen that the antibodies will target. If the cell's receptors exhibit a high affinity for the antigen, high affinity antibodies will be produced, however cells with receptors exhibiting lower affinity for the antigen will produce antibodies of reduced affinity.[88] Measurements must be made in near ideal conditions using purified antibody and antigen where the equilibrium concentrations of bound and unbound antigen are known. Even measurements made under the most ideal of conditions still represent an average.[88]

4.3.1.2 Antibody – Antigen Binding Kinetics

The kinetics of antibody antigen binding can prove very difficult to measure as certain antibodies are polyvalent permitting them to bind multiple antigen molecules.[89] Most antibodies have the ability to bind two antigens at the same time permittitng the formation of lattice like antibody – antigen complexes. This crosslinking ability expedites the removal of the foreign material by the immune system.[89] Likewise antigens themselves can be polyvalent and possess multiple binding sites for the antibody. This polyvalency can result in the formation of aggregates yielding data that does not necessarily reflect the rate of the primary interaction. It is known however that the rate of the binding event between antibody and antigen happens rapidly.[88] Occasionally, the process is so rapid that often mixing of the antibodies and antigens is the rate limiting step. This difficulty can sometimes be overcome by working with very dilute solutions of both components.[88]

Using the general reaction shown in Figure 4.3 the rate of bound antibody antigen complex can be depicted using a differential equation as given by equation (4.3).

$$\mathrm{Ab} + \mathrm{Ag} \underset{k_{21}}{\overset{k_{12}}{\rightleftharpoons}} \mathrm{AbAg}$$

Figure 4.3 – Representation of the reversible association and dissociation of an antibody and its antigen. k_{12} represents the rate of antibody – antigen association, while k_{21} represents the rate of antibody – antigen complex dissociation.

$$\frac{d[AbAg]}{dt} = k_{12}[Ab][Ag] - k_{21}[AbAg] \quad (4.3)$$

Since the net rate of antibody – antigen complex formation is zero at equilibrium, equation (4.3) can be rearranged to yield equation (4.4) where the equilibrium constant K is given in terms of the rate constants for the association and dissociation processes.[88]

$$\frac{k_{12}}{k_{21}} = \frac{[AbAg]}{[Ab][Ag]} = K \quad (4.4)$$

Having presented a basic introduction to both serpins and their role in insect immune response, and the properties and function of antibodies I will begin discussing our attempts to prepare microscale immunoaffinity columns for the purification of insect serpins in an attempt to extend the ability to analyze these proteins to smaller individual insects.

4.4 Materials and Methods

4.4.1 Fritted Column Assembly and Preparation

4.4.1.1 Column Packing

Rabbit serum containing polyclonal antibodies to different serpin proteins was generously provided by Dr. Michael Kanost of Kansas State University. Protein A coated polystyrene microspheres with an average diameter of 5.5 μm and 9.7 μm were purchased from Bangs Labs (Catalog # CP02N: Fishers, IN). Fused silica capillary was obtained from Polymicro Technologies (Phoenix, AZ). Sodium borate, sodium azide, sodium chloride, sodium hydroxide, sodium phosphate, hydrochloric acid, methanol, and Tween 20 was purchased from Fisher Scientific (Pittsburgh, PA). Glycine was supplied by ICN Biomedicals (Irvine, CA). Dimethyl pimelimidate, ethanoloamine and triethanolamine were provided by Sigma – Aldrich (St. Louis, MO). Ultrapure water was generated from a Barnstead E-pure system (Dubuque, IA). High pressure micrcolumn fittings as well as PEEK tubing were purchased from Upchurch Scientific (Oak Harbor, WA).

Double Fritted Column

During work on this project, two different fritted columns were prepared. The first microcolumn involved three different segments of fused silica capillary as well as two microcolumn filter assemblies as depicted in Figure 4.4. The total column length was ~24 cm,

with ~10 cm dedicated to the loading region, a ~4 cm packed bed, and a ~10 cm eluent region. The inner diameter of the capillary was 150 µm. When preparing to pack the column, the microcolumn filter assembly "A" contained a frit-less capsule union, while filter assembly "B" contained a 1µm porous titanium frit. This would allow for flow of the microspheres through the first fitting while retaining them against the frit of the second fitting. The setup for capillary packing is shown in Figure 4.5.

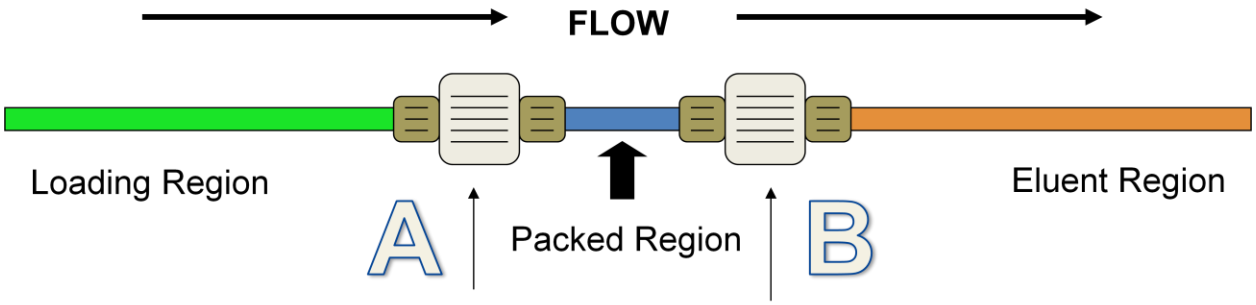

Figure 4.4 – Diagram of double fritted immunoaffinity column design.

With the column inserted in the pressure bomb, it was first rinsed with methanol, followed by water, and finally column buffer (0.1% Tween 20 & 0.02% sodium azide in phosphate buffered saline). Following the rinse steps, the microspheres were sonicated and then 100 µL of the microsphere solution was added to 900 µL of column buffer. The resulting microsphere slurry was placed into the pressure bomb with the loading column inserted into it. The bomb was then pressurized to 300 psi for 20 minutes (the flow rate under these conditions was about 1 µL/min) with the air pushing down on the surface of the liquid in the solution container within the bomb, and forcing the liquid and microspheres up the column where the spheres would be retained by the frit in the second microcolumn filter assembly.

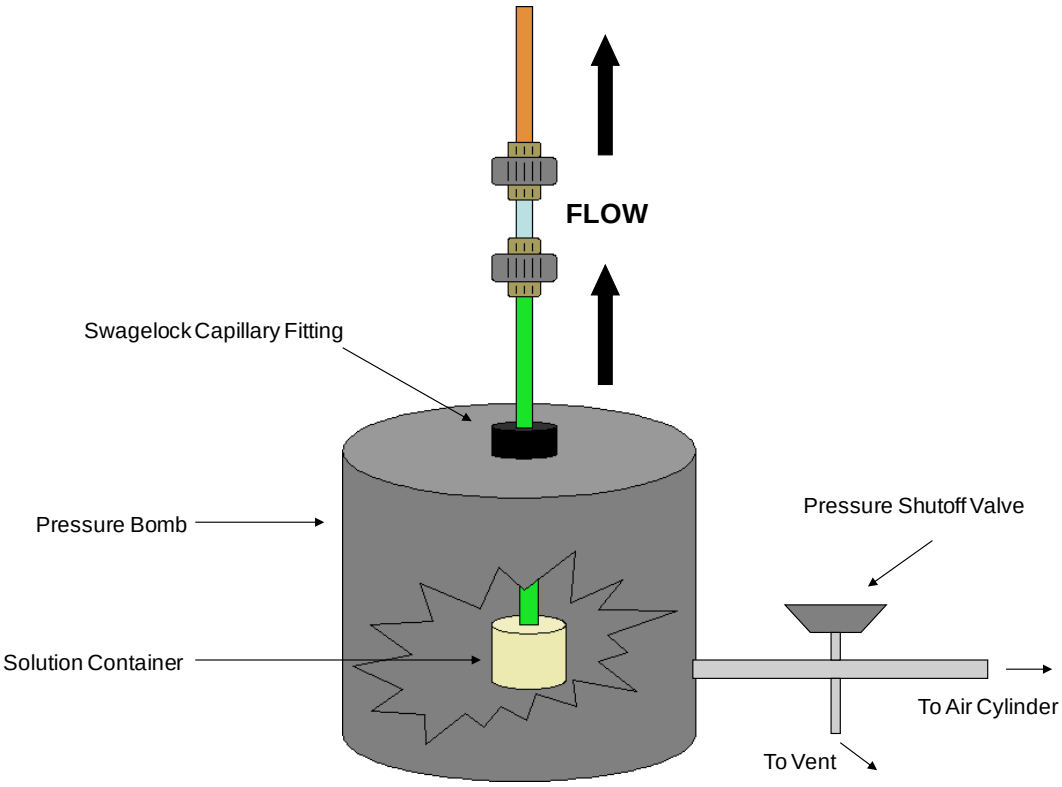

Figure 4.5 – Diagram of column assembled into an in-house constructed packing pressure bomb.

Following the 20 min packing step, microcolumn filter assembly "A" was carefully disassembled, and the fritless capsule union was replaced by the same 1μm titanium frit that was already installed in fitting "B". The loading column was then replaced with a new capillary segment of the same length, and fitting "A" was put in place resulting in a packed bed of Protein A coated microspheres contained between two 1 μm titanium frits. The packed column was now ready to receive the antibody and could be stored full of column buffer in the refrigerator.

Single Fritted Column

The second column was similar to the first in that it incorporated the use of a single microcolumn filter assembly. The total column length was ~24 cm, with ~14 cm dedicated to the loading region and ~10 cm to the eluent region as illustrated in Figure 4.6. The inner diameter of the capillary was 150 μm. The single microcolumn filter assembly contained a 1 μm porous titanium frit. With the column inserted in the pressure bomb, the column is first rinsed with methanol, followed by water, and finally column buffer (0.1% Tween 20 & 0.02% sodium azide in phosphate buffered saline). Following the rinse steps, the microspheres were sonicated

and then 100 µL of the microsphere solution was added to 900 µL of column buffer. The resulting microsphere solution was placed into the pressure bomb with the loading column inserted into it. The bomb was then pressurized to 300 psi for 20 min (the flow rate under these conditions was about 1 µL/min) with the air pushing down on the surface of the liquid in the solution container within the bomb, and forcing the liquid and microspheres up the column where the spheres would be retained by the frit in the microcolumn filter assembly. Following packing, the micrcolumn was flushed with column buffer and was now ready to receive antibodies.

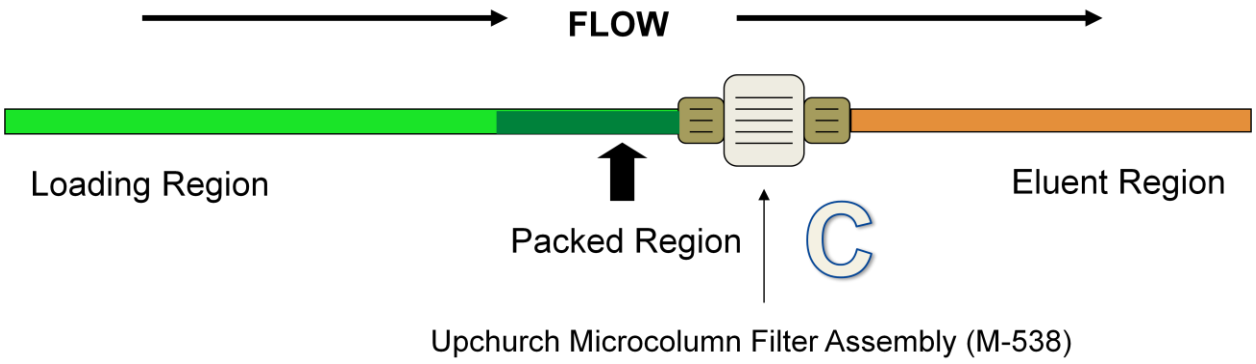

Figure 4.6 – Diagram of single fritted micro-immunoaffinity column.

4.4.2 Magnetic Column Assembly

Preparation of the magnetic device began with a 5.08 cm × 7.62 cm (2 in × 3 in) glass slide from Corning Inc. (Corning, NY). On this glass slide were placed four neodymium iron boride rare earth metal magnets with dimensions of 1.22 cm × 0.64 cm × 0.16 cm ($^1/_2$ in × $^1/_4$ in × $^1/_{16}$ in) that were supplied by K&J Magnetics (Jamison, PA). These were oriented north to south so that all four magnets were attracted to each other (

Figure 4.7 and Figure 4.8). A 381 µm (0.015 in) thick teflon spacer was placed in between the two columns of magnets holding them apart despite their magnetic attraction. Standard 10:1 ratio poly(dimethylsiloxane) (Sylgard 184: Dow Corning – Midland, MI) was then poured over the magnets and glass slide as shown in

Figure 4.7 and Figure 4.8. Following curing of the PDMS in an 80 °C oven for 2 hours, the Teflon spacer was removed and the PDMS successfully prevented the magnets from snapping together resulting in a narrow channel running between the magnets. A 40 – 50 cm segment of fused silica capillary, with an outer diameter of 665 µm and an inner

diameter of 300 µm, was placed down into the narrow channel between the magnets so that the magnetic device was approximately centered on the capillary segment. There appears to be some relaxation of the PDMS when the Teflon spacer is removed resulting in a wider groove than initially formed by the spacer. A drop of PDMS was placed over the capillary near the ends of the magnetic chip, as shown in

Figure 4.7 and Figure 4.8, and the device was placed in the 80 °C oven for 1 h to cure the PDMS. These drops of PDMS simply serve as anchor points preventing the capillary column from popping out of the magnetic cradle.

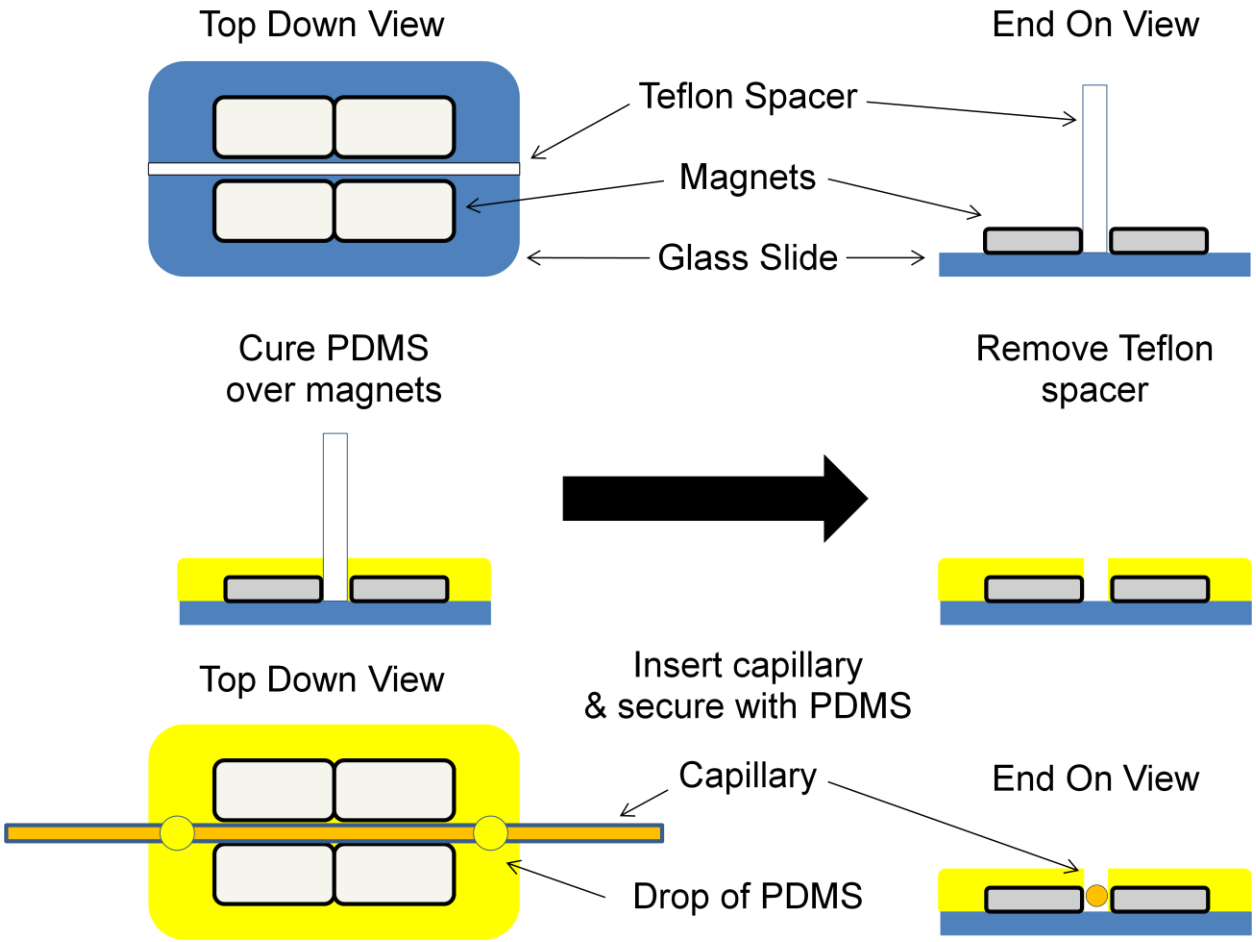

Figure 4.7 – Diagram illustrating assembly and fabrication of the magnetic immunoaffinity column device.

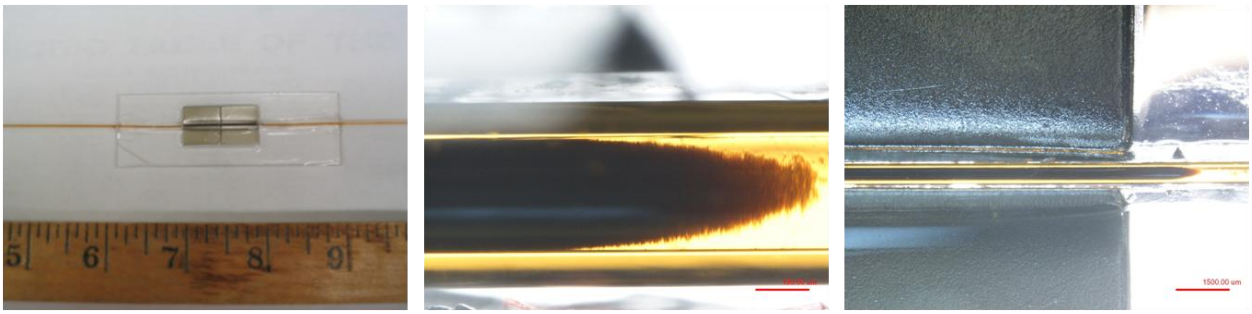

Figure 4.8 – Images of Magnetic Immunoaffinity Column device. Scale bars represent 190 μm and 1500 μm for the center and right images respectively.

4.4.2.1 Magnetic Column Packing

Protein A coated Dynabeads® were purchased from Invitrogen (Carlsbad, CA). Dynabeads are 2.8 μm diameter polymer coated iron oxide with Protein A covalently linked to the bead surface. Packing of these magnetic beads into the column required the use of two syringe pumps as well as a two-way switching valve and a 6-port manual injector with 4 μL loop connected as shown in Figure 4.9. To pack the column, the magnetic region was placed onto the stage of an inverted microscope to observe the bead filling process. To eliminate air bubbles, the entire system in Figure 4.9 was flushed with antibody binding buffer, which consisted of 100 mM sodium phosphate at pH 8.2 with 0.01% Tween 20 (v/v). Once all of the fluid lines were full, a microcentrifuge tube containing 20 μL of the Dynabeads® slurry was diluted into 180 μL of binding buffer was placed at the column outlet labeled "Fraction Collection" in Figure 4.9. At this time, one of the syringe pumps was set to "withdraw" so as to pull beads into the magnetic region where they would be captured. The other syringe pump was set to infuse and simply pumped its solution to a waste reservoir. Both pumps were operated at 10 μL/min. Beads were drawn into the magnetic bed until a packed segment approximately the length of the two magnets was achieved. Care was taken to avoid pulling beads into the 6-port manual injection valve. Once the packed segment was isolated, both syringe pumps were set to infuse and buffer was pumped through the packed bed to ensure its retention. The fluid flow rate was again 10 μL/min. The magnetic bed was now ready to receive antibodies.

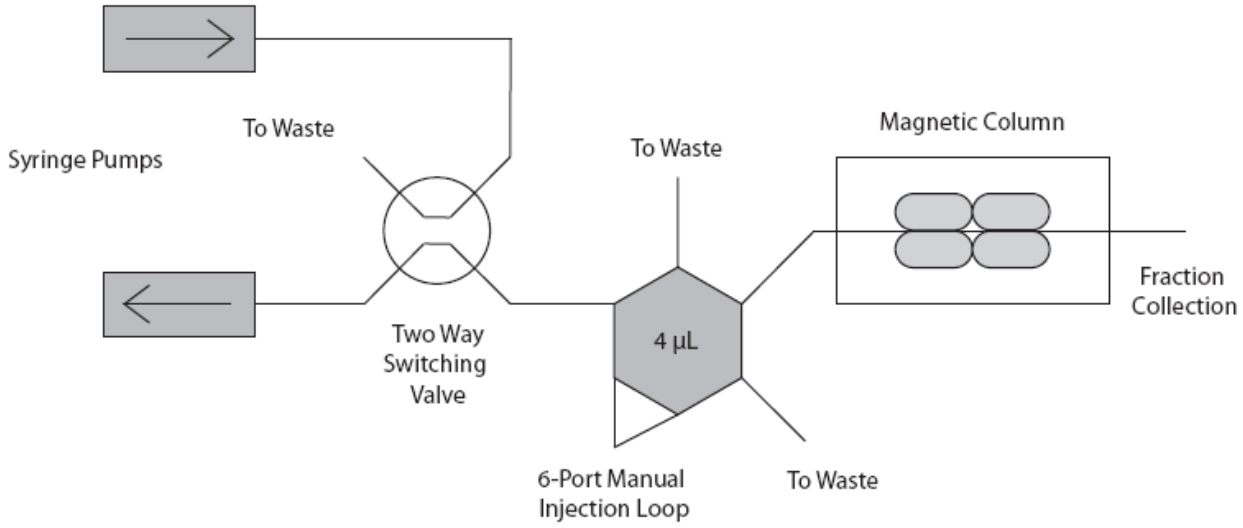

Figure 4.9 – Experimental setup for magnetic immunoaffinity column.

4.4.3 Antibody Binding and Crosslinking

4.4.3.1 Binding

Fritted Columns

Serum from a rabbits inoculated with different serpins was obtained from the Kanost labs. First, 10 µL of the serpin antibody serum solution was diluted to 1 mL with 990 µL of PBS at time of use. Using the pressure bomb, PBS was first run through the column at 300 psi for 20 min. Next, the PBS solution was replaced with the diluted serpin antibody solution which was then forced through the column at 300 psi for 120 min. Fractions of the eluent of the antibody solution were collected in 20 min intervals. These eluent samples were then run on slab gels using SDS-PAGE to determine if protein concentration of the eluent visibly increased as more and more active sites on the stationary phase were occupied (as the microspheres become more saturated with antibody molecules, more unbound protein should simply pass through the column and over time result in darker bands when samples are run on a slab gel). Following the 2 h antibody treatment, the antibody solution in the pressure bomb was traded for PBS which was run through the column for 20 min to clear out any unbound protein. Now, antibody must be cross-linked to the protein A coated microspheres.

Alternatively, the fritted column was also connected to an HPLC and fluid flow was achieved using the pumping system of an HP 1090 (Agilent Technologies: Santa Clara, CA). Fluidic connections between the HPLC's PEEK tubing and the column's fused silica tubing were made using a tubing adapter from Upchurch Scientific. Instead of continuous flow collection over a 2 hour period, a series of four 10 μL serum injections were performed using the autosampler system of the HPLC, and during this time, eluting fractions were collected for 10 min at a flow rate of 10 μL/min following each injection.

Magnetic Column

Following the flushing of the system with binding buffer, a syringe containing the cell-free serpin antibody rabbit serum was used to fill the 4 μL injection loop of the 6-port manual injector. When the loop was full, the syringe was removed and the valve was rotated to the "inject" position. This allowed the binding buffer to sweep through the sample loop carrying the loop's contents onto the column. The column eluent was collected for 10 min following the injection. This antibody serum injection process was repeated until a total of 4 injections had been performed, each one yielding a different eluent sample. Following the fourth injection, the system was flushed with binding buffer for 10 minutes to remove any unbound protein while the column eluent was being collected.

4.4.3.2 Crosslinking

To prepare the crosslinking solution, 66 mg of dimethyl pimelimidate (DMP) was added to 10 mL of crosslinking buffer which contained 200 mM triethanolamine at pH 8.2 resulting in a final DMP concentration of 20 mM.

Fritted Columns

Using the pressure bomb, PBS was first flowed through the packed column for 10 min at 300 psi. Next, 0.2 M sodium borate pH 9 was flowed through the column for 10 min at 300 psi. Third, crosslinking solution was placed in the pressure bomb and forced through the column for 30 min at 300 psi. The crosslinking solution was followed by the 0.2 M ethanolamine pH 8 solution for 2 h at 300 psi. Finally the column was rinsed with the column buffer solution for 10 min at 300 psi. The column could now be stored in the fridge and was ready to use for the isolation of proteins from hemolymph.

Crosslinking of the antibodies to the Protein A with the column connected to the HPLC was achieved by pumping the crosslinking solution through the column at 10 μL/min for 30 min using the HPLC pumping system. During this 30 min period the eluent was collected.

Magnetic Column

One of the syringes on the two different syringe pumps containing binding buffer was replaced with a syringe filled with DMP crosslinking solution. The two way switching valve was rotated so that the crosslinking solution flowed on-column while the binding buffer was directed to waste. The crosslinking solution was administered for 30 min at 10 μL/min while the eluent was being collected. Following the 30 min crosslinking step, the syringe containing the crosslinking solution was switched out with a syringe containing quenching buffer composed of 50 mM Tris at pH 7.5. The quenching solution was applied to the column for 10 min at 10 μL/min while the eluent was collected. Following the quenching, the two way switching valve was rotated directing the binding buffer onto the column and the quenching solution to waste. The column was re-equilibrated with binding buffer for 10 min at 10 μL/min. After re-equilibration, the column was ready to receive antigens.

4.4.4 Antigen Capture

Insect hemolymph extracted from *Manduca sexta* was generously provided by Dr. Michael Kanost. When collected, the hemolymph was diluted 1:1 with anti-coagulation buffer.

4.4.4.1 Fritted Columns

A vial containing the *Manduca sexta* hemolymph was placed in the pressure bomb, and the end of the capillary was inserted into the solution. The bomb was pressurized at 300 psi for 2 h while the column eluent was collected.

For administering the hemolymph to the column while it was connected to the HPLC, a series of four 4 μL injections of insect hemolymph was performed using the attached autosampler. During these injections, the system pumped binding buffer at 10 μL/min, and following each injection the column eluent was collected for 10 min.

4.4.4.2 Magnetic Column

A syringe was loaded with the hemolymph and used to load the 4 μL sample loop of the 6-port manual injection valve. The valve was then switched to the "inject position" allowing the binding buffer to flush the contents of the sample loop onto the column. The eluent was collected for 10 min at 10 μL/min. This injection process was repeated 3 additional times resulting in the collection of 4 total hemolymph injection fractions. Following the fourth hemolymph injection, the column was flushed with binding buffer for at least 10 min (without performing any injections) to wash out any unbound substances.

4.4.5 Antigen Release

Releasing the bound antigen from the columns was achieved by using a 100 mM glycine buffer with a pH of 2.8. When application of the antigen release buffer to the column was completed, all versions of the column were re-equilibrated with binding buffer.

4.4.5.1 Fritted columns

To pump the antigen releasing buffer through the column, a microcentrifuge tube containing the glycine buffer was placed in the pressure bomb and the end of the column was inserted into the solution. The bomb was then pressurized at 300 psi and elution fractions were collected at selected time intervals.

With the column attached to the HPLC system, application of the antigen release buffer was achieved by simply using the built in solvent system and internal pumps to administer the buffer to the column. The flow rate for antigen release was again 10 μL/min and elution fractions were collected at 10 min intervals.

4.4.5.2 Magnetic Column

Release of the antigens using the magnetic column assembly was achieved by placing a syringe full of the low pH glycine buffer in one of the syringe pumps and then turning the two-way switching valve so that its flow was directed on column. The syringe pump flow rate was set to 10 μL/min and elution fractions were collected at 10 min intervals.

4.4.6 SDS-PAGE

To prepare the samples for sodium dodecyl sulfate-polyacrylamide gel electrophoresis (SDS-PAGE), 10 μL from each fraction was mixed with 10 μL of 2X sample reducing buffer

which contained 20% glycerol (v/v), 4% SDS (w/v), 0.02 mg/mL bromothymol blue, and 10% β-mercaptoethanol (v/v). The samples were vortexed and then incubated in a block heater at 95 °C for 3 – 5 min to denature the proteins. Following heat incubation, the samples were loaded into the polyacrylamide gel wells. For protein separations NuPAGE® Novex 4-12% Bis-Tris Gel 1.0 mm from Invitrogen were used. The separation buffer system employed was a near neutral pH 3-(N-morpholino)propanesulfonic acid (MOPS) buffer. This buffer was supplied in a 20X concentrated form by Invitrogen. The electrophoresis unit used was an Xcell SureLock™ Mini-Cell from Invitrogen. Separations on the gel were carried out using a power supply from E-C Apparatus (St. Petersburg, FL) at 200 V (generating about 87 mA) for 45 min. Following separation, the gel was removed from its cassette and prepared for Western blotting.

4.4.7 Western Blotting

The membrane chosen for Western transfer was a Nitrobind 0.45 μm pore nitrocellulose purchased from the GE Osmonics Labstore (Minnetonka, MN) and cut to 9 cm × 7.5 cm. Six pieces of blotting paper from MidSci (St. Louis, MO) were cut to same dimensions as the membrane and soaked, with the membrane, in Western transfer buffer containing 48 mM Tris pH 9.2, 39 mM glycine, 1.3 mM SDS, and 20% methanol (v/v) on an orbital shaker table from VWR Scientific. The Western transfer was prepared by layering 3 pieces of the blotting paper on the surface of the Trans-Blot SD Semi-Dry transfer cell (Bio-Rad: Hercules, CA), followed by the membrane, the gel, and lastly, the remaining three pieces of blotting paper. The Western transfer unit lid was then attached and transfer of the protein bands from the gel to the membrane was carried out at 8 – 10 V for 1.75 h.

A milk solution was then prepared by dissolving 0.3 g dry milk in 50 mL of Tween 20 – Tris buffered saline buffer (T-TBS) which contained 137 mM NaCl, 2.7 mM KCl, 25 mM Tris pH 7.4 and 0.05% Tween 20 (v/v). The membrane was allowed to incubate in this milk solution for 1 – 1.5 h on a shaker table. Next, 10 μL of primary antibody solution was added directly to the milk solution and the membrane was allowed to incubate for an additional hour. After this incubation period, the membrane was washed 3 times for 5 min each in T-TBS buffer. Upon discarding the third wash solution a fresh milk solution was prepared and 10 mL of this solution was added to the tray containing the membrane. Secondary antibody was added directly to the milk solution. The secondary antibody was a goat-anti-rabbit alkaline phosphatase conjugate

from Bio-Rad and 3 μL was added to the milk solution. The membrane was incubated for 1 h with the secondary antibody solution after which time the membrane was washed three times for 2 min each in Tris buffered saline buffer (TBS) which contained 137 mM NaCl, 2.7 mM KCl, and 25 mM Tris pH 7.4.

For development of the membrane, a commercial 25X AP color development buffer kit from Bio-Rad (Hercules, CA) was used. To prepare the developing solution, 400 μL of 25X color development buffer was diluted into 9.6 mL of distilled water. Just prior to addition of the developing buffer solution to the membrane, 100 μL of both color reagent A and color reagent B were added to the solution followed by vigorous mixing. The developing buffer was then added to the tray containing the membrane and it was allowed to incubate for no longer than 15 min while resting on the shaker table. During this time the formation of colored protein bands was observed. Following development, the membrane was rinsed with water and then allowed to air dry.

4.4.8 Purification of Serpin-1 Antibodies

4.4.8.1 Protein Immobilization

A commercially available AminoLink Plus Immobilization kit from Pierce (Rockford, IL) was used for the purification of serpin antibodies. Serpin-1 protein had been previously purified by the Kanost group and was stored in a 20 mM Tris, 50 mM sodium chloride buffer. The serpin-1 protein was first dialyzed into pH 7.2 coupling buffer (which consisted of 100 mM sodium phosphate and 150 mM sodium chloride) using a 10,000 molecular weight cut-off (MWCO) Slide-A-Lyzer dialysis cassette from Pierce according to the manufacturer's instructions. The resin in the AminoLink column was suspended with end-over-end mixing. The top cap of the column was removed followed by the bottom tab. To the column 2 mL of pH 7.2 coupling buffer was added and allowed to drain. This rinsing was repeated with an additional 2 ml of coupling buffer. The bottom tab was replaced on the column, and 2 – 3 mL of the dialyzed serpin-1 protein in the coupling buffer was added to the column. In a fume hood, 40 μL of sodium cyanoborohydride solution was added to the column slurry (resulting in ~ 50 mM sodium cyanoborohydride). The top cap of the column was replaced so that both ends of the column were sealed, and the column was incubated with end-over-end mixing overnight.

Following this incubation period, the top and bottom column caps were removed and the eluent containing all of the non-bound protein was collected.

4.4.8.2 Blocking of Remaining Column Active Sites

The column was washed with 2 mL of quenching buffer which consisted of 1 M Tris·HCl and 0.05% sodium azide at pH 7.4. The bottom cap of the column was replaced and in a fume hood 40 µL of sodium cyanoborohydride was added to 2 mL of quenching buffer and the resulting solution was added to the column. The top cap was placed back on the column which was then incubated for 30 min with end-over-end mixing.

4.4.8.3 Column Washing

The top cap was removed from the column with care as the blocking reaction may have generated gas pressurizing the column. The bottom cap was then removed and the quenching buffer was drained from the column. The column was washed four times with 2 mL of washing solution which consisted of 1 M sodium chloride and 0.05% sodium azide (w/v). Next, the column was re-equilibrated with three 2 mL washes using storage buffer. The storage buffer consisted of coupling buffer containing 0.05% sodium azide (w/v). Finally the bottom cap was replaced and 2 mL of storage buffer was added to the resin bed. At this point the top cap was replaced and the column could be stored upright at 4 °C until use.

4.4.8.4 Affinity Purification

For affinity purification, the following solutions were required: phosphate buffered saline (PBS), anti-serum sample dissolved or exchanged into PBS, elution buffer consisting of 100 – 200 mM glycine·HCl pH 2.5 – 3.0, and neutralization buffer consisting of 1 M sodium phosphate pH 8.5 – 9.0. The column was prepared by inserting the porous disk supplied in the kit to within 1 mm of the top of the resin bed using the provided plunger. The column was then equilibrated to room temperature. With the bottom cap still in place, 2 mL of anti-sera sample (dissolved in PBS) was added to the column. The bottom cap was then removed to permit the sample to enter the resin bed. As soon as the sample had made its way into the resin bed, the bottom cap was replaced followed by the top cap. The column was then incubated with gentle rocking at room temperature for 15 – 60 min. After the incubation period, the top cap and then the bottom cap were removed and the column eluent was collected. Next, 1 mL of PBS was added to the top of

the column and the eluent was collected in the same tube. The column bed was then washed four times with 2 mL portions of PBS. To a collection tube was added 50 μL neutralization buffer, and then 1 mL of elution buffer was added to the head of the column and the eluent was collected into the tube containing the neutralization buffer. This process was repeated 5 additional times yielding 6 tubes containing eluted fractions. This eluted protein could be used directly for SDS-PAGE or microplate protein assay. The column was then immediately equilibrated with 4 mL of PBS. The bottom of the column was capped and then 4 mL of PBS containing 0.05% sodium azide was added to the top of the column and the top cap was replaced to preserve the column for long term storage. According to the manufacturer's documentation, this affinity column could be used about 10 times. The column was then stored upright at 4 °C.

After collection of the eluted serpin-1 antibody fractions, a SDS-PAGE of fraction aliquots followed by Western blot was performed. The appearance of appropriately sized protein bands confirmed the presence of protein possessing a size consistent with the molecular weight of antibodies to serpin-1. The intensity of the protein bands served to qualitatively identify which fractions contained the highest concentration of serpin-1 antibodies. Aliquots of the elution fractions were also submitted to a microplate protein concentration assay using a PowerWave XS microplate reader from BioTek (Winooski, VT) to quantitatively determine total protein concentrations of the elution fractions containing the purified serpin-1 antibodies.

4.5 Results and Discussion

4.5.1 Fritted Column Properties

Using the pressure bomb was an effective and relatively fast way of forming the packed immunoaffinity beds retained by the titanium frits. Initial work with the double fritted column proved that following packing, solutions could be administered to the column using the pressure bomb; however, operation of the pressure bomb within the range of pressures deemed safe generated low flow rates (≤ 1 μL/min). At this flow rate, some of the column treatment steps such as antibody attachment, crosslinking, and antigen attachment required long application times to ensure that the bed was exposed to appropriate amounts of fluid. Some of the biological solutions applied to the column such as antibody containing serum and insect hemolymph were quite a bit more viscous than the aqueous buffers. The increased viscosity coupled with the

already low flow rates further lengthened the amount of time required to collect useful volumes of fluid for further analysis. From a mechanical standpoint, the double fritted column required the disassembly of the first inline column filter assembly to remove the capsule union and replace it with a second titanium frit, resulting in an entirely contained column straddled by two frits. This step proved to be challenging as it was very easy to crush the end of the packed fused silica capillary segment upon retightening of the fittings leading to complete flow cessation. To circumvent this issue, the single fritted column was adopted. The single fritted column was more user friendly as no disassembly/reassembly of the fittings was required. It was observed that the packed bed retained its integrity despite not being entirely retained between two frits. While the single fritted column was more user friendly, upon application of fluids using the pressure bomb, it actually exhibited flow rates similar to that observed with the double fritted column. It was also noted that over the course of the application of the antibody containing serum, the flow rate continued to drop further, to as little as 0.03 μL/min. It was decided that the pressure bomb simply could not safely supply the pressure necessary to maintain a useful flow rate and the use of this fritted column would require attachment to an HPLC pumping unit.

With the fritted column connected to the HPLC and the flow rate set to 20 μL/min, a backpressure of 2900 psi was generated. The finger-tight Upchurch fittings were rated up to 6000 psi, so this operational pressure was acceptable. During the course of experiments, however, the flow rate was typically 5 – 10 μL/min and this ensured lower backpressures as well as increased the residence time of the antibodies and antigens within the packed bed. Longer residence times increased the opportunity for proper orientation of the antibodies and antigens to be achieved, and thus increased the likelihood of their respective binding events. Use of the HPLC's built-in solvent delivery system permitted seamless switching between different buffers. In addition the use of the auto-sampler system facilitated metered delivery of antibody and antigen solutions by performing multiple injections of equal volumes.

Despite the simplicity of this experimental setup, clogging of the column was frequently observed during steps involving the injection of biological components, either the antibodies or the antigen. It is at present unknown what was responsible for these clogs as all solutions were often diluted to reduce viscosity, filtered to eliminate particulate, centrifuged to remove cells, and spiked with various inhibitors to prevent coagulation and the activation of different immune responses that could lead to the formation of melanin.

Following the application of antibodies to the column, their subsequent crosslinking, isolation of antigen, and its subsequent release, samples were taken to the Kanost labs at Kansas State University to perform SDS-PAGE and Western blotting experiments.

4.5.2 Magnetic Column Properties

The single greatest advantage of the magnetic column lies in its dynamic packed bed. The fact that the packed region was not contained between frits provided it with enough give to virtually eliminate instances of clogging. While this experimental setup was more complicated than the fritted column with the HPLC it offered much better performance. The magnets provided a high enough field to retain the packed bed even with flow rates of 10 μL/min. Higher flow rates could be implemented; however they would often result in the leakage of some of the beads out of the column which would eventually find their way into the elution fractions. While the amount of beads lost at a flow rate of 20 μL/min was probably not significant, the increased residence time offered by the lower flow rate was deemed a greater priority than speed.

One important factor observed during packing is the necessity for close proximity of the capillary to the magnets on either side. If the capillary was not centered between the magnets and rather was closer to one than the other, the bead density throughout the capillary would be visibly heterogeneous with tighter packing nearest the magnet and occasionally a small unpacked "headspace" on the opposite side. Thus distance between the magnets and capillary walls was minimized and equalized.

4.5.3 Column Binding Capacity

The binding capacity of the fritted column was dictated by the length of the packed bed created during column packing. Due to the irreproducible length of the packed beds produced when preparing multiple columns, the bed length would have to be measured and the binding capacity determined for each individual column. The total binding capacity of the column (C_b) could be calculated by using equation (4.5), where r_c is the capillary radius in cm; l_c is the length of the packed capillary segment in cm; ρ_b is the density of the Protein A coated beads in mg/cm^3; and B_{cap} is the binding capacity of the beads reported in terms of mass of IgG bound per mg of beads used (provided by bead manufacturer).

$$C_b = \left(\frac{3}{4}\right)\pi r_c^2 l_c \rho_b B_{cap} \tag{4.5}$$

For columns prepared using the pressure bomb for packing, the inner diameter of the capillary was 150 μm with a bead diameter of 9.65 μm resulting in a C_b typically ranged between 0.5 – 1.0 μg total IgG. For the magnetic columns, the length of the packed bed was a reproducible 2.54 cm as dictated by the length of the magnets. The inner diameter of the capillary was also increased to 300 μm while smaller diameter protein A coated microspheres were also used providing a higher surface area for binding. These two factors permitted maximized overall binding capacity in a limited packed bed length. Typical C_b values for the magnetic column were 10 – 14 μg IgG. Assuming complete saturation of the binding sites of the column with the antibodies, followed by complete saturation of the antibody binding sites with the serpin proteins, and finally efficient elution of the bound antigen, this would be a high enough binding capacity to observe protein bands on a Western blot membrane. However, there will most likely be a fairly substantial amount of sample loss, as the serpin anti-sera contains other antibodies relevant to the host rabbit's immune system and numerous other proteins that could potentially bind the column and occupy sites that could otherwise serve to bind antibodies to the serpin proteins. The only way to determine if the operational binding capacity of the columns was sufficient was to simply carry out the experiment. One way to optimize the column binding capacity would be to use purified serpin antibodies, thus eliminating many interferences that could take up residence on the column. Results of experiments using both unpurified and purified antibodies will be presented.

4.5.4 Fritted Column Performance

Experiments using the fritted column assemblies were hindered by repeated instances of clogging. The double fritted column was susceptible to the crushing of the end of the fused silica capillary with the required disassembly and reassembly steps. Both the single and double fritted systems were prone to clogging upon the application of the higher viscosity biological fluids. In fact it was a rare occurrence when the column would survive the application of the entire cycle of fluids involved in the attachment of antibodies, their crosslinking, the attachment of the target antigen, and the elution of bound antigen. While it was occasionally possible to complete the cycle of fluids, flow rates were generally very low (< 5 μL/min). In an effort to reduce the

occurrence of column clogging, the diameter of the beads was changed from 5.50 µm to 9.65 µm as it is known that the pressure drop across a packed bed decreases with the square of the diameter of the packing material. The larger diameter packing material did not reduce the number of instances of clogging, and thus it became necessary to develop alternative column architecture.

Prior to switching to the magnetic column format, an initial qualitative test was performed using a single fritted column attached to the HPLC system where the goal was to determine if the antibodies were in fact being retained on the column. The results of this experiment are shown in Figure 4.10.

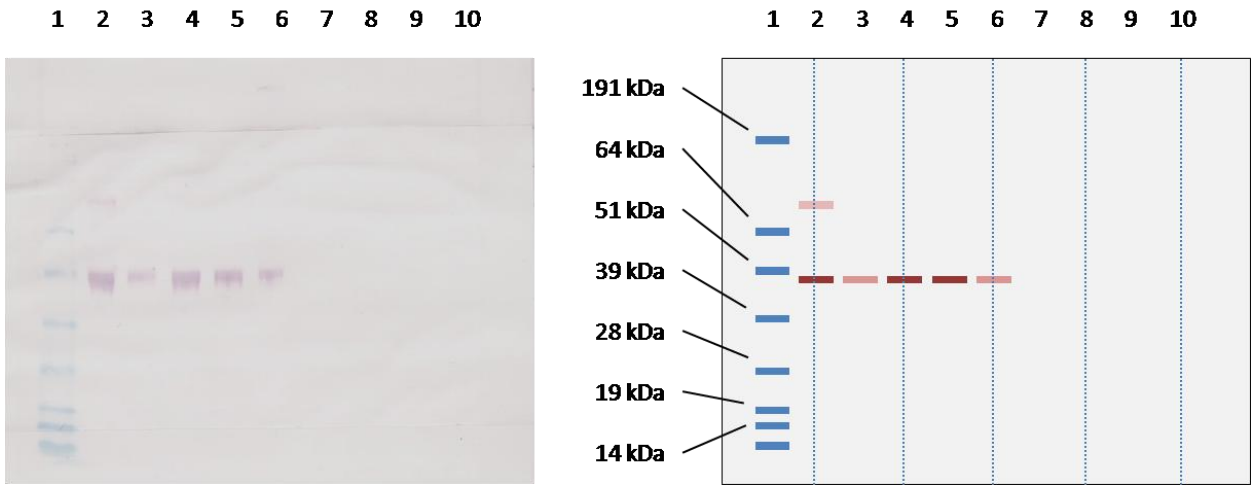

Lane IDs

1) Molecular Weight Marker
2) Serpin-1 anti-sera(Not applied to column)
3) 25 µL Injection of Serpin-1 anti-sera onto column
4) 25 µL Injection of Serpin-1 anti-sera onto column
5) 25 µL Injection of Serpin-1 anti-sera onto column
6) 25 µL Injection of Serpin-1 anti-sera onto column
7-10) No Samples Run

Figure 4.10 - Left: Western blot of single fritted immunoaffinity column elution fractions using serpin-1 anti-sera and purified serpin-1 protein. Right: analogous graphic depicting all major protein bands and their respective intensities and locations in the membrane. Identity of the samples run in each lane of the gel is indicated in the lane IDs list.

From the membrane shown in Figure 4.10 the protein band corresponding to injected serpin-1 anti-sera shown in lane 3 is less intense than the corresponding protein bands in lanes 4

and 5. This is to be expected, as some of the protein in the injected sample will be retained on the Protein A column. One could make the argument that this band appears lighter because not all of the injected sample had time to reach the column outlet and thus was not collected, however this was accounted for by determining the total system volume from injection to collection, and using an appropriate flow rate and fraction collection time to ensure that sufficient time was allowed for all of the sample to make its way to the system outlet. The other possibility that cannot be accounted for is the potential non-specific binding of the protein to the system surfaces. Loss of the protein due to surface adsorption would also result in a lighter protein band on the Western blot membrane. The lighter protein band in lane 6 is a result of a system blockage. During the collection of this fraction the column became clogged and the system pressure spiked resulting in leaks at some of the fluidic connections which contributed to sample loss. Thus this membrane provided cautious optimism as to the ability of the Protein A coated microspheres to retain the serpin antibodies.

4.5.5 Magnetic Column Performance

The first time isolation of serpin proteins was attempted on the magnetic micro-immunoaffinity column the results raised a number of questions. The experiment involved binding antibodies to serpin-5 from serpin-5 anti-sera to the column, crosslinking of the antibody to the column, and finally injection of purified serpin-5 protein from *M. sexta* for capture by the packed bed. The membrane from the Western blot of the SDS-PAGE separated proteins in the column elution fractions can be seen in Figure 4.11. In lanes 1 – 4 the protein bands corresponding to the injected anti-sera are clearly visible. The bands corresponding to serpin-5 antibodies (as well as all other IgGs in the sera) lie between the 51 and 39 kDa molecular weight marker bands, and have an appropriate apparent molecular mass of approximately 47 kDa. The barely visible bands in lanes 9 – 12 correspond to the injection of purified serpin-5 protein from *M. sexta*. This experiment conveyed the following information. First, no protein bands are observed in lanes 14 – 17.

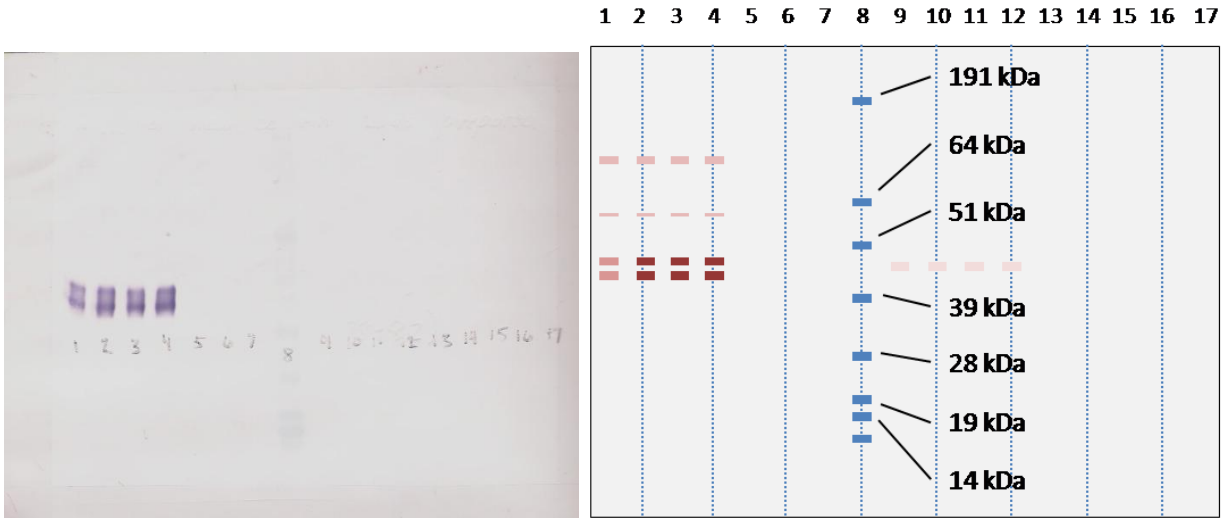

Lane IDs

1) 10 µL Serpin-5 anti-sera injection 1
2) 10 µL Serpin-5 anti-sera injection 2
3) 10 µL Serpin-5 anti-sera injection 3
4) 10 µL Serpin-5 anti-sera injection 4
5) 10 µL Post anti-sera injection wash
6) 10 µL Crosslinking fraction 1
7) 10 µL Post crosslinking wash
8) 10 µL SeeBlue molecular weight standard
9) 10 µL Serpin-5 injection 1
10) 10 µL Serpin-5 injection 2
11) 10 µL Serpin-5 injection 3
12) 10 µL Serpin-5 injection 4
13) 10 µL Post Serpin-5 injection wash
14) 10 µL Serpin-5 elution fraction 1
15) 10 µL Serpin-5 elution fraction 2
16) 10 µL Serpin-5 elution fraction 3
17) 10 µL Serpin-5 elution fraction 4

Figure 4.11 – Left: Western blot of magnetic immunoaffinity column elution fractions using serpin-5 anti-sera and purified Serpin-5 protein. Right: analogous graphic depicting all major protein bands and their respective intensities and locations in the membrane. The listed lane IDs convey the volume of solution loaded into the gel well as well as the sample loaded.

The absence of protein bands in these lanes indicates three main possibilities: the serpin-5 was not released during the elution, the concentration of the eluted protein was below the visible limit of detection, or the antibodies failed to bind the column in the first place and no isolated serpin-5 was available for elution. At this point it was believed that the protein was eluted, but present at a concentration below the visible limit of detection. This is a reasonable argument since the protein bands for the injection of the purified serpin-5 protein are already faint, meaning that little serpin-5 was available for isolation. Prior to their injection both the anti-sera solution as well as the serpin-5 protein solution was diluted in its appropriate buffer in an effort to reduce solution viscosity. This of course came at the expense of concentration. If the anti-sera was

diluted enough, it is possible that saturation of the columns binding sites was never achieved, resulting in a less than maximum total column binding capacity.

An experiment was performed in an attempt to confirm successful binding of the antibodies to the column. The results are shown in Figure 4.12.

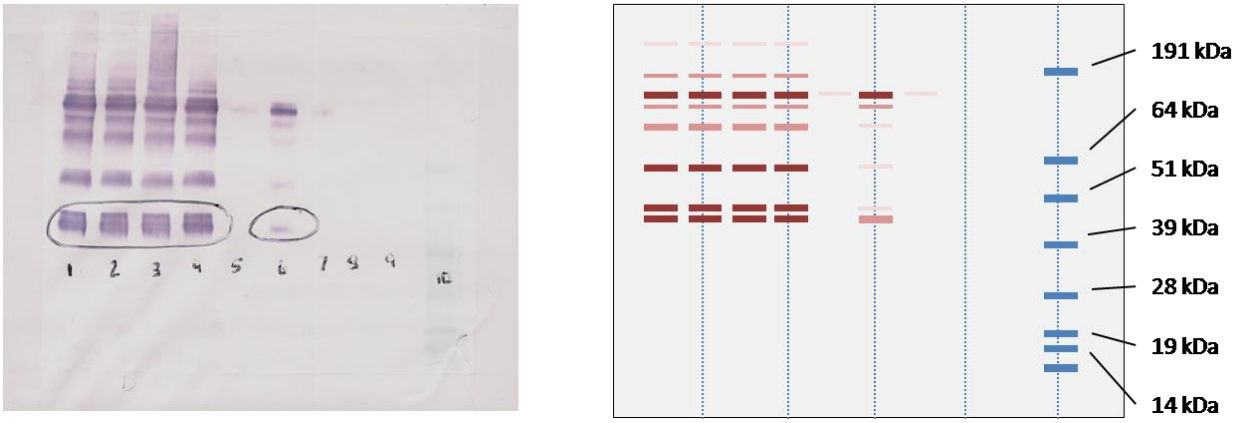

Lane IDs

1) Serpin-5 anti-sera injection 1
2) Serpin-5 anti-sera injection 2
3) Serpin-5 anti-sera injection 3
4) Serpin-5 anti-sera injection 4
5) Post anti-sera injection wash
6) Elution fraction 1
7) Elution fraction 2
8) Elution fraction 3
9) Elution fraction 4
10) SeeBlue molecular weight marker

Figure 4.12 – Left: Western blot of magnetic immunoaffinity column elution fractions using Serpin-5 anti-sera without crosslinking. Right: analogous graphic depicting all major protein bands and their respective intensities and locations in the membrane. The listed lane IDs convey the sample loaded into the gel wells. Circled bands on the Western blot membrane indicate the serpin-5 antibodies.

This Western blot confirms the successful binding of antibodies to the Protein A coated microspheres and their retention during a washing step. It is important to remember however that these are not purely antibodies to serpin-5. Rather, the circled protein bands represent all of the different antibodies in the serum. Antibodies to serpin-5 are only a fraction of these. Lanes 1 - 4 depict the column eluent fractions collected during the serpin-5 anti-sera injections. The protein content of undiluted anti-sera is quite high and the bands corresponding to the IgGs are quite dark indicating a high abundance of these antibodies in the sera. There are also a number of other proteins present in the anti-sera that could potentially take up residence on the column

and occupy sites otherwise reserved for serpin-5 antibodies resulting in a lowered total column binding capacity. Lane 5 is an elution fraction collected following the anti-sera injections where the column was simply being washed with the binding buffer to flush out any non-bound molecules, and a faint band is observed indicating the removal of a small amount of material, however no protein bands with a molecular weight similar to the serpin-5 antibodies is observed. The fraction shown in lane 6 was collected for 10 min while the antigen elution buffer was being applied to the column. Since the antibodies were not crosslinked to the Protein A, application of the elution buffer should result in their release from the column, and that is precisely what was observed. The appearance of these protein bands confirms that not only is the column retaining the antibodies, but also illustrates the degree to which other components of the anti-sera are also retained by the column. Another nice feature of the column is that elution of bound proteins appears to be a fairly rapid process as nearly all protein appears to be eluted in the first 10 min (100 μL) of application of the elution buffer. Lastly, this experiment suggests that the crosslinking of the antibodies to the Protein A was also successful, as in all previous experiments where the crosslinking buffer was applied, no protein bands corresponding to antibodies were ever observed from fractions collected during the application of the elution buffer.

The next logical step was to generate a column and perform the full range of the experiment by crosslinking the antibodies and then applying the antigen protein. For this experiment the column was prepared using serpin-5 anti-sera and purified serpin-5 protein as an antigen. For application of the antibodies, four 4 μL injections of the anti-sera were performed, and likewise, for the isolation of serpin-5, four 4 μL injections of purified serpin-5 were performed. The Western blot membrane corresponding to the elution fractions of this experiment are shown in Figure 4.13.

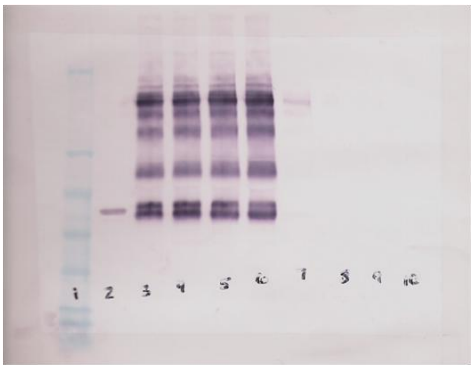

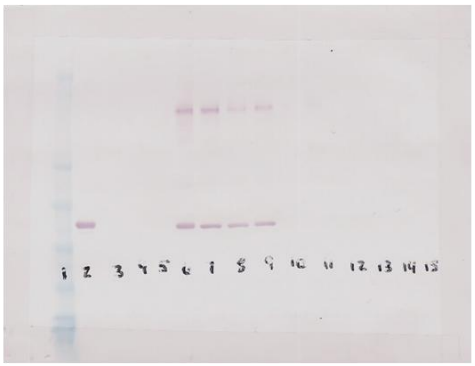

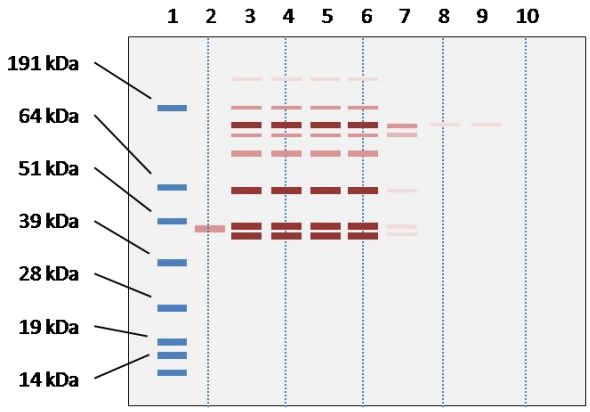

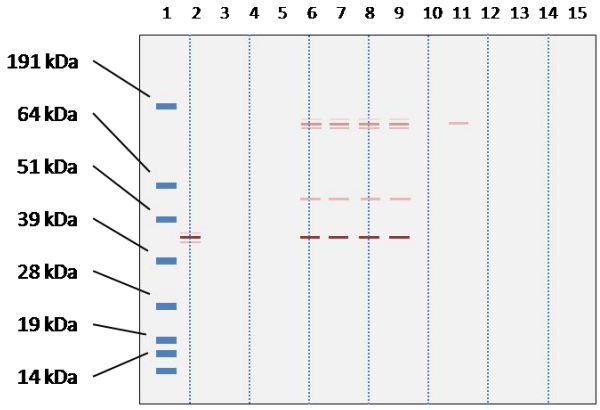

Lane IDs

1) SeeBlue molecular weight marker
2) Serpin-5 anti-sera standard
3) Serpin-5 anti-sera injection 1
4) Serpin-5 anti-sera injection 2
5) Serpin-5 anti-sera injection 3
6) Serpin-5 anti-sera injection 4
7) Post anti-sera injection wash - Fraction 1
8) Post anti-sera injection wash - Fraction 2
9) Crosslinking buffer wash
10) Crosslinking buffer with DMP - Fraction 1

Lane IDs

1) SeeBlue Molecular Weight Marker
2) Purified Serpin-5 antigen protein standard
3) Crosslinking buffer with DMP - Fraction 2
4) Crosslinking buffer with DMP - Fraction 3
5) Quenching buffer wash
6) Purified Serpin-5 injection 1
7) Purified Serpin-5 injection 2
8) Purified Serpin-5 injection 3
9) Purified Serpin-5 injection 4
10) Post Serpin-5 injection wash
11) Elution of bound protein from column – Fraction 1
12) Elution of bound protein from column – Fraction 2
13) Elution of bound protein from column – Fraction 3
14) Elution of bound protein from column – Fraction 4
15) Post elution wash

Figure 4.13 – Top: Western blot membranes of elution fractions of serpin-5 anti-sera immunoaffinity column with the injection and elution of purified serpin-5 protein. Bottom: analogous graphics depicting all major protein bands and their respective intensities and locations in the membrane. The listed lane IDs convey the sample loaded into the gel wells.

This column was prepared in the same manner as that used for the experiment depicted in Figure 4.12 with the exception that the antibodies were crosslinked to the Protein A. The effectiveness of the crosslinking is confirmed by the absence of the same protein bands in lane 11 as compared to those seen in lane 6 of Figure 4.12. According to lanes 6 – 9 on the 15-lane membrane, injection of the purified serpin-5 protein results in the displacement of the some of the higher molecular mass proteins from the packed bed. The source of this displacement is not currently known, but could be the result of some type of competitive binding. Other than one faint high molecular weight protein band in lane 11 of the 15-lane membrane, no protein bands are observed in lanes 11-14 which could correspond to serpin-5. This is an inconclusive result as either the serpin-5 is not being retained by the antibodies, not being released from the antibodies during application of the low pH elution buffer, or is being retained and released but is present in the elution fraction at a concentration below the visible detection limit of the Western blotting procedure.

In order to increase the concentration of serpin proteins in the elution fractions, the total binding capacity of the column can be increased, and one way to achieve this it through the application of purified antibodies to the Protein A coated spheres which would minimize occupation of useful binding sites on the column by other components in the anti-sera. An affinity column for the purification of serpin-1 antibodies was used as described in section 4.4.8.4 and the membrane from the Western blot performed on the eluted antibody fractions is shown in Figure 4.14. From this membrane it appears that elution fractions 4 and 5 have the highest concentration of serpin-1 antibody present. While the relative abundance of the serpin-1 antibody over other proteins in the anti-sera was dramatically increased, some other proteins are still present in relatively small amounts. The qualitative test performed on this membrane was supplemented with a microplate protein assay which determined the concentration of total protein to be 2.93, 5.34, 5.48, >10.45, >10.45, and 3.95 μg/mL for fractions 1 – 6 respectively. Samples 4 and 5 had slightly higher protein contents than the highest point on the calibration curve and thus their concentration could not be accurately determined.

Using this purified serpin-1 antibody, a new column was prepared and using four 4 μL injections of the purified serpin-1 antibody from fraction 4 (>10.45 μg/mL). Following the injection of antibodies, the maximum amount of serpin-1 antibody that could be retained on the column was 0.17 μg. Since IgG is a divalent antibody, it has the potential to bind two antigens,

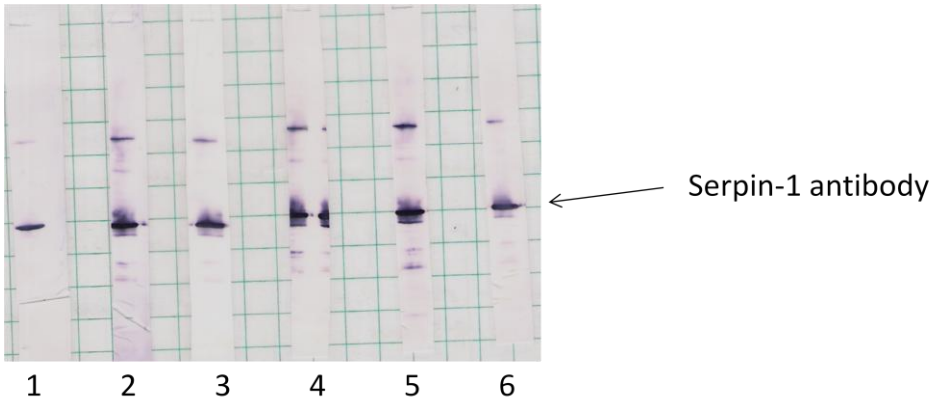

Figure 4.14 – Membrane strips visualizing the protein bands corresponding to the purified antibodies. The elution fraction run on membrane is indicated by the number below the strip. The heavy band in the middle of the membrane strips corresponds to Serpin-1 antibody.

thus the total column binding capacity is approximately 0.34 μg of serpin-1 protein assuming optimal conditions. This is an acceptable binding capacity as amounts of protein as small as few ng can be visualized on Western blot membranes. The concentration of the serpin-1 protein was also determined by microplate protein assay and found to be approximately 8.41 μg/mL. This solution was slightly diluted prior to injection on-column and following dilution the total amount of serpin-1 protein that was loaded was approximately 2.7 ng, enough to be just visible on a Western blot membrane. The Western blot membranes showing the results of SDS-PAGE performed on elution fractions collected from this column are shown in Figure 4.15. Clearly, protein bands corresponding to the injections of the purified antibody can be seen in lanes 4 – 7 of the 17 lane membrane. Also clearly visible are the protein bands corresponding to the injections of the purified serpin-1 protein in lanes 14 – 17 of the 17 lane membrane. The protein bands in lane 5 of the 10 lane membrane correspond to serpin-1 protein being released from the column upon the application of the low pH elution buffer. This protein band confirms that the microimmunoaffinity column is in fact working, and that the use of purified antibodies during column preparation increased the total binding capacity enough to isolate visible amounts of serpin proteins. While the same bands appearing in lane 5 of the 10 lane membrane also appear in the post antigen injection wash of lane 4, they are quite a bit darker in lane 5 indicating a higher abundance. The appearance of two protein bands in lane 5 of the 10 lane membrane is

likely due to the cleavage of the scissile bond of the serpins by proteases resulting in the loss of an amino acid sequence of approximately 30 residues in length.[80]

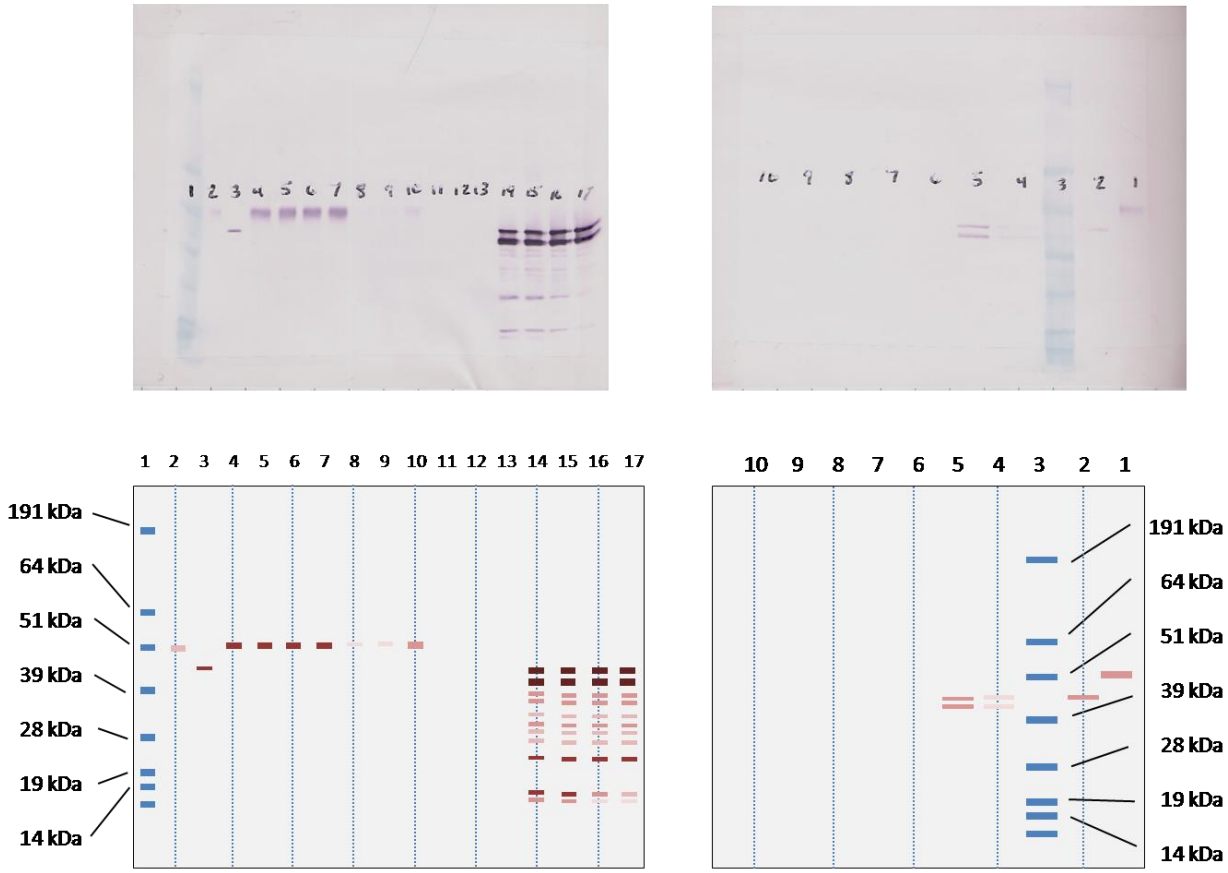

Lane IDs
1) SeeBlue molecular weight marker
2) Purified Serpin-1 antibody standard
3) Purified Serpin-1 antigen standard
4) Serpin-1 antibody injection 1
5) Serpin-1 antibody injection 2
6) Serpin-1 antibody injection 3
7) Serpin-1 antibody injection 4
8) Post Serpin-1 injection wash – Fraction 1
9) Post Serpin-1 injection wash – Fraction 2
10) Pre-crosslinking buffer wash
11) Crosslinking buffer with DMP
12) Quenching buffer wash
13) Equilibration buffer wash
14) Purified Serpin-1 injection 1
15) Purified Serpin-1 injection 2
16) Purified Serpin-1 injection 3
17) Purified Serpin-1 injection 4

Lane IDs
1) Purified Serpin-1 antibody standard
2) Purified Serpin-1 antigen standard
3) SeeBlue molecular weight marker
4) Post Serpin-1 antigen injection wash
5) Elution of bound protein from column – Fraction 1
6) Elution of bound protein from column – Fraction 2
7) Elution of bound protein from column – Fraction 3
8) Elution of bound protein from column – Fraction 4
9) Post elution wash
10) EMPTY

Figure 4.15 – Western blot membranes illustrating elution fractions that were collected using a column prepared with purified Serpin-1 antibodies.

4.6 Conclusion

Micro-immunoaffinity columns employing packed beds retained by rare-earth metal magnets can be used to solve many practical problems encountered by applying biological samples to columns whose packed bed is entirely restricted. The lack of any retaining frits on either end of the column permits the packed bed to adopt a semi-fluid nature. The bed possesses a certain amount of give which allows the beads to yield to particles and polymerized biological components that can form small clots. This semi-fluid nature all but completely eliminates any instances of column clogging. When using a fritted column, clogging became a recurring issue even when using beads 10 μm in diameter which produces much lower backpressures than the 2.8 μm diameter microspheres used in the magnetic column. The smaller diameter microspheres of the magnetic column will also form smaller interstitial spaces between individual beads of the packed region when compared to the interstitial spaces generated by the 10 μm diameter microspheres used in the fritted columns. This would lead one to believe that there would be increased susceptibility to clogging in the magnetic column, however due to the packed bed's ability to shift and make way for larger particles instances of clogging are virtually eliminated. The small volume of the system and the low flow rates used permits the analysis of very small amounts of fluid while keeping dilution to a minimum. Using small diameter beads creates packed beds of very high surface area and thus reasonable binding capacity given the length of the packed region. The column's high binding capacity coupled with its small dimension permits isolation of serpins from as little as a few μL of biological fluid. Elution of isolated serpins can be achieved in a total volume of less than 100 μL, as release of proteins bound to the column is rapid. This small elution volume helps to minimize the dilution of small amounts of total protein making this type of analysis useful for the analysis of serpins from individual insects of less than 100 mg total body weight.

With this current column setup, successful isolation of and elution of serine protease inhibitors was demonstrated in a proof-of-concept design. Admittedly, the execution of this analysis was performed under near ideal conditions involving the use of both purified antibodies and antigens, however column performance should be similar for both purified and unpurified antigens, as the target proteins are retained and isolated on-column as the concomitant substances are flushed through the column.

The application of fluids to the micro-immunoaffinity column could be further simplified by connecting it to an HPLC with an auto-sampler. This type of setup would allow much more seamless switching of fluids and minimize the chance for generating bubbles within the system. The attached auto-sampler would also simplify the injection of sample fluids, and incorporation of an automated fraction collector would propel the system nearer to complete automation. Alternatively, subsequent digestion of the column fractions followed by injection into a mass spectrometer could also help in identifying the amino acid sequences of the serpins present in different insects. Stimulation of the immune system of an insect by bacterial challenge that results in the up-regulation of certain serpins could increase the biological concentrations of the stimulated serpins to detectable levels and also help entomologists and biochemists identify the role of different serpins in an insect's immune response.

I would also like to thank Eve Metto, for her assistance with some of the data collected in this chapter as well as members of the Kanost Biochemistry Lab at Kansas State for their supply of biological samples and expertise.

Chapter 5 - Paper-Based Devices for Analysis of Clinically Relevant Analytes Present in Urine and Saliva

The majority of this chapter has been submitted for publication as: Scott A. Klasner, Alexander K. Price, Kurt W. Hoeman, Rashaun S. Wilson, Kayla J. Bell, Christopher T. Culbertson *Analytical and Bioanalytical Chemistry,* **2010**

5.1 .Introduction

Paper based microfluidic devices were first introduced in 2007 by Whitesides et al.[91] Since that time their potential use as templates for clinically relevant diagnostic assays has been investigated.[91-95] These devices are appealing because of their low cost, minimal required infrastructure, ease of fabrication, speed of fabrication, ease of use, potential to be used remotely, and ability to provide semi-quantitative results in a point-of-care fashion. These devices are fabricated on a paper substrate such as filter paper using photolithography of SU-8 photoresist,[91-93,96,97] inkjet printing,[95] wax patterning using either a wax pen or wax printer,[94,98,99] and plasma treatment of hydrophobic paper.[100] These devices, while all elegant, each have their own advantages and drawbacks. Devices patterned from SU-8 require over 20 min of fabrication time, as well as a post-production plasma oxidation step to render the device channels hydrophilic. These SU-8 devices, however, do permit precise control over feature dimensions resulting from the lithographic process.[96] Devices fabricated via inkjet printing require first coating the paper substrate with poly(styrene) for 2 h prior to printing. In addition, multiple print cycles were required to efficiently remove the poly(styrene) from what will be the hydrophilic channels. One nice feature of these devices is that not only are the channels fabricated via inkjet printing, but the detection reagents themselves are also applied to the devices using inkjet printing.[95] Using wax printing to construct paper-based microfluidic devices permits elimination of organic solvents from the fabrication process, however reduced control over precise channel dimensions is exhibited since following the administering of the wax to the paper substrate, a baking step is required to facilitate the melting of the wax into the paper forming a hydrophobic barrier throughout the thickness of the paper. The baking step allows the wax barriers to change size and shape eliminating the possibility of fabricating well defined small features.[94] In

addition, these wax based devices aren't well-suited for use with organic solvents as the solvents can penetrate the wax barriers or bleed organic dyes from the wax, which can create interferences when performing colorimetric detection. One must also take into account that wax printers can often be expensive investments.[99] Devices fabricated using plasma treatment of hydrophobic paper introduce simple mechanical flow switches, however preparation of the paper requires a 45 min cure of the polymer-soaked paper prior to patterning in the oxygen plasma chamber, which makes their fabrication time-consuming, and requires access to a plasma oxidation system.[100] While less expensive alternative photoactive polymers to SU-8 have been reported, due to their opacity, UV exposure fails to cure the polymer throughout the depth of the paper substrate. This requires the device to be flipped over, aligned, and re-exposed to ensure complete crosslinking throughout the paper.[101]

As demonstrations of the usefulness of these devices in diagnostic settings, colorimetric assays for urinary protein and glucose have been most commonly performed.[91-95,97] Using image manipulation software such as Adobe Photoshop CS4, the intensity of the color produced by these chemical reactions can be measured and related back to the concentrations of spotted reagents, which enables the construction of calibration curves for the different assays. For patients suffering from diabetes, close monitoring of glucose levels is necessary for the prevention of more serious medical complications. Failure to regulate glucose can result in hypoglycemia, diabetic ketoacidosis (DKA), and diabetic coma. In addition to performing glucose and protein assays, we have elected to adapt two other colorimetric assays to the paper microfluidic format for the testing our devices; assays for urinary ketones and salivary nitrite.

Diabetic Ketoacidosis (DKA) is a condition that can often affect untreated diabetics. In DKA, the levels of ketones present in the blood and urine are elevated as a result of low insulin levels. The ketone bodies produced are acetoacetate and beta-hydroxybutyrate. DKA is prominent in type 1 diabetes patients and can be fatal if left untreated. The heightened ketone levels in the blood also result in heightened ketone levels in the urine. Increased levels of ketone bodies in the urine can also be indications of starvation and low carbohydrate diets. Ketone levels in the body are typically monitored with urine tests since this type of analysis is less invasive than monitoring of the blood. Ketones will also appear in a patient's urine before they are seen in the blood, allowing for more rapid monitoring. This is especially useful because during pregnancy, ketoacidosis is a major contributor to intrauterine death if not treated early.[102]

Careful monitoring of DKA can greatly affect future treatments and prevent unnecessary complications.

Hemodialysis is a procedure used on patients with advanced and permanent kidney failure. Its purpose is to filter waste products from the blood stream when the kidneys are not functioning properly. Targeting primarily urea, potassium, and phosphate, this process can take several hours, several days a week, and there is no simple method of monitoring the treatment's progress.[103] Saliva has been found to contain many components derived from serum. These serum based components diffuse into the gingival crevices from the capillaries and eventually make their way into the bulk saliva.[104] Certain analytes present in serum may therefore be found in saliva which enables non-invasive monitoring of their concentrations. One such analyte is nitrite which has been identified as a potential biomarker for monitoring the progression of hemodialysis.[105]

Adaptation of the ketone and nitrite assays will both provide diabetic patients with the ability to perform multiplexed comprehensive screening of their urine with a single sample spotting helping them to better regulate their diet as well as treatment, as well as extend the usefulness of these devices to patients who have progressed beyond diabetes to the stages of kidney failure by providing a simplified method to monitor their hemodialysis treatments.

In this chapter I present the development of a novel polymer blend for the fabrication of paper-based microfluidic devices. This new polymer offers improved fabrication properties over most of the current technology as well as dramatically reduces the time necessary for fabrication. Also two new clinically relevant diagnostic assays are adapted to the paper-based device format which extend the usefulness of these devices to biological fluids other than urine and also demonstrate for the first time the ability of these devices to perform two-step spatially separated on-line chemical reactions.

5.2 Materials and Methods

5.2.1 Reagents

Zipcone UA (PP1-ZPUA) was obtained from Gelest Inc. (Morrisville, PA). Norland Optical Adhesive 74 was obtained from Norland Products (Cranbury, NJ). Fisherbrand qualitative filter paper (09-795), acetone, ammonium chloride, calcium chloride, citric acid, dextrose, n,n-dimethyl formamide, magnesium sulfate, methanol, potassium chloride, potassium

iodide, potassium phosphate monobasic, potassium phosphate dibasic, sodium bicarbonate, sodium chloride, sodium hydroxide, sodium nitroprusside, sodium phosphate monobasic, sodium phosphate dibasic, sodium sulfate, sodium sulfide, and urea were purchased from Fisher Scientific (Pittsburgh, PA). Glycine, lactic acid, n-(1-napthyl)ethylenediamine, and sulfanilamide were obtained from Acros Organics (Morris Plains, NJ). Sodium nitrite was supplied by Mallinckrodt (Hazelwood, MO). Ethylacetoacetate, glucose oxidase, horseradish peroxidase and trehalose were purchased from Sigma-Aldrich (St. Louis, MO). All reagents were used as received.

5.2.2 Photomask Design

Photomasks for lithography were designed using either Microsoft Powerpoint or AutoCAD LT 2006 (Autodesk: San Rafael, CA) and subsequently printed onto a Hewlett-Packard (Palo Alto, CA) inkjet printer transparency using a Hewlett-Packard hp cp1160 inkjet printer. Following printing, the transparency was placed in an 80°C oven (Lindberg/Blue: Asheville, NC) for 10 min to dry the ink. Photomasks were then cut to size.

5.2.3 Paper Device Preparation

The polymer blend used to fabricate the channels was a 1:1 mixture of Zipcone UA, an acryloxy-terminated siloxane polymer, and Norland Optical Adhesive 74 (NOA 74), an acrylate based polymer. Upon mixing, the solution was vortexed vigorously and then degassed in an ultrasonic bath (Branson: Ultrasonics: Danbury, CT) for 15 min. Both the Zipcone UA and the NOA 74 come premixed with their appropriate photoinitiators, therefore the addition of photoinitiator to render the polymer blend photoactive is not necessary.

It was found that ~25 μL of polymer per cm^2 of filter paper was a sufficient amount to fully saturate the paper substrate with the polymer blend. A piece of filter paper was placed on a 2 × 3" (5.08 × 7.62 cm) glass slide (Corning: Corning, NY) and the area of the filter paper was measured so that the amount of polymer required could be calculated. The calculated amount of the photoactive polymer was then slowly pipetted onto the paper and allowed to spread out until the filter paper was saturated. Next the transparency photomask was placed onto the wet polymer coated paper and placed into a UV flood exposure chamber (Oriel: Stratford, CT) for a 1.1 s exposure at 50.0 mW/cm^2. Following exposure, the photomask was peeled off of the paper device and could be cleaned for reuse by gently swabbing with acetone. The paper device was

then peeled off of the glass slide and rinsed with acetone to remove un-crosslinked polymer revealing the channel features defined by the photomask.

5.2.4 Glucose Assay

The glucose assay was based on that reported by Whitesides et al.[91-93] The reaction process for this assay is displayed in Scheme 5.1. Briefly, the glucose detection reagent involved 2 solutions that were spotted on top of each other in the detection zone of the paper device. Solution 1 consisted of 0.6 M potassium iodide and 0.3 M trehalose dissolved in a 100 mM phosphate buffer at pH 6.0. Solution 2 contained 5 parts of 120 units/mL glucose oxidase and 1 part 30 units/mL horseradish peroxidase. Initially, 0.5 μL of solution 1 was spotted in the detection zone of the paper device and allowed to dry for 5 min. Next, 0.5 μL of solution 2 was spotted directly on top of the spot of solution 1 and allowed to dry for 5 min. Dextrose was used as a standard and was dissolved in artificial urine that was prepared according to the formula reported by Brooks and Keevil.[106] Next, 5 μL of the sample was spotted on the sample pad and allowed to wick down a channel and into the detection zone where it comes into contact with the detection reagents.

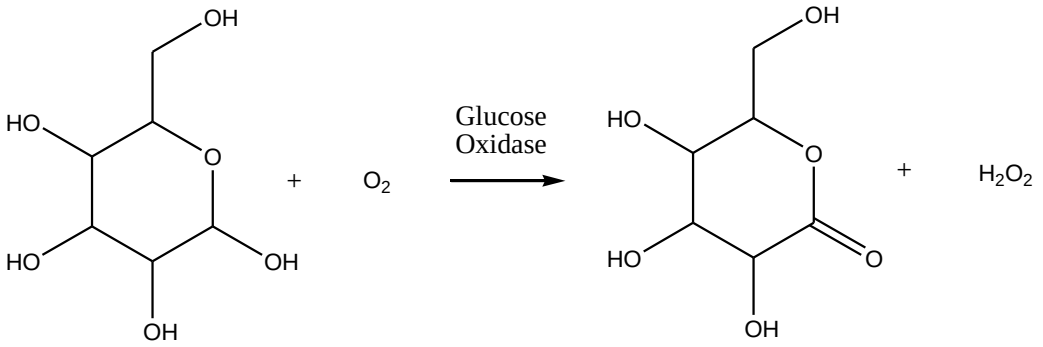

Scheme 5.1 – Enzymatic reactions of glucose oxidase and horseradish peroxidase. The visually detectable iodine produced can be quantified using digital imaging software.

The chip was then placed in a closed container that contained a small amount of water creating a humid environment which prevents the chip from drying out. The chip was left in the humidity

chamber for 20 min permitting the enzymes to metabolize the glucose and form the colored product. After 20 min, the chip was removed and allowed to dry at room temp for 10 min before it was placed on a flatbed scanner for image collection. The image was converted to grayscale in Adobe Photoshop® CS4 and gray intensities were recorded using the same software.

5.2.5 Ketone Assay

The specific chemical reactions governing this assay are depicted in Scheme 5.2. Using a pattern incorporating three spotting pads, 0.5 μL of 100 mM glycine in 100 mM phosphate buffer pH 9.4 was spotted on the middle zone. The final detection zone was spotted with 0.5 μL of 5% sodium nitroprusside (w/w) in 5% DMF (v/v) in water. This format allowed the target molecule, acetoacetate, to wick through the glycine region initiating a reaction between the two and forming an imine. This imine would wick down the second half of the channel into the detection pad containing the sodium nitroprusside and the reaction that occurs yields a magenta colored product. The sample spot was 7 μL of the desired amount of acetoacetate dissolved in synthetic urine. Following sample spotting the device was allowed to dry at room temperature for 15 min prior to image collection with a flatbed scanner. The image was converted to CMYK format in Adobe Photoshop® CS4 and the color intensity was recorded using the magenta channel.

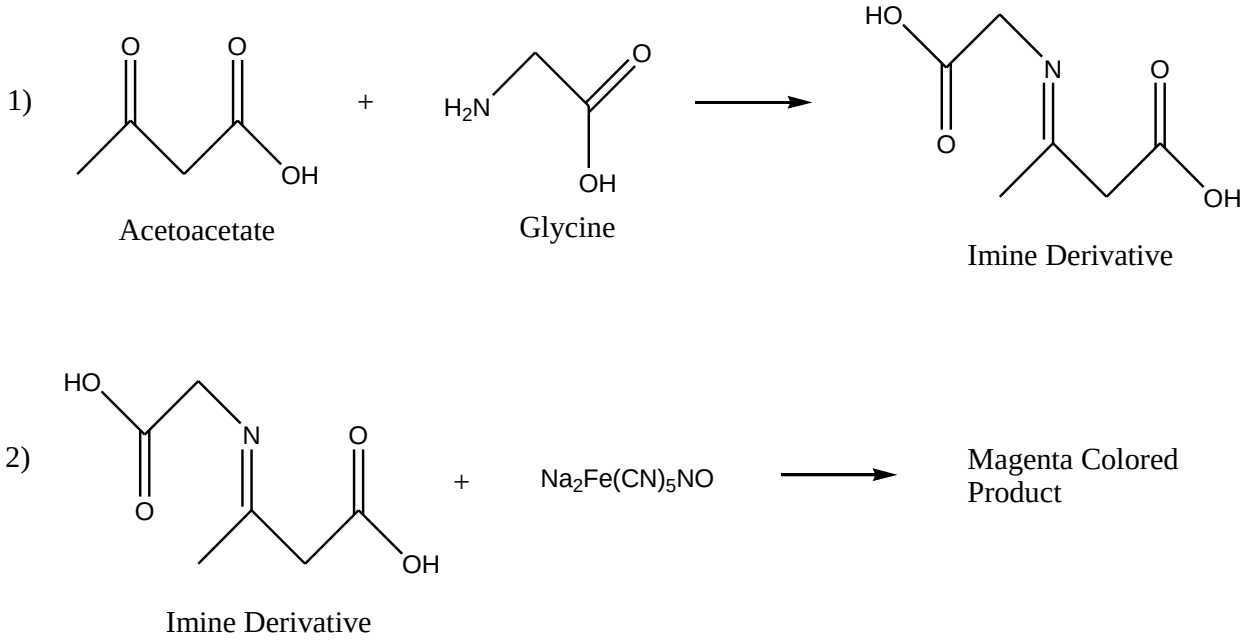

Scheme 5.2 – Reaction scheme for colorimetric determination of ketones in urine.

5.2.6 Protein Assay

The protein assay was modified from previously demonstrated colorimetric assays.[91-95] The assay was performed in a two-step fashion. The chip design involved three different spotting regions connected in series; one for the sample, a second for citrate buffer, and a third for the tetrabromophenol blue (TBPB) colorimetric reagent. For the spotting of the reagents, 0.5 μL of 300 mM citrate buffer pH 2.2 was placed in the middle spotting region so that when the sample was spotted it would wick through this region buffering the sample prior to reaching the TBPB detection pad. For the TBPB spotting, 0.5 μL of 3.3 mM TBPB in 95% ethanol was used. The sample spot consisted of 7 μL of the desired amount of BSA dissolved in the same synthetic urine used for the glucose assay. The sample would wick through the citric acid buffer zone adjusting the pH of the sample before reaching the TBPB. Upon reaction of the buffered sample with the TBPB, a blue color formed indicating the presence of protein. Following spotting, the device was allowed to dry at room temperature for 15 min and was then scanned using a flatbed scanner. The image was converted to CMYK in Adobe Photoshop CS4 and mean color intensities were measured using the cyan channel.

5.2.7 Nitrite Assay

The nitrite assay was adapted from previously reported methods for the preparation of nitrite salivary dipsticks.[105] The nitrite assay was a single step analysis based on the reaction depicted in Scheme 5.3. The detection solution consisted of 50 mM sulfanilamide, 330 mM citric acid, and 10 mM n-(1-napthyl)ethylenediamine in methanol; 0.5 μL of this solution was spotted in the detection zone. The sample consisted of a known amount of sodium nitrite dissolved in artificial saliva, and 5 μL of this was spotted onto the sample zone. The artificial saliva was prepared according to the method of Yildirmaz et al. and contained sodium chloride (0.4 mg/mL), potassium chloride (0.4 mg/mL), calcium chloride (0.8 mg/mL), sodium phosphate monobasic (0.69 mg/mL) and sodium sulfide nonahydrate (0.05 mg/mL).[107] Following spotting, the device was allowed to dry at room temperature for 15 min prior to recording an image with a flatbed scanner. Recorded images were converted to CMYK format in Adobe Photoshop CS4 and color intensity measurements were recorded using the magenta channel.

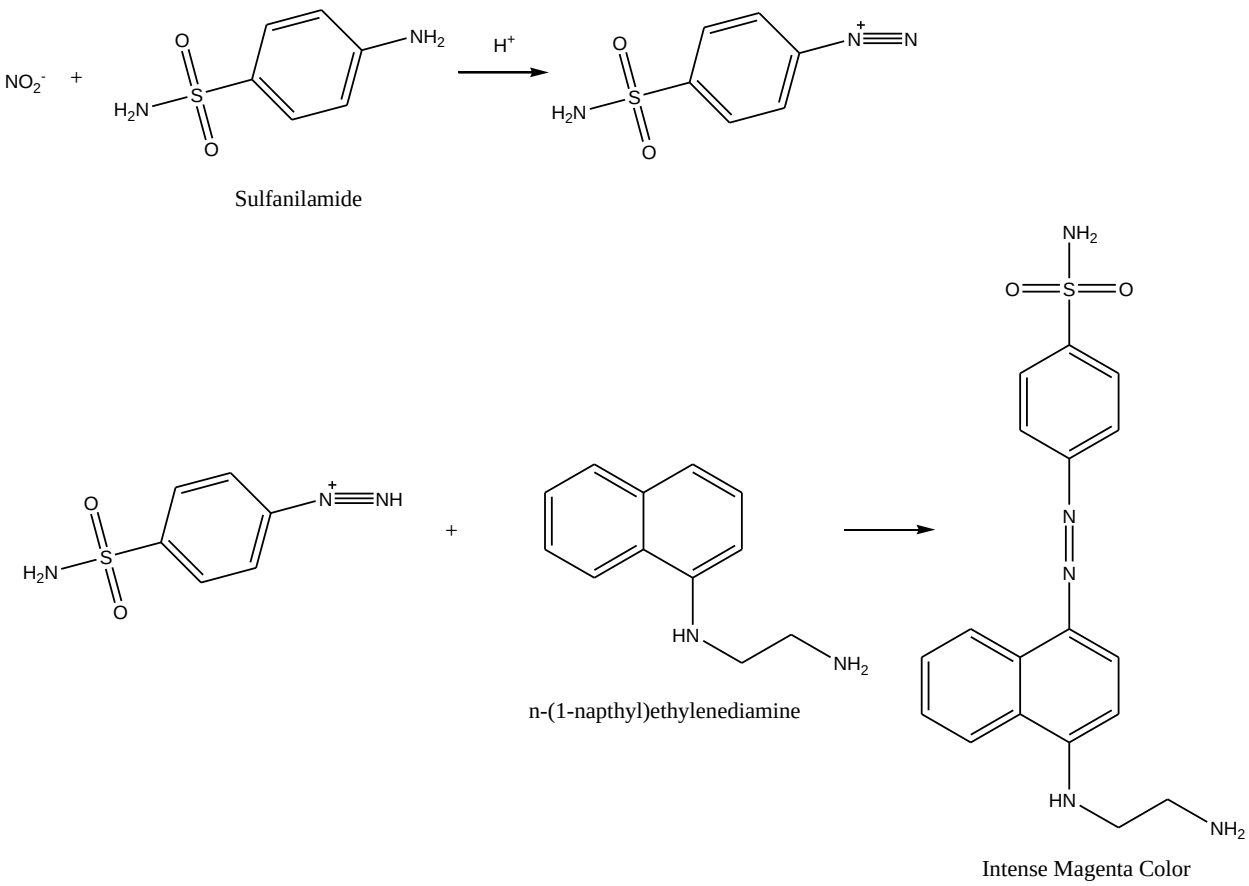

Scheme 5.3 – Reaction scheme for colorimetric determination of nitrite. Nitrite is first converted to nitrous acid by citric acid. Nitrous acid then reacts with sulfanilamide to form a diazo compound. The resulting diazo compound reacts with n-(1-naphthyl)ethylenediamine to form the colored product.[106]

5.2.8 Data Analysis

Image acquisition was performed using a flatbed scanner (Microtek Scanmaker 4800). Images were recorded in the TIFF format at 600 dpi. Adobe Photoshop CS4 was used to convert the images from RGB to either the CMYK or grayscale format and to select the relevant area of the image and then calculate the mean color intensity over that area. Calculated mean color values were imported into IGOR Pro 6.04 (Wavemetrics: Lake Oswego, Oregon) and used to generate calibration curves.

5.3 Results and Discussion

5.3.1 Material Characteristics

Initial attempts to find a polymer amenable to simpler and more rapid fabrication of paper-based microfluidic devices involved the use of the Zipcone UA exclusively. Fabrication of well-defined channels could be achieved, however after about 1 h, the device would begin to crack extensively due to shrinking of the polymer, and flexing of the device only exacerbated the cracking. We then attempted using Norland Optical Adhesive 74 using the same methodology. The result was a poorly defined pattern and a sticky textured device, however the device would not crack when subjected to flexing. It became readily apparent that alone, the two polymers would not yield usable devices, however by mixing them together in a 1:1 ratio, the best attributes of each could be taken advantage of and formed well defined, pliable, and hydrophilic devices.

These devices were particularly sensitive to exposure time, as too short of an exposure resulted in incomplete curing of the polymer on the underside of the device, while too long an exposure resulted in over curing of the polymer on the underside of the device resulting in narrower features on the underside of the chip as opposed to the top. For our purposes an exposure of 1.1 s at 50 mW/cm^2 was found to be optimal. The exposure intensity of 50 mW/cm^2 over a 1.1 s period converts to 55 mJ/cm^2. Knowing this energy, chips can alternately be exposed to sunlight for curing. We were able to produce sun-cured chips by taking devices outside for the exposure period and monitoring the total amount of energy the device had received using a photometer. On January 30th 2009 at 4:00 PM under clear skies, the required exposure time to reach the prescribed 55 mJ/cm^2 energy dosage was 100 s, which showed a 72% decrease in exposure time over reported sun-crosslinked SU-8 based devices.[96]

The final cost of the polymer used to manufacture these paper based devices was approximately 91¢ per gram of 1:1 Zipcone : NOA 74 blend. This cost could be decreased however by adjusting the ratio to favor the NOA 74 as it is the cheaper of the two components in the blended polymer. The cost corresponding to the fabrication of usable devices is dictated solely by the amount of polymer used and thus the size of the device (the cost of the filter paper substrates is negligible). The minimum volume of polymer required for fabrication is 30 μL/cm^2. With a density of 1.02 g/cm^3 at 20 °C, this amounts to a cost of $0.03 per cm^2 of device fabricated. Typical device size could be around 2.54 cm × 2.54 cm for a total cost per device of $0.19.

5.3.2 Patterning Properties

To examine the limitations of the polymer on the effective size of features that could be patterned, we mimicked the approach of Whitesides et al. and found both the smallest patterned channels that would successfully wick fluid as well as the minimum barrier size that would impede fluid flow from one channel to an adjacent one.[96]

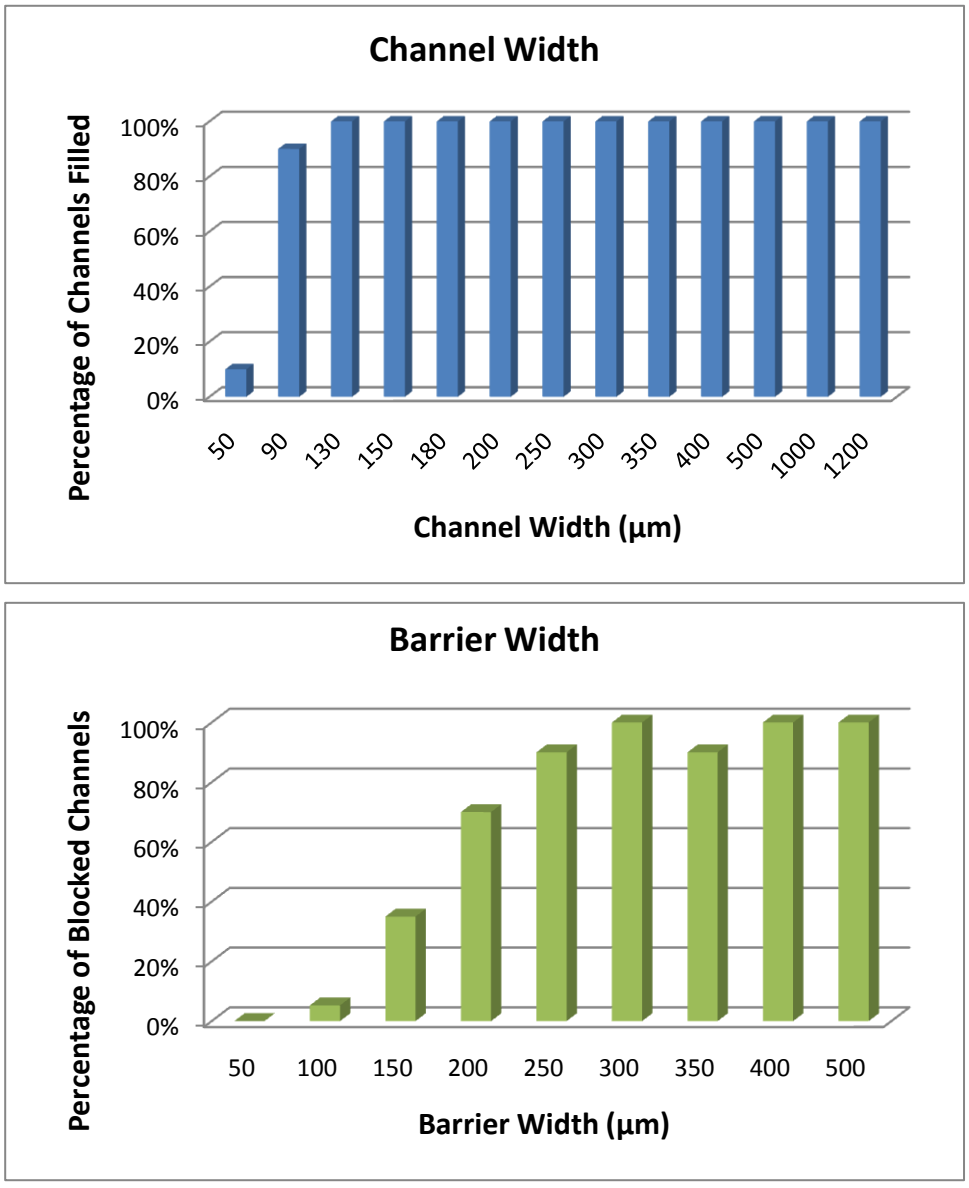

Figure 5.1 – Top: Graph illustrating the percentage of channels with different dimensions from 20 chips that successfully wicked fluid. Bottom: Graph illustrating the percentage of barriers with various widths from 20 chips that successfully blocked fluid flow.

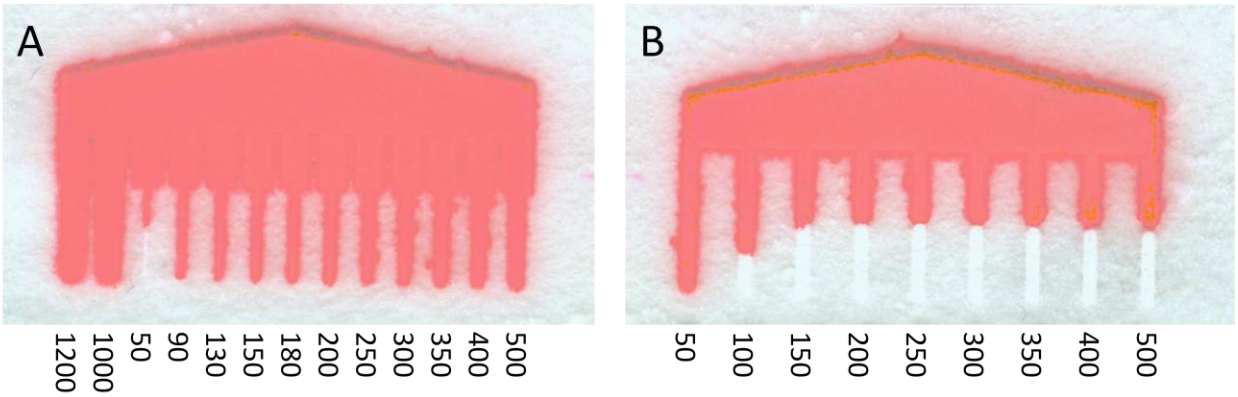

Figure 5.2 – Images of paper devices with different (A) channel widths and (B) barrier widths. All labeled dimensions in μm, 30 μL of red food coloring diluted in water spotted on each device.

Limiting ourselves to a 90% rate of success (Figure 5.1), the minimum channel width that would wick fluid was found to be 90 μm, while the minimum barrier width to prevent fluid penetration into an adjacent channel was 250 μm (Figure 5.2). The smallest features recorded for SU-8 paper based devices are 200 μm and 250 μm for channel and barrier features respectively.[96] The barrier feature is much more susceptible than channel features to fabrication defects such as bubbles or failure of the polymer to entirely saturate the depth of the paper substrate as these defects will decrease the effective width of the barrier and increase the likelihood of fluid carryover into an adjacent channel.

5.3.3 Glucose Assay

The glucose assay has become a fairly standard analysis performed on paper devices and therefore we decided to demonstrate the ability of our devices to perform this assay. Performed in the presence of water and oxygen, in this reaction glucose is oxidized by glucose oxidase to form gluconic acid and hydrogen peroxide. The hydrogen peroxide that has been produced is then reduced to water by horseradish peroxidase with simultaneous oxidation of iodide to iodine (Scheme 5.1). A glucose level in urine above 1.4 mM is typically an indicator of illness. In Figure 5.3 an image of a representative paper device is shown on which an assay for glucose in the range of 3 - 50 mM was performed. From devices such as this we were able to generate calibration curves for the data. While the Whitesides group reports a linear range between 1 – 5 mM, our linear range extends from 3 – 50 mM (Figure 5.4). Initially, our data also exhibited a

rollover yielding a linear range that covered glucose concentrations of 1 – 5 mM, much like Whitesides et al.[92] We thought of a number of ways to extend this linear range; first, if the concentration of glucose is high, then the enzymes become saturated and can't metabolize the glucose fast enough to make discernable color changes above the concentration at which the enzymes are saturated. Second, if the concentration of iodide is too low, then glucose could continue to be metabolized without yielding any additional color change. Third, if the channels dry out, the reactions cease, and if this occurs prematurely, the appropriate signal for a given concentration may not be achieved. In order to improve the linear dynamic range we therefore attempted the following: after spotting of the samples, the devices were placed in a closed humidity chamber and allowed to incubate for 20 min after which they were removed and allowed to dry for an additional 15 min prior to data collection. The humidity chamber ensured that all channels remained wet and thus had ample time for generation of the colored I_2 product. We next attempted to increase the concentrations of the reagents to extend the linear range of the curve. Increased amount of enzyme escalated the rate at which the glucose was metabolized resulting in faster signal generation and reduced incubation times. Initial experiments where detection reagents were spotted multiple times, resulting in higher concentrations of enzymes on the detection pads, did show increased signal production over the use of a single spotting, however signal reproducibility was decreased.

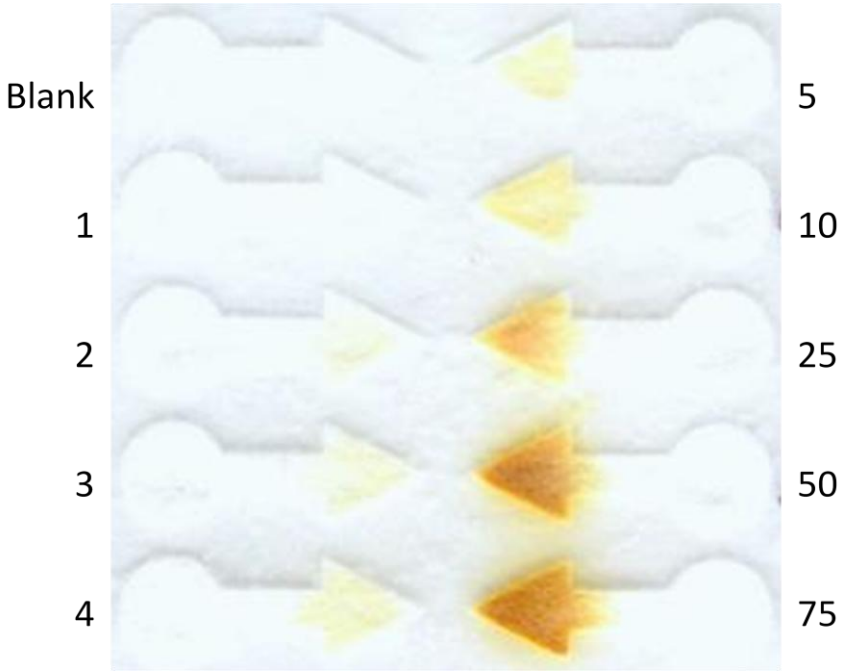

Figure 5.3 – Representative glucose chip. Numbers indicate mM concentrations of glucose.

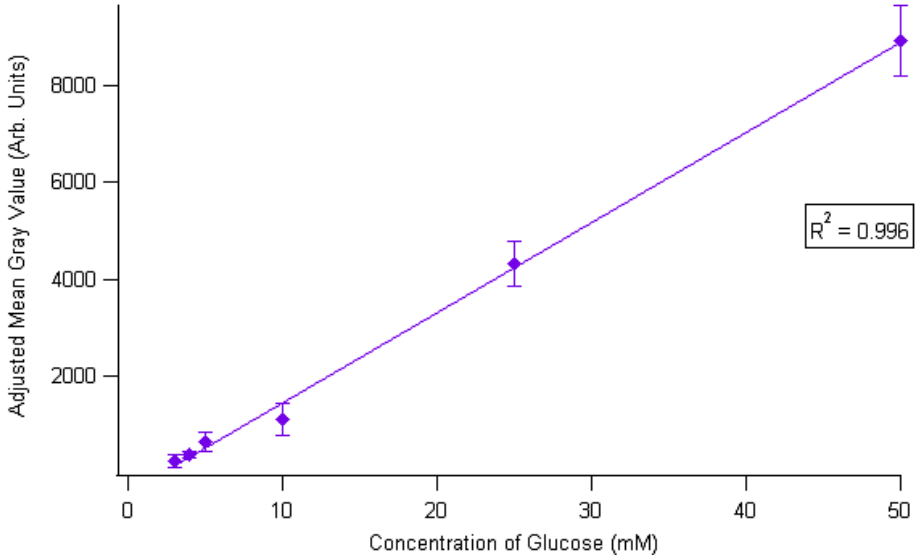

Figure 5.4 – Calibration curve generated for the range of 3 – 50 mM urinary glucose. Based on trendline, the limit of detection for this assay is 2.8 mM. Measurements were taken using the grayscale channel only. (N = 8)

The urinary glucose concentrations that are clinically tested fall in the range of 0 – 550 mM. The typical cutoff for glucose concentration of a urine sample that signals disease is about 1.4 mM.[92] The limit of detection of our glucose assay is just above that value at 2.8 mM, so while we are currently not able to detect glucose at 1.4 mM these devices could be used as a rapid initial screening and if glucose is detected it would indicate that more thorough, costly, and labor intensive tests may be required. We however, do not believe that the detection limit that we report is intrinsic to our chip format rather that it is a function of the methodology employed, and with some optimization, the limit of detection can be improved.

5.3.4 Protein Assay

The protein assay, like the glucose assay has become a standard assay performed on these paper-based devices. We chose to briefly examine the ability of our paper-based devices to detect protein in urine. The basis for the color change observed in this assay is referred to as the "protein error of a pH indicator". The pH at the surface of a protein differs from that of its bulk solution, and thus adsorption of pH indicators to the surface of proteins can result in color changes reflecting those pH differences.[108] Although typically not performed in this manner, we chose to separate this assay into a two part process. Initially, we struggled with this test getting many false positive results, however after much trial and error; we determined that the most

important aspect of this reaction is that the sample be properly buffered before reaching the detection zone. Most groups that perform this protein assay spot two different reagent solutions on the detection pad on top of one another. One is typically a low pH citrate buffer, and the other, a tetrabromophenol blue indicator solution. We have chosen to spot our citrate buffer and our indicator solution in two serial reservoirs. This approach allows the sample to wick into the buffering region prior to interaction with the detection reagents thus ensuring that the sample solution is properly buffered when it reaches the detection zone. Using a two part approach such as this dramatically reduced the occurrence of false positives

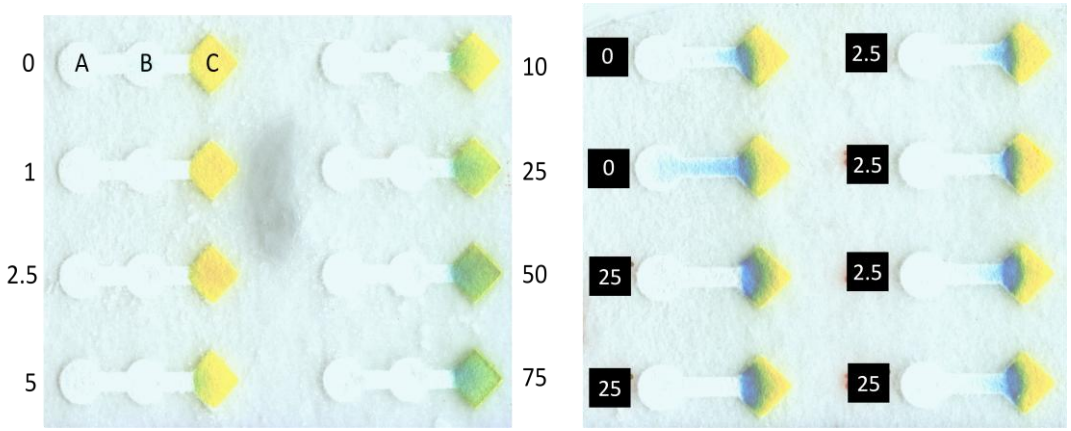

Figure 5.5 – Left - Representative device depicting an assay for protein in urine. Concentration of BSA (μM) in artificial urine of each sample is shown in margins. In regions (B) and (C) 0.5 μL of 300 mM citrate buffer pH 1.8 and 0.5 μL of 3.3 mM tetrabromophenol blue in 95% ethanol were respectively spotted and allowed to dry at which time 7.0 μL of sample was spotted in region (A). Right – Demonstration of false positive readings obtained when citrate buffer and TBPB are spotted in same reservoir. Concentrations of BSA (μM) in sample listed next to corresponding lanes.

The ability of this assay to quantify urinary proteins is depicted in Figure 5.6. For the curve spanning the entire range of concentrations examined, we attempted to fit our data to a number of different types of relationships including polynomial, double exponential, and logarithmic. The goodness of the fit was determined using chi squared χ^2 values, with the smallest value of χ^2 indicating the best fit. Over the range of 5 – 50 μM this assay clearly exhibits the common trend of signal rollover at higher concentrations of BSA. A fairly linear range does exist in the narrow range of 5 – 25 μM, however truly accurate quantitation would

require additional data points as it appears that curve rollover begins to occur at approximately 25 µM. That being the case, quantitation over the entire range is examined as the data fits very well to a logarithmic trend line. Using the linear region of the curve to calculate a limit of detection generated a LOD of 1.5 µM. The typical clinical range for urinary protein is from 0.3 – 60 µM,[92] and using a logarithmic relationship should facilitate fairly accurate determination of protein levels between 5 and 50 µM.

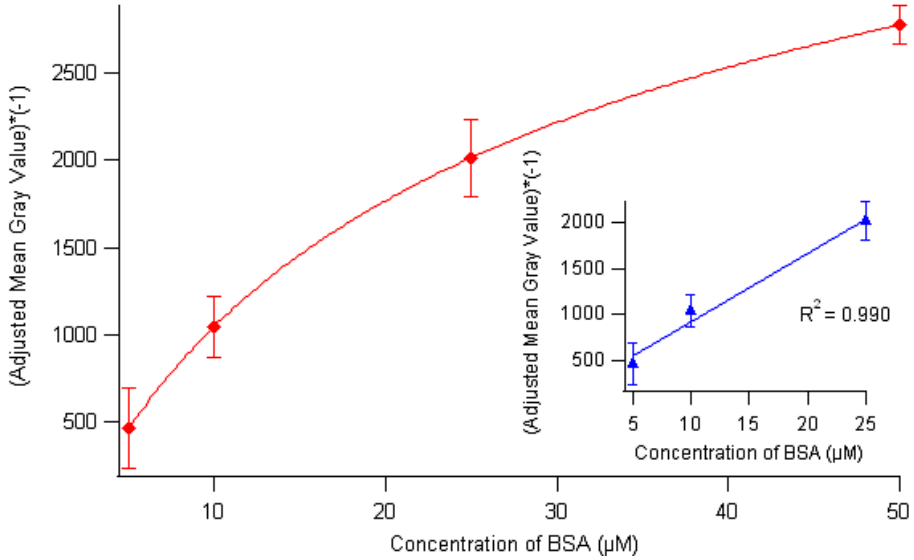

Figure 5.6 – Calibration curves for the concentration of BSA in artificial urine. Main – curve for the full range of concentrations examined. Inset – Expansion of linear range of curve from 5 – 25 µM BSA. All color intensity measurements were taken using the cyan channel only. Main data set was fit to a logarithmic trendline with an equation of the general formula:

$$y = y_0 + Ae(-[\ln\{x/x_0\}/width]^2)$$

with values for y_0, A, x_0, and $width$ calculated using IGOR Pro's regression curve fitting feature.

5.3.5 Ketone Assay

Most of the work collected with respect to the ketone assay has been previously reported by Hoeman.[4] Some additional data analysis has since been performed and those details are presented here. The assay for urinary ketones demonstrated for the first time the ability of these devices to perform online chemical derivatization. This assay uses a two-part format allowing

chemical modification prior to detection. Acetoacetate in urine first reacts with glycine forming an imine derivative. The imine derivative then continues wicking along the channel until it reaches the detection pad and reacts with sodium nitroprusside forming a deep violet colored complex (Scheme 5.2 and Figure 5.7). The success of the on-line reaction between acetoacetate and glycine is confirmed by the fact that if either of the two components comes into contact with the sodium nitroprusside individually, no color change is observed, rather the two reagents must be mixed and react before any color change with the nitroprusside salt is observed.

We determined that our data was best represented with a logarithmic relationship by using χ^2 values (similar to the protein assay). Since the results of this assay already blanket the clinically relevant range, we did not determine the limit of detection. At this time we are still trying to understand why no linear range of concentrations was ever achieved with this assay. The kinetics of this reaction have been studied by Laios and Pardue, and based on their findings the best hypothesis that we can offer is that part of the colored product begins to noticeably decay, even as new product is formed, after a period of about 30 minutes.[109] This fact could account for the increased linearity of the data the sooner it is collected. However, as previously discussed, the signal intensity of this assay increases with time until about 50 min after spotting where the signal plateaus.[4] So, with competing reactions producing new colored product while at the same time resulting in the decay of older product, we currently believe that the lack of curve linearity is founded in the complex kinetics of the system combined with the added complexity of a 2-step spatially separated reaction. The color intensity produced in the detection pad is not only a function of the concentration of ketone in the sample, but also a function of the efficiency of the reaction forming the imine derivative. Any differences in the amount of imine produced as a result of ketone concentration will inevitably be reflected by the amount of color generated on the detection pad. Despite the curve's lack of linearity, it was reproducible and thus useful for the quantitation of analytes.

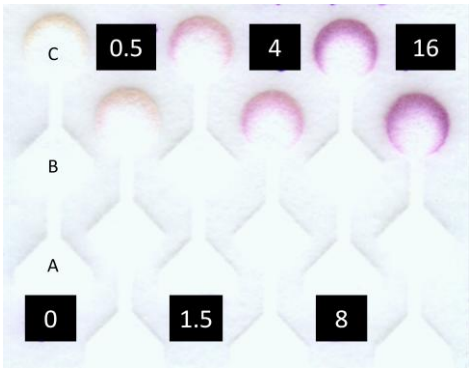

Figure 5.7 – Scanned image of a ketone assay paper-based device. Concentrations of acetoacetate are mM. (A) Sample spotting pad: 10 µL of ketone spiked artificial urine spotted. (B) Glycine derivatization zone: 0.7 µL 100 mM glycine dissolved in 100 mM phosphate buffer pH 9.4 spotted. (C) Detection pad: 0.7 µL on 5% sodium nitroprusside (w/w) in a 5% DMF (v/v) in water solution spotted. Sample spotted in "A" wicks to "B" where imine formation occurs and then on to "C" where complexing with sodium nitroprusside yields a deep purple colored product.

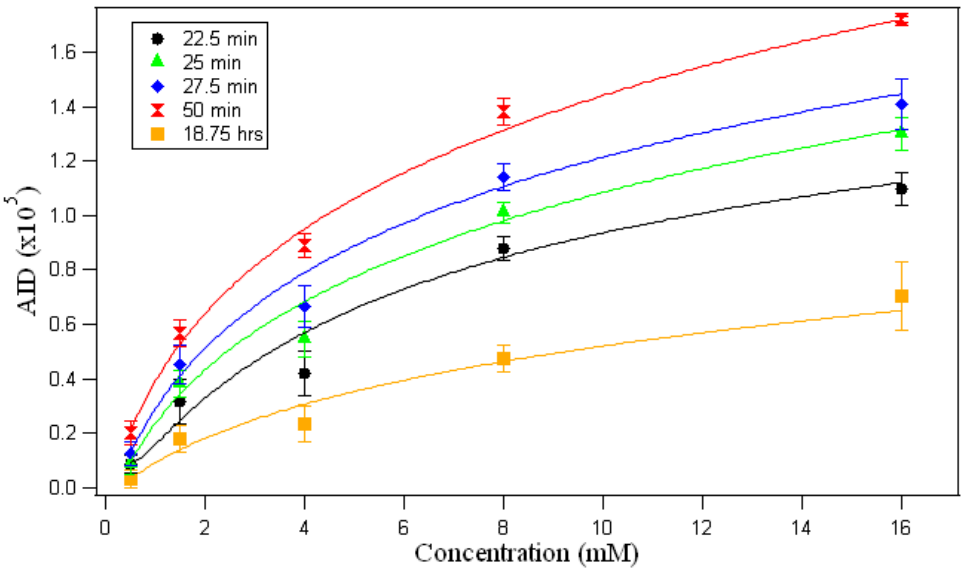

Figure 5.8 – Calibration curves for ketone assay. Adjusted integrated density; Integrated density values measured in Adobe Photoshop CS4 were corrected for the blank and then multiplied by (-1) to yield y-axis values. Measurements were taken using magenta channel only. Signal intensity changes with elapsed time after sample spotting. Data sets were fit to a logarithmic trendline with an equation of the general formula:

$$y = y_0 + Ae(-[\ln\{x/x_0\}/width]^2)$$

with values for y_0, A, x_0, and $width$ calculated using IGOR Pro's regression curve fitting feature.

Urinary tests for ketones are normally negative. However, when present, laboratories routinely categorize the patient as having low, moderate, or high levels of ketones in their urine. The concentrations corresponding to these three levels are ≤ 1.9 mM for "low", between 2.9 – 3.9 mM for "moderate" and ≥ 7.8 mM for "high".[110]

5.3.6 Nitrite Assay

In order to extend the functionality of these devices to biological samples other than urine, we adapted a dipstick based colorimetric test for salivary nitrite to our format. Nitrite has been identified as a useful biomarker to identify the progression of hemodialysis on patients with end stage renal disease. This assay is based on the Griess reaction for the quantization of NO_2^- (Scheme 5.3).[111] As hemodialysis progresses, NO_2^- will be filtered out of the blood along with other waste products. As this occurs, the diminished nitrite concentration in the blood will also be reflected in the patient's saliva, permitting real-time point-of-care monitoring of dialysis progression. A representative device for the analysis of nitrite is shown in Figure 5.9. Since this assay functions only to qualitatively monitor the progression of dialysis, it is less important to have a wide linear response to varied nitrite concentrations, however our data does appear to be linear in the range of concentrations of most relevance. Of twelve patients with end stage renal disease (ESRD) examined by Blicharz et al., all had salivary nitrite concentrations prior to dialysis of between 40 and 160 μM.[105] Following a 4 h dialysis treatment, that concentration window decreased to between approximately 1 – 40 μM. While all patients had different initial salivary nitrite concentrations, all exhibited a net decrease following dialysis treatment. This assay produces a linear response over the fairly wide range of 25 to 250 μM (Figure 5.10). At concentrations above ~250 μM, the linearity of our curve ceases and begins to plateau rapidly. This could be due to complete consumption of our color forming reagents, evaporation of the artificial saliva causing the paper to dry before the colored product has completely formed, or even a decreased sensitivity of our data acquisition methods to increasingly dark shades. We found that it was important to closely monitor the elapsed time between sample spotting and scanned image collection as color would develop over time after the device had dried producing

false positives and high backgrounds, however this typically wasn't a significant problem until the device had sat for several hours.

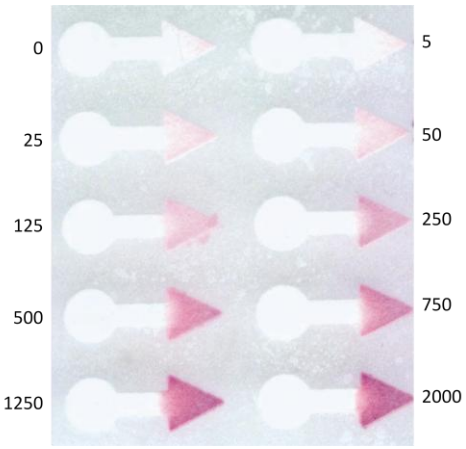

Figure 5.9 – Representative nitrite assay chip with concentrations (μM) of nitrite dissolved in artificial saliva listed in margins.

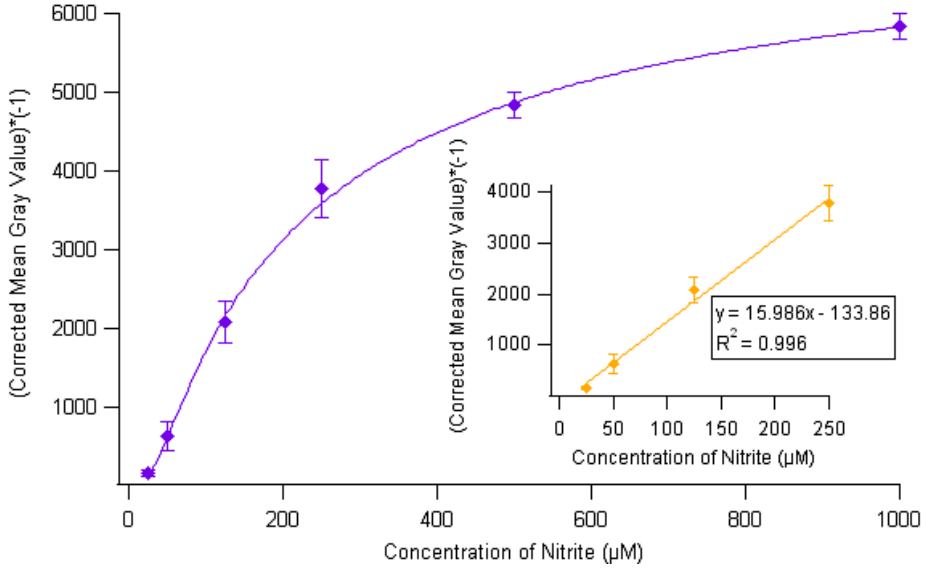

Figure 5.10 - Calibration curves for the concentration of Nitrite in artificial saliva. Large - curve for the full range of concentrations examined. Inset – Expansion of linear range of curve from 5 – 250 μM nitrite. All color intensity measurements were taken using the magenta channel only.

5.4 Conclusion

We have introduced a new photoactive polymer that dramatically decreases the both the fabrication time and complexity of paper-based devices. We have demonstrated their ability to

perform traditionally practiced paper based clinical assays for glucose and protein in urine as well as adapted two new assays for ketones in urine and nitrite in saliva to the paper microfluidic format. This polymer permits the fabrications of smaller channel features on paper-based devices in a fraction of the time compared to SU-8 devices. We also demonstrated for the first time the ability of paper based devices to successfully execute on-line chemical derivatization as required for the analysis of ketones in urine. The introduction of an assay for urinary ketones when coupled with the urinary glucose and protein assays on a paper-based device provides for a comprehensive screening tool for diabetics. Also, the extension of the use of these devices to salivary analysis introduces other possible avenues for noninvasive monitoring of analytes in bodily fluids.

Chapter 6 - Future Direction and Outlook

6.1 PDMS-PEO

6.1.1 Thermally Cured PDMS-PEO

With the current state of the PDMS-PEO material, I don't believe that it is a viable option for widespread use in the fabrication of microfluidic devices due to its difficulty of fabrication, lack of mechanical strength, decreased conformal adhesion, and failure to provide improved separation efficiencies. There is simply too much about the cured material that is not understood. The hydrosilation reaction between the vinyl and hydride groups should be stoichiometric. The question of why excessive equivalents of crosslinker are required to form a suitable material with the mechanical strength required to be considered for use as a microfluidic template still remains unanswered. Devices fabricated from standard poly(dimethylsiloxane) use elastomers that contain silica particles as a mechanical filler to impart structural integrity to the crosslinked material. The PDMS-PEO devices prepared in our lab do not use any reinforcing fillers, and this could explain why PDMS-PEO materials are less robust. However, despite this absence of reinforcing fillers the PDMS-PEO materials display a Young's modulus that is in some instances greater than standard PDMS materials. A future study incorporating the use of fillers in the PDMS-PEO may improve the functional durability of these materials and reduces their susceptibility to damage by shear.

The degree of conformal contact exhibited by PDMS-PEO devices is far less than that possessed by PDMS. The origin of the attraction of two PDMS surfaces with each other is rooted in Van der Waals interactions resulting from the hydrophobic nature of the material. As the hydrophilicity of the material increases due to incorporation of poly(ethylene oxide) units it is logical that the magnitude of the conformal interaction between the two surfaces would reflect a decrease. Thus it would appear that the degree of hydrophilicity achievable with a PDMS-PEO device will be limited by the amount of attractive interaction needed to seal two pieces of material together without fluid leakage. Without further characterization of the cured material and increased knowledge regarding how the polymer crosslinking is occurring, it is difficult to suggest avenues which may increase the overall reliability of the material. It does appear that it

will be necessary to balance the desired characteristics with the required characteristics in order to develop optimal formulations.

While it is possible to perform analytical separations of simple mixtures of amino acids on these devices now, separations of more hydrophobic molecules will be required. By increasing the hydrophilicity of the bulk material we hope to reduce the tendency of biomolecules to adsorb to its surface facilitating the separations of proteins while obviating the many different types of surface modifications used on standard PDMS devices to make these separations possible. If these devices don't exhibit increased compatibility with hydrophobic compounds it may not be worthwhile to pursue their optimization.

6.1.2 Photocured PDMS-PEO

Photocurable PDMS-PEO is extremely simple to prepare. The block copolymer is commercially available and is rendered photoactive via simple mixing with a photoinitiator. Curing is much more rapid than with thermally prepared PDMS-PEO, and irreversible sealing of two layers is also straightforward. The native fluorescence of the material however, prevents its use as a template for microfluidic devices. The source of this fluorescence is most likely the commercially added inhibitors used to prevent crosslinking of the block copolymer during shipping and storage. Discussions with technical personnel at Gelest have conveyed that there is a method to remove these inhibitors from the block copolymer, however it is proprietary. Depending on how stable the acryloxy groups are in the absence of the inhibitors it should be possible to prepare photoactive PDMS-PEO with little or no native fluorescence. It is likely that removal of the inhibitors using a silica gel column is possible; however this would require determination of the appropriate silica gel and selection of an optimal solvent system, followed by removal of the solvent from the PDMS-PEO block copolymer. Typically solvents can be removed from a mixture such as this by using high vacuum. Often times, mixtures will be heated to facilitate solvent evaporation. Depending on the reactivity of the acryloxy groups in the absence of the inhibitors, the application of heat to remove the solvent may be enough to initiate crosslinking of the block copolymer. Regardless, of the difficulties, the fluorescent inhibitors must be removed for this block copolymer to be a viable option for microfluidic chip fabrication. If removal of the inhibitors can be achieved, photocurable PDMS-PEO devices, with

their ease of fabrication, should be conducive to rapid production permitting in depth characterization of their different properties.

6.2 Analysis of Ecdysteroids

A variety of methods were developed and examined in an attempt to fluorescently tag and separate ecdysteroids. In the process, a quantitative analysis scheme for fluorescently labeled progesterone was developed, but in reality this assay is restricted in its application as the fluorescently labeled progesterone is not fully separated from a common fluorescently tagged metabolite of very similar structure. Some of the results obtained using ecdysteroids were hopeful, but inconclusive. Some very small new peaks were occasionally observed, but it was not possible to confidently assign them to labeled ecdysteroids.

The main sources of difficulty with this project were both scientific as well as economic. The functional group targeted by the fluorescent tag was an α,β-unsaturated ketone. It was believed that this group would be prone to attack by a hydrazide functional fluorophore, and the multiple labeling of the progesterone molecule confirmed this suspicion, however attempts to apply the same labeling methodology to the ecdysteroids failed to produce a tagged adduct. The question remains as to why the enone on progesterone can be derivatized while the enone on the ecdysteroids does not appear to react.

The second more practical impediment to progress was the exceedingly high cost of the reagents. Both the fluorescent tag and the ecdysteroids cost more than $100.00 for a few mg. This required sparse use of the reagents by performing multiple iterations of an experiment with very dilute concentrations of analyte. The use of dilute analyte in the midst of high levels of fluorescent molecules makes any recognition of minor peaks exceedingly difficult. This was further complicated by the fact that the fluorophore itself often exhibited a number of peaks. The collection of more reliable information will require, at least initially, the use of more concentrated solutions of analyte. This means either accepting the financial costs associated with the analysis, or the development of a means to more easily isolate or synthetically prepare ecdysteroids leading to increased commercial availability and a reduction in price. Also, continued development of new fluorescent molecules may lead to the introduction of a more affordable, and stable probe.

The methods for the analysis of ecdysteroids using capillary electrophoresis with laser induced fluorescence exist, however, at this time they are not useful without a means of effectively and confidently fluorescently labeling the ecdysteroid. Using the currently proposed reagents will require a thorough understanding of the chemistry involving enones, and an optimization of the coupling conditions for linking it to a hydrazide.

6.3 Microimmunoaffinity Column

Investigation into the preparation of a micro-scale immunoaffinity column initially resulted in the assembly of columns based around the use of stationary frits to retain packed beds of functionalized microspheres. Designs based on this format presented recurrent instances of column clogging as a result of both disassembly and reassembly of the column for the purposes of frit installation, or the application of biological fluids with increased viscosity. By adopting the magnetically isolated packed bed format for the micro-immunoaffinity column we all but eliminated these instances of clogging. This magnetic column proved to be quite reliable as far as containment of the functionalized magnetic microspheres. Once the column was assembled, all experimental steps including the application of antibodies, crosslinking of the antibodies to the column, application of the antigen molecules, and elution of the antigen molecules were performed on-line. Initial experiments confirmed the successful crosslinking of antibodies to the column as well as the isolation and elution of antigen molecules. Experiments were admittedly performed under near ideal conditions. But with the optimistic outlook of the preliminary results collected, more "real" samples should be investigated. Tests that validate the capability of these columns to isolate serpin proteins from real samples like insect hemolymph will naturally be required. Due the small amounts of serpins that will inevitably be present in smaller insects from which limited volumes of hemolymph can be collected, it may be necessary to improve the column eluent collection method by reducing the collection window from 10 minutes. For instance, if fractions are collected every 60 s instead of 600 s and it becomes apparent that a majority of the protein is eluted within a 60 s window, additional fractional collection time will result in up to a 10-fold sample dilution. This dilution may result in amounts of protein below the visible limit of detection on the membrane.

The other remaining concern is non-specific binding. Application of the elution buffer releases the proteins from the system, as they are detected in the Western blots of the elution

fractions, however we do not definitively know if these proteins are being released from the packed bed, or the inner surfaces of the system tubing. We are however optimistic that non-specific binding is minimal, as upon injections of the antibodies onto the system, they would be the first proteins with an opportunity to non-specifically bind system surfaces. Since it is not possible to crosslink non-specifically bound proteins they would be released upon the application of the elution buffer. On the western blots we have performed, following the crosslinking of the antibodies and application of the elution buffer, no protein bands corresponding to released antibody protein are observed in the elution fractions. This means that either non-specific binding is minimal, or the relative surface area of the system surfaces available is negligible relative to the surface area of the small packed bed and that the binding capacity of the packed bed is much higher than the non-specific binding capacity of the system.

While additional experiments with this system are required to further optimize conditions and improve sample collection, the initial results presented are optimistic. Coupling this system to additional instrumentation would provide a great deal of supplemental information about the proteins collected. Injecting the column eluent directly into a mass spectrometer (MS) could provide specific structural and sequence information. Spotting column eluent onto a MALDI plate for subsequent tryptic digest and analysis by MS could also help to identify and characterize these proteins.

6.4 Paper-Based Microfluidics

Paper-based microfluidic devices do offer potential as useful, cheap, and disposable point-of-care diagnostic tools. They exhibit multiple avenues for fabrication each with their own advantages and disadvantages. So far these devices have been shown capable of semi-quantitative analysis of many urinary analytes relevant to diabetes. The main limitations of the devices produced in our lab lies in their limit of detection, linear ranges, and reproducibility. While we were capable of generating fairly good data, Implementation of these types of devices in a real clinical setting will undoubtedly generate lower quality results due to the complexity of real samples.

The simple elegance of these devices is one of the features that makes them so fascinating, however there are still demands that need to be met before they will suitable for real-world deployment. The method of data collection needs to be further evaluated. Types of

images collected (JPEG, TIFF, BMP); the resolution of the collected image in dpi; and the image format (RGB, CMYK, grayscale) could all impact the quantification of colored analytes using the image analysis software, and any impact due to these factors will require investigation and analysis.

With the current state of development for paper-based devices, I believe that pursuant to their in depth characterization, wax based devices will be the dominant device form produced due to the environmental friendliness of the fabrication process as well as its simplicity. The focus of these devices to this point has been on diagnostic applications, but with the ability of these devices to perform online chemical reactions, they may have potential as a template for small scale preliminary testing of multi-step chemical synthesis by spotting a series of reagents in different regions and then allowing a sample reagent to wick through them performing multiple derivatization steps until the new product can be collected at a final zone and used for subsequent analysis such as NMR or MS.

References

(1) Giddings, J. C. *Unified Separation Science*; John Wiley & Sons Inc.: New York, NY, 1991.
(2) Heiger, D. N. *High Performance Capillary Electrophoresis - An Introduction*; 2nd ed.; Hewlett-Packard Company: France, 1992.
(3) Jacobson, S. C.; Culbertson, C. T. In *Separation Methods in Microanalytical Systems*; Kutter, J. P., Fintschenko, Y., Eds.; CRC Press: Boca Raton, FL, 2006, p 19-54.
(4) Hoeman, K., W., Kansas State University, 2009.
(5) Schoch, R. B.; Han, J.; Renaud, P. *Rev Mod Phys* **2008**, *80*, 839-883.
(6) Poole, C. F. **2003**.
(7) Terabe, S.; Otsuka, K.; Ichikawa, K.; Tsuchiya, A.; Ando, T. *Anal Chem* **1984**, *56*, 111.
(8) Alescaron, G.; Petr, B.; rcaron; Petr, B.; Pavel, A.; Juraj, S.; ccaron; ík; Panagiotis, T.; Jitka, U. *J Sep Sci* **2001**, *24*, 723-728.
(9) Cunico, R. L.; Gooding, K. M.; Wehr, T. *Basic HPLC and CE of Biomolecules*; Bay Bioanalytical Labaratory, Inc.: Richmond, CA, 1998.
(10) Karger, B. L.; Snyder, L. R.; Horvath, C. *An Introduction to Separation Science*; John Wiley & Sons: New York, NY, 1973.
(11) de Mello, A. *Lab Chip* **2002**, *2*, 31N-36N.
(12) McCormick, R. M.; Nelson, R. J.; Alonso-Amigo, M. G.; Benvegnu, D. J.; Hooper, H. H. *Anal Chem* **1997**, *69*, 2626.
(13) Probstein, R. F. *Physiochemical Hydrodynamics*; 2nd ed.; John Wiley & Sons, Inc.: Hoboken, NJ, 2003.
(14) Duffy, D. C.; McDonald, J. C.; Schueller, O. J. A.; Whitesides, G. M. *Anal Chem* **1998**, *70*, 4974-4984.
(15) Huang, B.; Kim, S.; Wu, H.; Zare, R. N. *Anal Chem* **2007**, *79*, 9145-9149.
(16) Roman, G. T.; Carroll, S.; McDaniel, K.; Culbertson, C. T. *Electrophoresis* **2006**, *27*, 2933-2939.
(17) Roman, G. T.; McDaniel, K.; Culbertson, C. T. *The Analyst* **2006**, *131*, 194-201.
(18) Wu, D.; Luo, Y.; Zhou, X.; Dai, Z.; Lin, B. *Electrophoresis* **2005**, *26*, 211-218.
(19) Zhang, Q.; Xu, J.; Lian, H.; Li, X.; Chen, H. *Anal Bioanal Chem* **2006**, *384*, 265.
(20) Dou, Y.-H.; Bao, N.; Xu, J.-J.; Meng, F.; Chen, H.-Y. *Electrophoresis* **2004**, *25*, 3024-3031.
(21) Cui, H.; Horiuchi, K.; Dutta, P.; Ivory, C. F. *Anal Chem* **2005**, *77*, 1303-1309.
(22) Liu, Y.; Henry, C. S. In *Microchip Capillary Electrophoresis* 2006, p 57.
(23) Liu, Y.; Fanguy, J. C.; Bledsoe, J. M.; Henry, C. S. *Anal Chem* **2000**, *72*, 5939-5944.
(24) Jones, B. J.; Hayes, M. A. In *Microchip Capillary Electrophoresis* 2006, p 49.
(25) Chen, L.; Ren, J.; Bi, R.; Chen, D. *Electrophoresis* **2004**, *25*, 914-921.
(26) Hu, S.; Ren, X.; Bachman, M.; Sims, C. E.; Li, G. P.; Allbritton, N. *Anal Chem* **2002**, *74*, 4117-4123.
(27) Wu, D.; Zhao, B.; Dai, Z.; Qin, J.; Lin, B. *Lab Chip* **2006**, *6*, 942-947.

(28) Hu, S.; Ren, X.; Bachman, M.; Sims, C. E.; Li, G. P.; Allbritton, N. L. *Langmuir* **2004**, *20*, 5569-5574.
(29) Hu, S.; Ren, X.; Bachman, M.; Sims, C. E.; Li, G. P.; Allbritton, N. L. *Anal Chem* **2004**, *76*, 1865-1870.
(30) Patrito, N.; McCague, C.; Chiang, S.; Norton, P. R.; Petersen, N. O. *Langmuir* **2006**, *22*, 3453-3455.
(31) Wu, D.; Qin, J.; Lin, B. *Lab Chip* **2007**, *7*, 1490-1496.
(32) Xiao, D.; Le, T. V.; Wirth, M. J. *Anal Chem* **2004**, *76*, 2055-2061.
(33) Roman, G. T.; Culbertson, C. T. *Langmuir* **2006**, *22*, 4445-4451.
(34) Roman, G. T.; Hlaus, T.; Bass, K. J.; Seelhammer, T. G.; Culbertson, C. T. *Anal Chem* **2005**, *77*, 1414-1422.
(35) Abate, A. R.; Lee, D.; Do, T.; Holtze, C.; Weitz, D. A. *Lab Chip* **2008**, *8*, 516-518.
(36) Hellmich, W.; Regtmeier, J.; Duong, T. T.; Ros, R.; Anselmetti, D.; Ros, A. *Langmuir* **2005**, *21*, 7551-7557.
(37) Wang, A.-J.; Feng, J.-J.; Fan, J. *J Chromatogr A* **2008**, *1192*, 173.
(38) Guo, D.-J.; Han, H.-M.; Jing, W.; Xiao, S.-J.; Dai, Z.-D. *Colloid Surface A* **2007**, *308*, 129.
(39) Wang, A.-J.; Xu, J.-J.; Chen, H.-Y. *J Chromatogr A* **2007**, *1147*, 120.
(40) Jukarainen, H.; Ruohonen, J.; Lehtinen, M.; Ala-Sorvari, J.; Seppala, J.; (Leiras Oy, Finland). Application: WO, 1999, p 15 pp.
(41) Galin, M.; Mathis, A. *Macromolecules* **1981**, *14*, 677-683.
(42) Haesslin, H. W.; Eicke, H. F.; Riess, G. *Makromolekul Chem* **1984**, *185*, 2625-2645.
(43) Haesslin, H. W. *Makromolekul Chem* **1985**, *186*, 357-366.
(44) Guo, Q.; Chen, F.; Wang, K.; Chen, L. *J Polym Sci Pol Phys* **2006**, *44*, 3042-3052.
(45) Rutnakornpituk, M.; Ngamdee, P. *Polymer* **2006**, *47*, 7909.
(46) Rutnakornpituk, M.; Ngamdee, P.; Phinyocheep, P. *Polymer* **2005**, *46*, 9742.
(47) Park, J. H.; Bae, Y. H. *Biomaterials* **2002**, *23*, 1797.
(48) Roman, G. T.; Hlaus, T.; Bass, K. J.; Seelhammer, T. G.; Culbertson, C. T. *Anal. Chem.* **2005**, *77*, 1414-1422.
(49) Stevens, M. P. *Polymer Chemistry. 2nd Ed*, 1990.
(50) Harris, D. C. *Quantitative Chemical Analysis*; 7th ed.; W.H. Freeman Company: New York, NY, 2007.
(51) Lee, C. S.; McManigill, D.; Wu, C. T.; Patel, B. *Anal Chem* **1991**, *63*, 1519-1523.
(52) Lee, C. S.; Blanchard, W. C.; Wu, C. T. *Anal Chem* **1990**, *62*, 1550-1552.
(53) Ocvirk, G.; Munroe, M.; Tang, T.; Oleschuk, R.; Westra, K.; Harrison, D. J. *Electrophoresis* **2000**, *21*, 107-115.
(54) Jacobson, S. C.; Ramsey, J. M. *Anal Chem* **1996**, *68*, 720-723.
(55) Jukarainen, H.; Clarson, S. J.; Seppala, J. V. *ACS Sym Ser* **2000**, *729*, 353-358.
(56) Wang, X.; Chen, Z.; Shen, Z. *Sci China Ser B* **2005**, *48*, 553.
(57) Vickers, J. A.; Caulum, M. M.; Henry, C. S. *Anal Chem* **2006**, *78*, 7446-7452.
(58) Mark, J. E.; Pan, S. J. *Makromol Chem-Rapid* **1982**, *3*, 681-685.
(59) Ninc, Y.-P.; Mark, J. E. *J Appl Polym Sci* **1985**, *30*, 3519-3522.
(60) Mark, J. E. *Acc Chem Res* **2004**, *37*, 946-953.

(61) Tandon, V.; Bhagavatula, S. K.; Nelson, W. C.; Kirby, B. J. *Electrophoresis* **2008**, *29*, 1092-1101.
(62) Vickers, J. A.; Caulum, M. M.; Henry, C. S. *Anal Chem* **2006**, *78*, 7446.
(63) *Ecdysone: From Chemistry to Mode of Action*; Koolman, J., Ed.; Thieme Medical Publishers Inc.: New York, 1989.
(64) Nijhout, H. F., Princeton University Press, 1994.
(65) Lafont, R.; Dinan, L. *J Insect Sci* **2003**, *3*, 7.
(66) Skoog, D. A. H., F. James; Nieman, Timothy A. *Principles of Instrumental Analysis*; 5th ed.; Saunders College Publishing, 1998.
(67) Gallo, M. B. C.; Beltrame, F. L.; Vieira, P. C.; Cass, Q. B.; Fernandes, J. B.; da Silva, M. F. d. G. F. *J Chromatogr B* **2006**, *832*, 36.
(68) Kubo, I.; Komatsu, S. *J Chromatogr A* **1986**, *362*, 61.
(69) Kubo, I.; Komatsu, S. *Agric Biol Chem* **1987**, *51*, 1305-1309.
(70) Yasuda, A.; Ikeda, M.; Naya, Y. *Nippon Suisan Gakk* **1993**, *59*, 1793-1799.
(71) Santagati, N. A.; Tropea, S.; Ronsisvalle, G. *J Chromatogr A* **2005**, *1081*, 77-86.
(72) Davis, P.; Lafon, R.; Large, T.; Morgan, E.; Wilson, I. *Chromatographia* **1993**, *37*, 37.
(73) Báthori, M.; Máthé, I.; Guttman, A. *Chromatographia* **1998**, *48*, 145.
(74) Katayama, M.; Nakane, R.; Matsuda, Y.; Kaneko, S.; Hara, I.; Sato, H. *Analyst* **1998**, *123*, 2339-42.
(75) Hoeman, K. W.; Culbertson, C. T. *Electrophoresis* **2008**, *29*, 4900-4905.
(76) Hyytiaeinen, M.; Appelblad, P.; Ponten, E.; Stigbrand, M.; Irgum, K.; Jaegfeldt, H. *J Chromatogr A* **1996**, *740*, 279-283.
(77) Michel, K.; Kafatos, F. C. *Insect Biochemistry and Molecular Biology* **2005**, *35*, 677.
(78) Suwanchaichinda, C.; Kanost, M. R. *Gene* **2009**, *442*, 47.
(79) Silverman, G. A.; Bird, P. I.; Carrell, R. W.; Church, F. C.; Coughlin, P. B.; Gettins, P. G. W.; Irving, J. A.; Lomas, D. A.; Luke, C. J.; Moyer, R. W.; Pemberton, P. A.; Remold-O'Donnell, E.; Salvesen, G. S.; Travis, J.; Whisstock, J. C. *Journal of Biological Chemistry* **2001**, *276*, 33293-33296.
(80) Tong, Y.; Jiang, H.; Kanost, M. R. *J Biol Chem* **2005**, *280*, 14932-14942.
(81) Silverman, G. A.; Lomas, D. A.; Editors *Molecular and Cellular Aspects of the Serpinopathies and Disorders in Serpin Activity*, 2007.
(82) Huntington, J. A.; Read, R. J.; Carrell, R. W. *Nature* **2000**, *407*, 923.
(83) Irving, J. A.; Pike, R. N.; Lesk, A. M.; Whisstock, J. C. *Genome Research* **2000**, *10*, 1845-1864.
(84) Vassilis, J. M.; Nektarios, D. C.; Christos, G. Z. *Archives of Insect Biochemistry and Physiology* **1996**, *31*, 119-133.
(85) Michael, R. K.; Haobo, J.; Xiao-Qiang, Y. *Immunological Reviews* **2004**, *198*, 97-105.
(86) Osta, M. A.; Christophides, G. K.; Vlachou, D.; Kafatos, F. C. *J Exp Biol* **2004**, *207*, 2551-2563.
(87) Padlan, E. A. *Antibody-Antigen Complexes*; R.G. Landes Company: Georgetown, TX, 1994.
(88) Steward, M. W. *Antibodies: Their Structure & Function*; Chapman and Hall: New York, NY, 1984.

(89) Voet, D.; Voet, J. G.; Pratt, C. W. *Fundamentals of Biochemistry*; John Wiley & Sons Inc.: New York, NY, 2002.
(90) Catty, D. In *The Practical Approach Series*; Catty, D., Ed.; IRL Press: Oxford, England, 1988; Vol. 1, p 7-18.
(91) Martinez, A. W.; Phillips, S. T.; Butte, M. J.; Whitesides, G. M. *Angew Chem Int Ed* **2007**, *46*, 1318-1320.
(92) Martinez, A. W.; Phillips, S. T.; Carrilho, E.; Thomas, S. W.; Sindi, H.; Whitesides, G. M. *Anal Chem* **2008**, *80*, 3699-3707.
(93) Martinez, A. W.; Phillips, S. T.; Whitesides, G. M. *Proc Nat Acad Sci USA* **2008**, *105*, 19606-19611.
(94) Lu, Y.; Shi, W.; Jiang, L.; Qin, J.; Lin, B. *Electrophoresis* **2009**, *30*, 1497-1500.
(95) Abe, K.; Suzuki, K.; Citterio, D. *Anal Chem* **2008**, *80*, 6928-6934.
(96) Martinez, A. W.; Phillips, S. T.; Wiley, B. J.; Gupta, M.; Whitesides, G. M. *Lab Chip* **2008**, *8*, 2146-2150.
(97) Ellerbee, A. K.; Phillips, S. T.; Siegel, A. C.; Mirica, K. A.; Martinez, A. W.; Striehl, P.; Jain, N.; Prentiss, M.; Whitesides, G. M. *Anal Chem* **2009**, *81*, 8447.
(98) Lu, Y.; Shi, W.; Qin, J.; Lin, B. *Anal Chem* **2009**, *82*, 329.
(99) Carrilho, E.; Martinez, A. W.; Whitesides, G. M. *Anal Chem* **2009**, *81*, 7091.
(100) Li, X.; Tian, J.; Nguyen, T.; Shen, W. *Anal Chem* **2008**, *80*, 9131.
(101) Carrilho, E.; Phillips, S. T.; Vella, S. J.; Martinez, A. W.; Whitesides, G. M. *Anal Chem* **2009**, *81*, 5990.
(102) Fischbach, F.; Dunning, M. B. *A Manual of Laboratory and Diagnostic Tests*; 8th Ed. ed.; Wolters Kluwer Health - Lippincott, Williams, and Wilkins: Philadelphia, PA, 2009.
(103) Sherman, R. A.; Swartz, R. D.; Thomas, C. In *Kidney Failure Series* 2006; Vol. 2009.
(104) Griffiths, G. S. *Periodontol* **2003**, *31*, 32-42.
(105) Blicharz, T. M.; Rissin, D. M.; Bowden, M.; Hayman, R. B.; DiCesare, C.; Bhatia, J. S.; Grand-Pierre, N.; Siqueira, W. L.; Helmerhorst, E. J.; Loscalzo, J.; Oppenheim, F. G.; Walt, D. R. *Clin Chem* **2008**, *54*, 1473-1480.
(106) Brooks, T.; Keevil, C. W. *Lett Appl Microbiol* **1997**, *24*, 203-206.
(107) Yildirmaz, G.; Akgöl, S.; Yakup ArIca, M.; Sönmez, H.; Denizli, A. *React Funct Polym* **2003**, *56*, 103.
(108) Danielli, J. F. *Biochem J* **1941**, *35*, 470-478.
(109) Laios, I. D.; Pardue, H. L. *Anal Chem* **1993**, *65*, 1903.
(110) Silberberg, C. Medline Plus: Ketones - Urine. **2007** http://www.nlm.nih.gov/medlineplus/ency/article/003585.htm.
(111) Sun, J.; Zhang, X.; Broderick, M.; Fein, H. *Sensors* **2003**, *3*, 276-284.